

# **Integrated Ocean Drilling Program Expedition 321 Preliminary Report**

## **Pacific Equatorial Age Transect**

4 May–22 June 2009

Mitch Lyle, Isabella Raffi, Heiko Pälike, Hiroshi Nishi,  
Kusali Gamage, Adam Klaus,  
and the Expedition 320/321 Scientists



Published by  
Integrated Ocean Drilling Program Management International, Inc.,  
for the Integrated Ocean Drilling Program

## **Publisher's notes**

Material in this publication may be copied without restraint for library, abstract service, educational, or personal research purposes; however, this source should be appropriately acknowledged. Core samples and the wider set of data from the science program covered in this report are under moratorium and accessible only to Science Party members until 24 October 2010.

### Citation:

Lyle, M., Raffi, I., Pälke, H., Nishi, H., Gamage, K., Klaus, A., and the Expedition 320/321 Scientists, 2009. Pacific Equatorial Transect. *IODP Prel. Rept.*, 321. doi:10.2204/iodp.pr.321.2009

### Distribution:

Electronic copies of this series may be obtained from the Integrated Ocean Drilling Program (IODP) Scientific Publications homepage on the World Wide Web at [www.iodp.org/scientific-publications/](http://www.iodp.org/scientific-publications/).

This publication was prepared by the Integrated Ocean Drilling Program U.S. Implementing Organization (IODP-USIO): Consortium for Ocean Leadership, Lamont Doherty Earth Observatory of Columbia University, and Texas A&M University, as an account of work performed under the international Integrated Ocean Drilling Program, which is managed by IODP Management International (IODP-MI), Inc. Funding for the program is provided by the following agencies:

National Science Foundation (NSF), United States

Ministry of Education, Culture, Sports, Science and Technology (MEXT), Japan

European Consortium for Ocean Research Drilling (ECORD)

Ministry of Science and Technology (MOST), People's Republic of China

Korea Institute of Geoscience and Mineral Resources (KIGAM)

Australian Research Council (ARC) and New Zealand Institute for Geological and Nuclear Sciences (GNS), Australian/New Zealand Consortium

Ministry of Earth Sciences (MoES), India

## **Disclaimer**

Any opinions, findings, and conclusions or recommendations expressed in this publication are those of the author(s) and do not necessarily reflect the views of the participating agencies, IODP Management International, Inc., Consortium for Ocean Leadership, Lamont-Doherty Earth Observatory of Columbia University, Texas A&M University, or Texas A&M Research Foundation.

## Expedition 320 participants

### Expedition 320 scientists

**Heiko Pälike**  
**Co-Chief Scientist**  
National Oceanography Centre, Southampton  
University of Southampton  
European Way  
Southampton SO14 3ZH  
United Kingdom  
[heiko@noc.soton.ac.uk](mailto:heiko@noc.soton.ac.uk)

**Hiroshi Nishi**  
**Co-Chief Scientist**  
Department of Natural History Sciences  
Hokkaido University  
Kita-10, Nishi-8, Kita-ku  
Sapporo 060-0810  
Japan  
[hnishi@mail.sci.hokudai.ac.jp](mailto:hnishi@mail.sci.hokudai.ac.jp)

**Adam Klaus**  
**Expedition Project Manager/Staff Scientist**  
Integrated Ocean Drilling Program  
Texas A&M University  
1000 Discovery Drive  
College Station TX 77845-9547  
USA  
[aklaus@iodp.tamu.edu](mailto:aklaus@iodp.tamu.edu)

**Helen Evans**  
**Logging Staff Scientist**  
Borehole Research Group  
Lamont-Doherty Earth Observatory  
of Columbia University  
PO Box 1000, 61 Route 9W  
Palisades NY 10964  
USA  
[helen@ldeo.columbia.edu](mailto:helen@ldeo.columbia.edu)

**Trevor Williams**  
**Logging Staff Scientist**  
Borehole Research Group  
Lamont-Doherty Earth Observatory  
of Columbia University  
PO Box 1000, 61 Route 9W  
Palisades NY 10964  
USA  
[trevor@ldeo.columbia.edu](mailto:trevor@ldeo.columbia.edu)

**Gary D. Acton**  
**Paleomagnetist**  
Department of Geology  
University of California, Davis  
One Shields Avenue  
Davis CA 95616  
USA  
[gdacton@ucdavis.edu](mailto:gdacton@ucdavis.edu)

**Paul Bown**  
**Paleontologist (nannofossils)**  
Earth Sciences  
University College London  
Gower Street  
London WC1E 6BT  
United Kingdom  
[p.bown@ucl.ac.uk](mailto:p.bown@ucl.ac.uk)

**Margaret (Peggy) Delaney**  
**Inorganic Geochemist**  
Ocean Sciences  
University of California, Santa Cruz  
1156 High Street  
Santa Cruz CA 95064  
USA  
[delaney@ucsc.edu](mailto:delaney@ucsc.edu)

**Tom Dunkley Jones**  
**Paleontologist (nannofossils)**  
Earth Sciences  
University College London  
Gower Street  
London WC1E 6BT  
United Kingdom  
[tom.dunkleyjones@ucl.ac.uk](mailto:tom.dunkleyjones@ucl.ac.uk)

**Kirsty Edgar**  
**Paleontologist (planktonic foraminifers)**  
School of Ocean and Earth Sciences  
National Oceanography Centre  
European Way  
Southampton SO14 3ZH  
United Kingdom  
[kme@noc.soton.ac.uk](mailto:kme@noc.soton.ac.uk)

**Peter Fitch**  
**Physical Properties/Downhole Tools**  
**Specialist**

Department of Geology  
University of Leicester  
University Road  
Leicester LE1 7RH  
United Kingdom  
[pjf5@le.ac.uk](mailto:pjf5@le.ac.uk)

**Nikolaus Gussone**  
**Inorganic Geochemist**  
Institut für Mineralogie  
Westfälische Wilhelms-Universität Münster  
Corrensstrasse 24  
48149 Muenster  
Germany  
[nikolaus.gussone@uni-muenster.de](mailto:nikolaus.gussone@uni-muenster.de)

**Jens Herrle**  
**Sedimentologist**  
Institute of Geosciences  
Goethe University Frankfurt  
Altenhoferallee 1  
60438 Frankfurt  
Germany  
[jens.herrle@em.uni-frankfurt.de](mailto:jens.herrle@em.uni-frankfurt.de)

**Kiseong Hyeong**  
**Sedimentologist**  
Deep Sea Resources Research Center  
Korea Ocean Research and Development  
Institute  
ANSAN PO Box 29  
Seoul 425-600  
Korea  
[kshyeong@kordi.re.kr](mailto:kshyeong@kordi.re.kr)

**Shin-ichi Kamikuri**  
**Paleontologist (radiolarians)**  
Graduate School of Science  
Hokkaido University  
Kita-10, Nishi-8, Kita-ku  
Sapporo 060-0810  
Japan  
[kamikuri@geol.tsukuba.ac.jp](mailto:kamikuri@geol.tsukuba.ac.jp)

**Junichiro Kuroda**  
**Sedimentologist**  
Institute for Frontier Research on Earth  
Evolution (IFREE)  
Japan Agency for Marine-Earth Science and  
Technology (JAMSTEC)  
2-15 Natsushima-cho  
Yokosuka 237-0061  
Japan  
[kurodaj@jamstec.go.jp](mailto:kurodaj@jamstec.go.jp)

**Lizette Leon-Rodriguez**  
**Paleontologist (planktonic foraminifers)**  
Department of Earth Science  
Rice University  
6100 Main Street, MS-126  
Houston TX 77005  
USA  
[lizette@rice.edu](mailto:lizette@rice.edu)

**Theodore Moore Jr.**  
**Paleontologist (radiolarians)**  
Department of Geological Sciences  
University of Michigan  
1100 North University  
Ann Arbor MI 48109-1005  
USA  
[ted.moore@umich.edu](mailto:ted.moore@umich.edu)

**Brandon Murphy**  
**Sedimentologist**  
Earth and Planetary Sciences  
University of California, Santa Cruz  
1156 High Street  
Santa Cruz CA 95064  
USA  
[bmurphy@es.ucsc.edu](mailto:bmurphy@es.ucsc.edu)

**Hideto Nakamura**  
**Sedimentologist**  
Department of Natural History Sciences  
Hokkaido University  
Kita-10, Nishi-8, Kita-ku  
Sapporo 060-0810  
Japan  
[hideton@mail.sci.hokudai.ac.jp](mailto:hideton@mail.sci.hokudai.ac.jp)

**Christian Ohneiser**

**Paleomagnetist**

Geology Department

University of Otago

Leith Street Central

Dunedin

New Zealand

[christian.ohneiser@otago.ac.nz](mailto:christian.ohneiser@otago.ac.nz)

**Carl Richter**

**Stratigraphic Correlator**

Department of Geology and Energy Institute

University of Louisiana

PO Box 44530

Lafayette LA 70504-0002

USA

[richter@louisiana.edu](mailto:richter@louisiana.edu)

**Rebecca Robinson**

**Sedimentologist**

Graduate School of Oceanography

University of Rhode Island

South Ferry Road

Narragansett RI 02882

USA

[rebeccar@gso.uri.edu](mailto:rebeccar@gso.uri.edu)

**Ken Sawada**

**Organic Geochemist**

Department of Natural History Sciences

Hokkaido University

Kita-10, Nishi-8, Kita-ku

Sapporo 060-0810

Japan

[sawadak@mail.sci.hokudai.ac.jp](mailto:sawadak@mail.sci.hokudai.ac.jp)

**Howie Scher**

**Physical Properties/Downhole Tools**

**Specialist**

Department of Geological Sciences

University of South Carolina

701 Sumter Street, EWS 617

Columbia SC 29208

USA

[hscher@geol.sc.edu](mailto:hscher@geol.sc.edu)

**Hiroyuki Takata**

**Paleontologist (benthic foraminifers)**

Research Center for Coastal Lagoon

Environments

Shimane University

Nishikawatsu 1060

Matsue 690-8504

Japan

[yuu@soc.shimane-u.ac.jp](mailto:yuu@soc.shimane-u.ac.jp)

**Thomas Westerhold**

**Stratigraphic Correlator**

Center for marine Environmental Sciences

(MARUM)

University of Bremen

PO Box 330440

28334 Bremen

Germany

[tho@uni-bremen.de](mailto:tho@uni-bremen.de)

**Paul A. Wilson**

**Sedimentologist**

School Ocean and Earth Science

National Oceanography Centre, Southampton

European Way

Southampton SO14 3ZH

United Kingdom

[paw1@noc.soton.ac.uk](mailto:paw1@noc.soton.ac.uk)

**Yuhji Yamamoto**

**Paleomagnetist**

Marine and Core Research Center

Kochi University

B200 Monobe

Nankoku-City

Kochi 783-8502

Japan

[y.yamamoto@kochi-u.ac.jp](mailto:y.yamamoto@kochi-u.ac.jp)

## Shipboard personnel and technical representatives

Ron Grout  
Operations Superintendent

Roy Davis  
Laboratory Officer

Tim Bronk  
Assistant Laboratory Officer

Lisa Crowder  
Assistant Laboratory Officer

Gerald Bode  
Curator

William Crawford  
Imaging Specialist

Kelly VonDrehle  
Publications Specialist

Grant Banta  
Marine Computer Specialist

Michael Hodge  
Marine Computer Specialist

Randy Gjesvold  
Marine Instrumentation Specialist

Alwyn Burger  
Marine Instrumentation Specialist

Chris Bennight  
Chemistry Laboratory

Yulia Vasilyeva  
Chemistry Laboratory

Sarah-Jane Jackett  
Core Laboratory

Kazushi Kuroki  
Downhole Tools/Thin Section Laboratory

Trevor Cobine  
Paleomagnetism Laboratory

Thomas Gorgas  
Physical Properties Laboratory

Kristin Hillis  
Underway Geophysics Laboratory

Eric Jackson  
X-ray/Microbiology Laboratory

Dwight Hornbacher  
Applications Developer

Stephanie Zeliadt  
Applications Developer

Don Sims Jr.  
Database

Leslie Peart  
Education/Outreach

Dean Ferrell  
Drilling Engineer

Clayton Furman  
Schlumberger Logging Engineer

## Expedition 321 participants

### Expedition 321 scientists

**Mitchell W. Lyle**  
**Co-Chief Scientist**  
Department of Oceanography  
Texas A&M University  
TAMU 3146  
College Station TX 77840-3146  
USA  
[mlyle@ocean.tamu.edu](mailto:mlyle@ocean.tamu.edu)

**Isabella Raffi**  
**Co-Chief Scientist**  
Dipartimento di Geotecnologie per l'Ambiente e il Territorio  
DiGAT—CeRS Geo  
Università "G. D'Annunzio"  
Campus Universitario  
via dei Vestini 31  
66013 Chieti Scalo  
Italy  
[raffi@unich.it](mailto:raffi@unich.it)

**Kusali Gamage**  
**Expedition Project Manager/Staff Scientist**  
Integrated Ocean Drilling Program  
Texas A&M University  
1000 Discovery Drive  
College Station TX 77845-9547  
USA  
[gamage@iodp.tamu.edu](mailto:gamage@iodp.tamu.edu)

**Alberto Malinverno**  
**Logging Staff Scientist**  
Borehole Research Group  
Lamont-Doherty Earth Observatory  
of Columbia University  
PO Box 1000, 61 Route 9W  
Palisades NY 10964  
USA  
[alberto@ldeo.columbia.edu](mailto:alberto@ldeo.columbia.edu)

**Louise Anderson**  
**Logging Staff Scientist**  
Department of Geology  
University of Leicester  
Leicester LE1 7RH  
United Kingdom  
[lma9@le.ac.uk](mailto:lma9@le.ac.uk)

**Jan Backman**  
**Paleontologist (nannofossils)**  
Department of Geology and Geochemistry  
Stockholm University  
SE-10691 Stockholm  
Sweden  
[backman@geo.su.se](mailto:backman@geo.su.se)

**Catherine Beltran**  
**Sedimentologist**  
Laboratoire Biominéralisations et  
Paléoenvironnements (UPMC)  
Université Pierre et Marie Curie  
Case 116—4 Place Jussieu  
75252 Paris  
France  
[catherine.beltran@upmc.fr](mailto:catherine.beltran@upmc.fr)

**William Busch**  
**Physical Properties/Downhole Tools  
Specialist**  
Earth and Environmental Sciences  
University of New Orleans  
2000 Lakeshore Drive  
New Orleans LA 70148  
USA  
[wbusch@uno.edu](mailto:wbusch@uno.edu)

**James Channell**  
**Paleomagnetist**  
Department of Geological Sciences  
University of Florida  
241 Williamson Hall  
Gainesville FL 32611-2120  
USA  
[jetc@geology.ufl.edu](mailto:jetc@geology.ufl.edu)

**Pawan Dewangan**  
**Physical Properties/Downhole Tools  
Specialist**  
National Institute of Oceanography  
Dona Paula  
Goa 403 004  
India  
[pdewangan@nio.org](mailto:pdewangan@nio.org)

**Hitoshi Hasegawa**  
**Sedimentologist**  
Earth and Planetary Science  
University of Tokyo  
7-3-1 Hongo  
Bunkyo-ku  
Tokyo 113-0033  
Japan  
[hase@eps.s.u-tokyo.ac.jp](mailto:hase@eps.s.u-tokyo.ac.jp)

**Ed Hathorne**  
**Inorganic Geochemist**  
MARUM-Centre for Marine Environmental  
Sciences  
University of Bremen  
Leobener Strasse  
D-28359 Bremen  
Germany  
[ehathorne@marum.de](mailto:ehathorne@marum.de)

**Hiroki Hayashi**  
**Paleontologist (planktonic foraminifers)**  
Interdisciplinary Faculty of Science and  
Engineering  
Shimane University  
1060 Nishikawatsucho  
Matsue City  
Shimane 690-8504  
Japan  
[hayashi@riko.shimane-u.ac.jp](mailto:hayashi@riko.shimane-u.ac.jp)

**Ann Holbourn**  
**Paleontologist (benthic foraminifers)**  
Institut für Geowissenschaften  
Christian-Albrechts-Universität zu Kiel  
Olhausenstrasse 40  
24098 Kiel  
Germany  
[ah@gpi.uni-kiel.de](mailto:ah@gpi.uni-kiel.de)

**Steven Hovan**  
**Sedimentologist**  
Department of Geoscience  
Indiana University of Pennsylvania  
114 Walsh Hall  
Indiana PA 15705  
USA  
[hovan@iup.edu](mailto:hovan@iup.edu)

**Koichi Iijima**  
**Physical Properties/Downhole Tools  
Specialist**  
Institute of Biogeosciences  
Japan Agency for Marine-Earth Science and  
Technology  
2-15 Natsushima-cho  
Yokosuka 237-0061  
Japan  
[kijima@jamstec.go.jp](mailto:kijima@jamstec.go.jp)

**Takashi Ito**  
**Sedimentologist**  
Faculty of Education  
Ibaraki University  
2-1-1 Bunkyo  
Mito  
Ibaraki 310-8512  
Japan  
[tito@mx.ibaraki.ac.jp](mailto:tito@mx.ibaraki.ac.jp)

**Katsunori Kimoto**  
**Inorganic Geochemist**  
Institute of Observational Research for Global  
Change (IORGC)  
Japan Agency for Marine-Earth Science and  
Technology  
2-15 Natsushima-Cho  
Yokosuka 237-0061  
Japan  
[kimopy@jamstec.go.jp](mailto:kimopy@jamstec.go.jp)

**Daniel Murphy**  
**Sedimentologist**  
Department of Oceanography  
Texas A&M University  
MS 3146  
College Station TX 77845  
USA  
[dmurphy@ocean.tamu.edu](mailto:dmurphy@ocean.tamu.edu)

**Kaoru Ogane**  
**Paleontologist (radiolarians)**  
Institute of Geology and Paleontology  
Tohoku University  
Aoba 6-4  
Aramaki, Aoba-ku  
Sendai City 980-8578  
Japan  
[ogane@mtc.biglobe.ne.jp](mailto:ogane@mtc.biglobe.ne.jp)

**Oscar Romero**  
**Paleontologist (diatoms)**  
Instituto Andaluz de Ciencias de la Tierra  
Universidad de Granada  
Campus Fuentenueva  
18002 Granada  
Spain  
[oromero@ugr.es](mailto:oromero@ugr.es)

**Leah Schneider**  
**Paleontologist (Nannofossils)**  
Department of Geosciences  
Pennsylvania State University  
509 Deike Building  
University Park PA 16802  
USA  
[lschneid@geosc.psu.edu](mailto:lschneid@geosc.psu.edu)

**Appy Sluijs**  
**Sedimentologist**  
Palaeoecology, Institute of Environmental  
Biology  
Utrecht University  
Laboratory of Palaeobotany and Palynology  
Budapestlaan 4  
3584CD Utrecht  
The Netherlands  
[a.sluijs@uu.nl](mailto:a.sluijs@uu.nl)

**Jun Tian**  
**Stratigraphic Correlator**  
Laboratory of Marine Geology  
Tongji University  
Siping Road 1239  
Shanghai 200092  
PR China  
[tianjun@mail.tongji.edu.cn](mailto:tianjun@mail.tongji.edu.cn)

**Akira Tsujimoto**  
**Sedimentologist**  
Department of Geosciences  
Osaka City University  
3-3-138 Sugimoto  
Sumiyoshi-ku  
Osaka 558-8585  
Japan  
[tujimoto@sci.osaka-cu.ac.jp](mailto:tujimoto@sci.osaka-cu.ac.jp)

**Bridget Wade**  
**Paleontologist (planktonic foraminifers)**  
Department of Geology and Geophysics  
Texas A&M University  
College Station TX 77843  
USA  
[wade@geo.tamu.edu](mailto:wade@geo.tamu.edu)

**Roy Wilkens**  
**Stratigraphic Correlator**  
Hawaii Institute of Geophysics and  
Planetology  
University of Hawaii at Manoa  
1680 East West Road  
Honolulu HI 96822  
USA  
[rwilkens@hawaii.edu](mailto:rwilkens@hawaii.edu)

**Shinya Yamamoto**  
**Organic Geochemist**  
Institute of Low Temperature Science  
Hokkaido University  
N19W8, Kita-Ku  
Sapporo 060-0819  
Japan  
[s.yamamoto@pop.lowtem.hokudai.ac.jp](mailto:s.yamamoto@pop.lowtem.hokudai.ac.jp)

**Toshitsugu Yamazaki**  
**Paleomagnetist**  
Geological Survey of Japan, AIST  
1-1-1 Higashi, Tsukuba  
Ibaraki 305-8567  
Japan  
[toshi-yamazaki@aist.go.jp](mailto:toshi-yamazaki@aist.go.jp)

## Shipboard personnel and technical representatives

Heather Barnes  
Assistant Laboratory Officer

John Beck  
Imaging Specialist

Lisa Brandt  
Chemistry Laboratory

Chad Broyles  
Curator

Etienne Claassen  
Marine Instrumentation Specialist

David Fackler  
Applications Developer

Kazuho Fujine  
Chemistry Laboratory

Gus Gustafson  
Downhole Tools/Thin Section Laboratory

Margaret Hastedt  
Paleomagnetism Laboratory

Maarten in 't Hout  
Videographer

Jurie Kotze  
Marine Instrumentation Specialist

Zenon Mateo  
Core Laboratory

Mike Meiring  
Engineer

Erik Moortgat  
Underway Geophysics Laboratory

Matt Nobles  
Marine Computer Specialist

Bob Olivas  
X-ray/Microbiology Laboratory

Debbie Partain  
Publications Specialist

Chieh Peng  
Laboratory Officer

Steve Prinz  
Assistant Laboratory Officer

Michael Storms  
Operations Superintendent

Kerry Swain  
Logging Engineer

Andrew Trefethen  
Marine Computer Specialist

Maxim Vasilyev  
Petrophysics Laboratory

Hai (James) Zhao  
Applications Developer

## Abstract

Integrated Ocean Drilling Program Expedition 320/321, “Pacific Equatorial Age Transect” (Sites U1331–U1338), was designed to recover a continuous Cenozoic record of the equatorial Pacific by coring above the paleoposition of the equator at successive crustal ages on the Pacific plate. These sediments record the evolution of the equatorial climate system throughout the Cenozoic. As we have gained more information about the past movement of plates and when in Earth’s history “critical” climate events took place, it became possible to drill an age-transect (“flow-line”) along the position of the paleoequator in the Pacific, targeting important time intervals to reconstruct how the equatorial Pacific was involved in the climate change. The Pacific Equatorial Age Transect (PEAT) program cored eight sites from the sediment surface to basement, with basalt aged between 53 and 18 Ma, covering the time period following maximum Cenozoic warmth, through initial major glaciations, to today. The PEAT program allows the reconstruction of extreme changes of the calcium carbonate compensation depth (CCD) across major geological boundaries during the last 53 m.y. A very shallow CCD during most of the Paleogene makes it difficult to obtain well-preserved carbonate sediments during these stratigraphic intervals, but we recovered a unique sedimentary biogenic sediment archive for time periods just after the Paleocene/Eocene boundary event, the Eocene cooling, the Eocene–Oligocene transition, the “one cold pole” Oligocene, the Oligocene–Miocene transition, and the middle Miocene cooling. Together with older Deep Sea Drilling Project and Ocean Drilling Program drilling in the equatorial Pacific, we can also delineate the position of the paleoequator and variations in sediment thickness from ~150°W to 110°W longitude. Expedition 321, the second part of the PEAT program, focused on the time period roughly from 25 Ma forward. During Expedition 321 two major Neogene equatorial Pacific sediment sections were recovered at Sites U1337 and U1338.

## Scientific objectives, introduction, and background

### Scientific objectives

The Pacific Equatorial Age Transect (PEAT) program (Fig. F1) was designed to achieve an age transect of eastern Pacific sediments deposited within the equatorial region ( $\pm 2^\circ$  of the equator) on the Pacific plate. The age of sediments within the equatorial transect span from the early Eocene through the Pliocene, with Paleocene/Eocene and late Miocene to recent intervals being covered by previous Ocean Drilling Pro-

gram (ODP) Legs 138 and 199 (Pisias, Mayer, Janecek, Palmer-Julson, and van Andel, 1995; Lyle, Wilson, Janecek, et al., 2002). Drill sites target specific time intervals of interest (Fig. F2) at locations that provide optimum preservation of calcareous sediments (Figs. F3, F4, F5, F6, F7). The overall aim was to obtain a continuous well-preserved equatorial Pacific sediment section that addresses the following primary scientific objectives:

1. To detail the nature and changes of the calcium carbonate compensation depth (CCD) over the Cenozoic in the paleoequatorial Pacific;
2. To determine the evolution of paleoproductivity of the equatorial Pacific over the Cenozoic;
3. To validate and extend the astronomical calibration of the geological timescale for the Cenozoic, using orbitally forced variations in sediment composition known to occur in the equatorial Pacific, and to provide a fully integrated and astronomically calibrated bio-, chemo-, and magnetostratigraphy at the Equator;
4. To determine temperatures (sea surface and bottom water), nutrient profiles, and upper water column gradients;
5. To better constrain Pacific plate tectonic motion and better locate the Cenozoic equatorial region in plate reconstructions, primarily using paleomagnetic methods; and
6. To make use of the high level of correlation between tropical sedimentary sections and existing seismic stratigraphy to develop a more complete model of equatorial circulation and sedimentation.

Additional objectives include:

7. To provide information about rapid biological evolution and turnover rates during times of climatic stress;
8. To improve our knowledge of the reorganization of water masses as a function of depth and time, as our strategy also implies a paleodepth transect (Fig. F3);
9. To develop a limited north–south transect across the paleoequator, caused by the northward offset of the proposed sites by Pacific plate motion, providing additional information about north–south hydrographic and biogeochemical gradients; and
10. To obtain a transect of mid-ocean-ridge basalt (MORB) samples from a fixed location in the absolute mantle reference frame and to use a transect of basalt samples along the flow line that have been erupted in similar formation-water

environments to study low-temperature alteration processes by seawater circulation.

## Introduction

As the world's largest ocean, the Pacific Ocean is intricately linked to major changes in the global climate system that took place during the Cenozoic. Throughout the Cenozoic the Pacific plate motion has had a northward component. The Pacific is unique in that the thick sediment bulge of biogenic-rich deposits from the currently narrow equatorial upwelling zone is slowly moving away from the Equator. Hence, older sections are not deeply buried and can be recovered by drilling without extensive diagenesis. Previous Legs 138 and 199 were remarkably successful in giving us new insights into the workings of the climate and carbon system, productivity changes across the zone of divergence, time-dependent calcium carbonate dissolution, an integrated astronomically age-calibrated bio- and magnetostratigraphy, the location of the intertropical convergence zone (ITCZ), and evolutionary patterns for times of climatic change and upheaval. Together with older Deep Sea Drilling Project (DSDP) drilling in the eastern equatorial Pacific (Legs 8, 9, 16, and 85), ODP drilling also helped to delineate the paleoequatorial position on the Pacific plate and variations in sediment thickness from ~150° to 110°W longitude.

Legs 138 and 199 were designed as latitudinal transects across the paleoequator in order to study the changing patterns of sediment deposition across equatorial regions at critical time intervals. As we have gained more information about the past movement of plates and when in Earth's history "critical" climate events took place it became possible to drill an age transect ("flow line") along the track of the equatorial region on the Pacific plate, targeting important time slices where calcareous sediments have been preserved best and the sedimentary archive in general allows us the reconstruction of past climatic and tectonic conditions. Consequentially, the PEAT program will sharpen our understanding of extreme changes of the CCD across major geological boundaries during the last 53 m.y.

During most of the Paleogene the CCD was between 500 and 1300 m shallower than today. Thus, a very shallow CCD makes it difficult to obtain well-preserved sediments during these stratigraphic intervals because initial thermal subsidence of the ridge crest is rapid (Fig. F3). Nevertheless, the careful coring and site location strategy of the current PEAT Expedition 320/321 allowed us to drill the most promising sites and to obtain a unique sedimentary biogenic sediment archive for time periods just after the

Paleocene/Eocene boundary event, the Eocene cooling, the Eocene–Oligocene transition, the “one cold pole” Oligocene, the Oligocene–Miocene transition, and the Miocene. These new cores and data will significantly contribute to the objectives of the Integrated Ocean Drilling Program (IODP) Extreme Climates Initiative and are a new archive for detailed paleoceanographic study of the equatorial Pacific.

## Background

The circulation of the equatorial surface ocean is inescapably linked to the trade wind system. The equatorial Pacific is the classic “world ocean” example of this linkage. It is dominated by wind-driven circulation and is largely unfettered by ocean boundaries. Here, the Equator itself is characterized by a narrow zone of divergence that results from the change in the sign of the Coriolis effect and that gives rise to a band of high biologic productivity (Fig. F6). The strength of the equatorial circulation and of this divergence is linked to the strength of the trade winds, which are in turn strongly tied to the global climate system. Variations in global climate, interhemispheric differences in temperature gradients, and marked changes in the ocean boundaries are all imprinted on the biogenic-rich sediments that are accumulating in the equatorial zone. The PEAT program was designed to provide an understanding of equatorial Pacific circulation, carbonate production, deposition, and dissolution for the last ~53 m.y. at a scale where orbital forcing can be resolved. Combined with seismic reflection data (Lyle et al., 2006, 2002) following in the vein of Mitchell et al. (2003) and synthesized with earlier drilling (e.g., Moore et al., 2002, 2004, 2008b; Lyle et al., 2005) we can reconstruct equatorial Pacific history with high confidence and substantially improve upon work from the early stages of DSDP and recent ODP Legs.

Deciphering the sedimentary history of the equatorial Pacific has been greatly simplified by favorable motion of the Pacific plate. Throughout the Cenozoic, the movement of the Pacific plate has had a northward latitudinal component of ~0.25°/m.y. This northward movement transports the equatorial sediments gradually out from under the zone of highest sediment delivery, resulting in a broad mound of biogenic sediments (Fig. F8). This transport prevents older equatorial sections from being buried deeply beneath younger sections as the crust moves northward. The diminished overburden resulting from this transport also allows relatively good preservation of biogenic sediments and minimizes burial diagenesis. In addition, it allows us to core nearly all sediment sections using the advanced piston corer (APC). The northward tectonic displacement, however, is not so large that a traverse of the equatorial zone (within 2° latitude of the Equator) was too rapid to record a reasonable period of equa-

torial ocean history. Typically drill sites remain within the equatorial zone for 10–20 m.y. before passing beyond the northern edge of high-biogenic sedimentation. Older equatorial sections are thus buried beneath a thin veneer of younger sediments as the crust moves northwestward.

In his summary of DSDP results in the equatorial Pacific, van Andel (1975) gave a general view of the development of the equatorial mound of sediments in the Pacific Ocean, based mostly upon three early DSDP legs (5, 8, and 16). They showed how both temporal and spatial variation in sediment accumulation rates resulted from plate movement, varying biologic productivity at the equatorial divergence, and carbonate preservation. The buildup of the Pacific equatorial mound of sediment has been more recently documented and discussed by Mitchell (1998) and Mitchell et al. (2003) (Fig. F8).

Drilling across the Pacific equatorial mound was addressed again some 20 y after the van Andel (1975) compilation when an equatorial latitudinal transect along 10 Ma crust was drilled during ODP Leg 138 (Pisias, Mayer, Janecek, Palmer-Julson, and van Andel, 1995), and then again 10 y later when a similar transect along 56 Ma aged crust was conducted during Leg 199 (Lyle, Wilson, Janecek, et al., 2002). The newer drilling, coupled with major advances in geochronology, has documented the remarkable correlation of paleoceanographic events over thousands of kilometers in the equatorial Pacific, caused by the large scale of Pacific equatorial circulation (Fig. F9). It was thus possible during the PEAT program, with the addition of a relatively small number of new sites, to build detailed reconstructions of equatorial Pacific circulation throughout the Cenozoic.

Earlier drilling missed most of this detail because of the lack of important drilling technologies such as extended core barrel (XCB) and APC coring, which allow the collection of relatively undisturbed sediments, multisensor track correlation, core-log integration, the rebuilding of a continuous sediment column from individual cores, and the correlation to seismic reflection data. Together with an improved knowledge of the plate tectonic regime, these advances allow us to locate the areas of enhanced depositional rates associated with paleoequatorial positions. Combining multiple sites along the equator, as in the PEAT drilling plan, will result in a detailed sediment record from the Pleistocene to the Paleocene. These records will also be invaluable for the continued development of the Cenozoic timescale as well as for the paleoceanographic information they contain.

Excellent sections were recovered during Legs 138 and 199, on which the detailed orbital tuning of the geologic timescale has been carried out. These sections give a much clearer picture of variations in sedimentation rates, isotopic evolution of the oceans, biologic evolution and zoological provenance, variations in carbonate preservation, and variations in geochemical fluxes that result from paleoceanographic and paleoclimate changes. Parts of the Cenozoic timescale still require further refinement and verification of the proposed orbital tuning. The timescale older than the late Eocene has not been calibrated sufficiently, even though there is evidence of orbital frequencies in parts of the records recovered from this older interval (e.g., Norris and Röhl, 1999; Röhl et al., 2001).

To develop a detailed history of the Pacific equatorial current system, the strategy pursued in the most recent ODP legs (199 and 138) was to drill along a line of equal oceanic crustal age, thus obtaining an approximate north–south transect across the major east–west currents during time intervals of particular interest.

During the Paleocene and Eocene, the shallow CCD prevents deposition of carbonate except at shallow ocean crust. Drilling near the paleoposition of the ridge crest at the critical time interval allows the recovery of the shallowest sections available in the pelagic oceans and thereby assures the best possible preservation of the carbonate sediments recovered. As the crust cools and sinks, the seafloor on which the sediments are deposited approaches the lysocline and CCD. Thus, the best preserved part of the sections recovered in such “time line” transects is restricted by the depth at which carbonate dissolution significantly increases, as well as by the northward movement of sediment sections out of the region of high equatorial productivity. This limitation was exemplified by the results from Leg 199, during which only limited amounts of carbonate prior to the Eocene/Oligocene boundary were recovered (e.g., at ODP Site 1218 on 42 Ma crust).

For the PEAT program, we planned to overcome this limitation of the time line strategy by pursuing an equatorial age transect, or flow line strategy (Figs. [F1](#), [F3](#)), to collect well-preserved equatorial sections through the Cenozoic while also making use of the Pacific plate motion to add an oblique latitudinal transect across all time slices.

We drilled a series of sites on the paleoequator at key intervals in the evolution of the Cenozoic climate. These intervals span the extremely warm times of the early Eocene, the cooling of the late Eocene through Oligocene, the early Miocene time of relatively warm climates (or low ice volume), and sections deposited during the development

of the major Southern and Northern hemisphere ice sheets (Fig. F2). There are very few previous drill sites that match our site selection criteria. Each site is selected to be close to the geographic paleoequator and on crust aged slightly older than the age intervals of particular interest.

In this way we were able to track the paleoceanographic conditions at the paleoequator in the best preserved sediments obtainable. We can also make use of the high level of correlation between tropical sediment sections and seismic stratigraphy to develop a more complete model of equatorial productivity and sedimentation.

### ***Understanding the interplay between the CCD, CaCO<sub>3</sub> dissolution, and productivity***

The Pacific Ocean, specifically the equatorial upwelling zone, is the largest oceanic source of CO<sub>2</sub> to the atmosphere and controls atmospheric CO<sub>2</sub> levels (Dore et al., 2003). The release and uptake of CO<sub>2</sub> is the direct consequence of calcium carbonate deposition and the interplay between nutrient supply, carbonate dissolution, surface water productivity, and export of biogenic carbonate from the surface waters to the sediment pile. Distinguishing between the effects of carbonate dissolution and productivity has been a field of intense study in the past. An important objective of the PEAT program is to address the detailed workings of depth-dependent carbonate dissolution, which is intricately linked to the climate system and paleoceanography. In the standard model for carbonate dissolution, accumulation rates locally decrease linearly from a lysocline down to a CCD, reflecting a linearly increasing rate of dissolution. The depth of both of these mappable surfaces varies spatially and in time as a result of climatic and physical processes. The equatorial Pacific is one of the classic areas where the lysocline-CCD model was first developed, but little subsequent effort has been made to test it—a necessary step, considering that the functional form of dissolution is now known to depend in a more complex way on organic carbon burial and water mass properties. The age transect will provide the necessary additional data with which to test the carbonate paradigm and recover previously unavailable carbonate material from important Paleogene time slices in the Pacific.

Specifically, the recovery of shallowly buried carbonate sediments from near the paleoequatorial upwelling zone would contribute significantly toward separating the various processes that affect carbonate deposition and preservation and reduce some of the processes that affect climatic proxy records, such as diagenetic recrystallization (Pearson et al., 2001a). Neogene productivity has been strongly oriented parallel to the equator, so differences in carbonate thicknesses at a common latitude but differing depth permit the effect of dissolution to be isolated (Lyle, 2003; Mitchell et al.,

2003; Mitchell and Lyle, 2005). In addition, the strategy adopted in this program provided new data throughout the Cenozoic with which it will be possible to map the spatial evolution of the equatorial CCD with time (see “**Results and highlights**”). This is because the northward component of the Pacific plate movement results in the multiple recovery of the same time slice at different sites but with a slightly different paleolatitude (Fig. **F3**).

Recovering more detailed records from the best possible material will also allow a better understanding of physical processes that might affect or hinder our interpretation of carbonate proxy records, such as the “carbonate ion effect”—an observed and modeled influence of the carbonate ion concentration on stable isotope fractionation in carbonate (Spero et al., 1997; Zeebe and Wolf-Gladrow, 2001; Lear et al., 2008).

Preliminary work with seismic data (Mitchell et al., 2003) has revealed a surprising lack of correlation between dissolution and depth in the westerly region of this study area. Our aim is to develop a more extensive three-dimensional model for the stratigraphy of the equatorial Pacific deposits that links all existing core data using a grid of high-resolution seismic reflection profiles, including more recent data from the PEAT site survey AMAT03 (Lyle et al., 2006). A numerical stratigraphic model will then be used to assess carbonate dissolution and, in particular, the spatial pattern of sharp changes in dissolution, such as the extremely abrupt change in the CCD at the Oligocene/Eocene boundary, which has been linked to a possible abrupt onset of continental weathering. The sediment archive recovered during the PEAT program will allow the application of the substantial array of carbonate-based proxies with which the wider regional seismic study can be constrained and calibrated.

### ***Reconstructing paleoceanographic properties and sea-surface temperature***

A large number of paleoceanographic interpretations rely on obtaining proxy data such as stable isotope measurements, element ratios such as Mg/Ca, sea-surface temperature (SST) estimates from faunal distributions and isotope data, alkenone proxies, TEX86, geochemical productivity, and so on. In turn, a very large number of these measurements rely on the presence of biogenic calcium carbonate. For the Pacific Ocean, the PEAT drilling strategy was designed to recover this important material with the best possible preservation and the least amount of diagenetic effects for long intervals throughout the Cenozoic.

### ***Spatial range considerations***

The age transect siting strategy necessarily implies a restricted north–south transect, even though the northward movement of the Pacific plate does allow us to recover identical time slices multiple times at different paleolatitudes (separated by several degrees) (Fig. F5). However, we note that the regional seismic study to be developed as part of our site survey work gives us the opportunity to integrate data from older drill sites with the new drilling. The site survey linked the new sites to key drill sites from DSDP Legs 9 and 85 and ODP Legs 138 and 199. Combining data from these expeditions and surveys will allow us to construct a site-to-site correlation and, finally, a Pacific “megasplice” of high-resolution data spliced together to cover most of the Cenozoic.

### ***Paleomagnetic objectives***

One important aspect of the PEAT program is the recovery of high-quality paleomagnetic data so that attempts to improve existing geologic timescales (Gradstein et al., 2004) can be extended further back in time. Results from Leg 199 demonstrate that these records can be recovered from near-equatorial carbonate sediments (e.g., Lanci et al., 2004, 2005). Almost all magnetic reversals from the Paleogene to the present were recovered during Leg 199. However, neither biogenic carbonate sediments through most of the Eocene nor for ages younger than the lower Miocene were recovered during Leg 199. Thus, although the paleomagnetic record during these times was of high quality, global stratigraphic correlation is hindered by the lower mass accumulation rate, the absence of a detailed isotope stratigraphy, and sparser biostratigraphic control. In order to facilitate the development of an integrated magneto- and biostratigraphic framework with a stable isotope stratigraphy (necessary to enable global correlation), recovery of magnetic reversals within carbonate sediment is desirable. In addition, further detailed paleomagnetic, magnetostratigraphic, and magnetic rock fabric data, most importantly from the Eocene, will help to resolve the suggestion that the geographic equator, as determined from the biogenic sediment bulge, might not coincide with the paleoequator position backtracked with a fixed-hotspot reference frame (Moore et al., 2004; Tarduno, 2003; Parés and Moore, 2005).

### ***Ancillary benefits (MORB, basement)***

Our drilling aimed to recover basement samples at all sites. A transect of MORB samples from a fixed location in the absolute mantle reference frame is a unique sample suite for mantle geochemists. A transect of basalt samples along the flow line that

have erupted in similar environments will be of interest for low-temperature alteration studies (see, e.g., Elderfield and Schultz, 1996).

## Site selection strategy and site targets

Time slices drilled during the PEAT program were chosen to cover the overall climatic history of the Cenozoic and to target particular times of marked changes in the climatic regime. The spacing of the sites was determined by what we knew of the Cenozoic evolution of the lysocline from previous drilling. Where the CCD is particularly shallow, the spacing in time of age transect sites must be closer than when the CCD is deep (Fig. F3). As a guide, Site 1218 was drilled on 42 Ma crust during times when the CCD was near 3.3 km. Nannofossil oozes were deposited at this location to ~37 Ma before the crust at this site sank below the CCD. An age separation between drill sites of 2–5 m.y. is a maximum for the shallow CCD of the Eocene; for good preservation of foraminifers an even closer spacing should be used. The results of our paleoequator reconstruction and drill site locations are shown in Figure F1.

### *Site location strategy*

In pursuing the history of the equatorial Pacific Ocean through both time line and flow line transects, we have two major advantages over the efforts that took place in the earlier days of scientific ocean drilling. Although previous drill sites have targeted the general area, they mostly do not fulfill all of our criteria in terms of (1) a sufficient number of holes to obtain a continuous record, (2) modern coring technology to obtain undisturbed sediments, (3) location inside the paleoequatorial zone, or (4) location on the right crustal age to ensure the presence of calcium carbonate at the targeted time slice. We positioned Sites U1331 through U1338 somewhat south of the estimated paleoequatorial position at their target ages (Fig. F6) to maximize the time that drill sites remain within the equatorial zone (i.e.,  $\pm 2^\circ$  of the equator), to allow for some error in positions (evidence suggests a southward bias of the equatorial sediment mound relative to the hotspot frame of reference [Knappenberger, 2000]), and to place the interval of maximum interest above the basal hydrothermal sediments.

To determine the site and site survey location, we used the digital age grid of seafloor ages from Müller et al. (1997), heavily modified and improved with additional magnetic anomaly picks from Petronotis (1991) and Petronotis et al. (1994), as well as DSDP/ODP basement ages. For this grid, each point is backrotated in time to zero age using the fixed-hotspot stage-poles from Koppers et al. (2001) and Engebretson et al. (1985) and the paleopole data from Sager and Pringle (1988). From the backtracked

latitudes for each grid point, we obtained the paleoequator at the crustal age by contouring all backrotated latitudinal positions.

### ***Eocene (Sites U1331–U1334)***

The Eocene was a time of extremely warm climates that reached a global temperature maximum near 52 Ma, a period around the Early Eocene Climatic Optimum (EECO) (Fig. F2) (Zachos et al., 2001a; Shipboard Scientific Party, 2004). From this maximum there was a gradual climatic cooling through the Eocene to the Eocene/Oligocene boundary. There appears to have been a slight reversal to this trend within the middle Eocene near 43 Ma and in the late Eocene at 34–36 Ma, just prior to the pronounced drop in oxygen isotopes that marks the Eocene/Oligocene boundary and one of the most dramatic changes of the CCD (Fig. F3).

Throughout the Eocene, the CCD lay near a depth of 3.2–3.3 km, albeit with potentially significant short-term fluctuations (Lyle et al., 2005). Thus, recovering well-preserved carbonate sediments from the equatorial region is a substantial challenge but not impossible if the depth of the East Pacific Rise lay near the global average of 2.7 km. We presently lack calcareous sediments from the region of the equatorial circulation system during this time of maximum Cenozoic warmth (Zachos et al., 2001a), elevated atmospheric pCO<sub>2</sub> concentrations (Lowenstein and Demicco, 2007), and a shallow early Eocene CCD estimated between 3200 and 3300 m water depth (Lyle, Wilson, Janecek, et al., 2002; Lyle et al., 2005; Rea and Lyle, 2005). The Eocene equatorial upwelling system appears to differ from the modern equatorial upwelling regime by having strong secondary upwelling lobes ~10° in latitude away from the primary equatorial region (Figs. F10, F11). They produce a much broader region of (relatively) high productivity than is present today.

### ***Early and middle Eocene (Sites U1331 and U1332; ~53 Ma and 50 Ma crust)***

During Leg 199, a north–south transect across the equatorial region was drilled on ~56 Ma oceanic crust. Sites on this transect had generally drifted below the CCD by 52–53 Ma. Thus, we have yet to recover calcareous sediments from the equatorial Pacific during the time of maximum Cenozoic warmth. Site U1331 is on crust with an estimated age of ~53 Ma in order to intercept the interval between 53 and 50 Ma in basal carbonate sediments above the shallow early Eocene CCD (4200–4300 m), whereas Site U1332 is located on 50 Ma crust to collect a carbonate interval from ~50–48 Ma.

Average (noncarbonate) accumulation rates in the early Eocene were moderate, showing only slight increases in some of the more northern sites on the Leg 199 transect (Sites 1215 and 1220). What is particularly interesting in the records of Leg 199 is that the very shallow CCD of this early Eocene time appears to deepen to the north, perhaps suggesting a northern source for the bottom waters. Sites targeting this time interval would ideally give us sediments with sufficient carbonate material to better constrain the isotopic and biotic characteristics of the near surface equatorial waters.

During the early Eocene, a very shallow CCD and typical rapid tectonic plate subsidence of young crust near the shallow ridge crest conspire to make the time window above the CCD short (~2–5 Ma). Thus, although good records of pelagic carbonates during and just after the Paleocene/Eocene Thermal Maximum (PETM) were recovered during Leg 199 (Lyle, Wilson, Janecek, et al., 2002; Nuñez and Norris, 2006; Raffi et al., 2005), the time period of the EECO (Zachos et al., 2001b) is not well sampled.

Sites U1331 (53 Ma crust) and U1332 (50 Ma crust) aim to provide the sedimentary archive to address several important questions that relate to causes and responses of the true Cenozoic “Greenhouse” world: the Eocene was a time of extremely warm climates that reached a maximum in temperatures near 52 Ma (Zachos et al., 2001a). From this maximum there was a gradual climatic cooling to the Eocene/Oligocene boundary. Good paleomagnetic stratigraphy from Leg 199 sites allowed a much improved calibration of nannofossil and radiolarian biostratigraphic datums throughout the Eocene. A north–south transect across the equatorial region at ~56 Ma was drilled during Leg 199. Although good records of pelagic carbonates during and just after the PETM were recovered at Leg 199 sites (Lyle, Wilson, Janecek, et al., 2002; Raffi et al., 2005; Nuñez and Norris, 2006), the time period of the EECO (Zachos et al., 2001) and the shallowest CCD is not well sampled.

### ***Middle and late Eocene (Site U1333; 46 Ma crust)***

Good paleomagnetic stratigraphy from Leg 199 sites allowed a much improved calibration of nannofossil and radiolarian biostratigraphic datum ages (Pälike et al., 2005; 2006b; Raffi et al., 2005, 2006; Moore et al., 2004). From the combined information a more detailed picture emerged of temporal variations in sediment accumulation through the middle and upper Eocene of the tropical Pacific. These data showed an increase of a factor of up to 2–3 in accumulation rates of siliceous ooze in the middle Eocene (41–45 Ma).

There are also several notable periods of highly fluctuating CCD associated with intervals in which carbonate is preserved as deep as 4000 m water depth, or ~700 m deeper than the average Eocene CCD (Lyle, Wilson, Janecek, et al., 2002; Lyle et al., 2005; Rea and Lyle, 2005; Bohaty et al., 2009). These fluctuations occur immediately prior to the Middle Eocene Climatic Optimum, which is associated with CCD shoaling (Bohaty and Zachos, 2003; Bohaty et al., 2009). Such fluctuations in the CCD are similar in magnitude to those at the Eocene/Oligocene boundary (Coxall et al., 2005). High siliceous sedimentation rates occur near an apparent short reversal in the middle Eocene cooling interval. It is difficult to interpret the cause of such a substantial change in silica flux during a very warm climatic regime.

The primary objective of coring at Site U1333 is to recover a complete sequence of carbonate sediments spanning the middle Eocene to Oligocene so we can evaluate changes in the temperature and structure of the near-surface ocean, bottom water temperatures, and the evolution of the CCD.

One of the additional objectives of the PEAT program is to provide a depth transect for several Cenozoic key horizons, such as the Eocene–Oligocene transition (Coxall et al., 2005) targeted at Sites U1331–U1334. Site U1333 forms the third deepest paleodepth constraint, with an estimated crustal paleodepth of <4 km and a paleolatitude of ~3° north of the paleoequator during the Eocene–Oligocene transition.

#### ***Eocene/Oligocene boundary (Site U1334; 38 Ma crust)***

Site U1334 sediments are estimated to have been deposited on top of late middle Eocene ~38 Ma crust, and this site targets the events bracketing the Eocene–Oligocene transition with the specific aim to recover carbonate-bearing sediments of latest Eocene age prior to a large deepening of the CCD that occurred during this greenhouse to icehouse transition (Kennett and Shackleton, 1976; Miller et al., 1991; Zachos et al., 1996; Coxall et al., 2005). The Eocene–Oligocene transition experienced the most dramatic deepening of the Pacific CCD during the Paleogene (van Andel, 1975), which has now been shown by Coxall et al. (2005) to coincide with a rapid step-wise increase in benthic oxygen stable isotope ratios interpreted to reflect a combination of growth of the Antarctic ice sheet and decrease in deep water temperatures (DeConto et al., 2008; Liu et al., 2009).

So far the most complete Eocene/Oligocene boundary section recovered from the equatorial Pacific has been Site 1218 on 42 Ma crust; however, it is far from pristine. Carbonate percentages drop markedly below the boundary and reach zero near 34 Ma

during a time of apparent global shoaling of the CCD just prior to the Eocene–Oligocene transition and CCD deepening (Bohaty et al., 2008). This prevented the recovery of information about paleoceanographic conditions prior to the Eocene–Oligocene transition and also has implications for the interpretation of paleotemperature proxies such as Mg/Ca ratios in foraminifer shells that were bathed in waters with very low carbonate ion concentrations (Lear et al., 2008; Elderfield et al., 2006). The integrated stratigraphy from Site 1218 has been correlated to the planktonic foraminifer marker extinction of the genus *Hantkenina* in exceptionally well-preserved shallow clay-rich sediments from Tanzania by Pearson et al. (2008), who demonstrated that the Eocene/Oligocene boundary falls within the middle plateau of the stable isotope double-step described by Coxall et al. (2005) just prior to the base of Chron C13n.

Data from Site 1218 allowed the astronomical time calibration of the entire Oligocene (Coxall et al., 2005; Wade and Pälike, 2004; Pälike et al., 2006b), but the lack of carbonate in the uppermost Eocene at this site made the detailed time control now available for the Oligocene much less certain for the late Eocene. Site U1334 is on crustal basement with an age of ~38 Ma and crossed the paleoequator shortly thereafter. It was located to provide the missing information about the crucial chain of events prior to and during the Eocene–Oligocene transition.

### ***Oligocene (Site U1336, ~32 Ma crust)***

Site U1336 targets the Oligocene and is on early Oligocene crust. This interval of time is noted for its markedly heavy benthic oxygen isotopes (Fig. F2) and its relatively deep CCD (Fig. F3). There was probably ice on Antarctica during this interval, but not the large ice sheets to be found there later in the middle Miocene. Compelling evidence does not exist for ice sheets in the Northern Hemisphere during the Oligocene and early Miocene. Thus, a time of low global ice volume, cold bottom waters, a cold South Pole, and a relatively warm North Pole apparently existed. This scenario of a “one cold pole” world has given rise to speculation on the impact of interhemispheric temperature imbalance on pole to Equator temperature gradients and on the symmetry of the global wind systems. The extent to which such an imbalance may have affected the trade winds, the position of the ITCZ, and the seasonal shifts in this zone should be seen in the wind-driven currents of the equatorial region.

The older low-resolution DSDP data indicate relatively high but variable sediment accumulation rates during this interval and better carbonate preservation to the south of the Equator (van Andel, 1975). In the Leg 199 equatorial transect, the highest accumulation rates encountered (>15 m/m.y.) occurred in the lower part of the Oligo-

cene, but these were in sites north of the Oligocene Equator or on relatively old (and therefore deep) crust. Thus we expected a better preserved thicker carbonate section at the Oligocene Equator. Studies of Oligocene sections from Leg 199 and other ODP sites (e.g., Paul et al., 2000; Zachos et al., 2001a; Billups et al., 2004; Pälike et al., 2006a) indicate the presence of strong eccentricity and obliquity cycles in carbonate preservation and suggest a strong (southern) high-latitude influence on the carbonate record. These cycles are leading to the development of an orbitally tuned timescale that reaches back to the base of the Oligocene (Pälike et al., 2006b). Such a timescale will make it possible to develop a very detailed picture of equatorial geochemical fluxes and of the degree of variability in the equatorial system of the Oligocene.

### ***Latest Oligocene–earliest Miocene (Site U1335; 26 Ma crust)***

Site U1335 was designed to focus on the paleoceanographic events in the late Oligocene and into the early and middle Miocene, including the climatically significant Oligocene–Miocene transition and its recovery. In conjunction with Sites U1336 and U1337, Site U1335 was also designed to provide a latitudinal transect for early Miocene age slices. A significant several million year long rise in the oxygen isotope record (Lear et al., 2004; Pälike et al., 2006b) at the end of the Oligocene is closely followed by a relatively short, sharp increase in oxygen isotope values. This increase has been interpreted as a major glacial episode (Mi-1) (Fig. F2) (Paul et al., 2000; Zachos et al. 1997, 2001a, 2001b; Pälike et al., 2006a) and correlated to a pronounced drop in sea level (Miller et al., 1991). The Mi-1 event is very close to the Oligocene/Miocene boundary and has now been astronomically age calibrated in several ocean basins (Shackleton et al., 2000; Billups et al., 2004). Although there are clear periodic isotopic signals indicating major changes in ice volume, ocean temperatures, and/or ocean structure, this biostratigraphic boundary has always been somewhat of an enigma. Unlike the major changes in the isotopic stratigraphy, the biostratigraphies of the planktonic microfossils show very little change across this boundary. In fact it is one of the most difficult epoch boundaries to pick using only microfossil biostratigraphy.

At Leg 199 Sites 1218 and 1219 this interval was well recovered; however, carbonate preservation still presented a problem for foraminifer stratigraphy. Both sites were deep and well within the lysocline, making the application of temperature proxies such as Mg/Ca ratios in foraminifer tests more difficult (Lear et al., 2008). At the time Miocene–Oligocene sediments were deposited, Site 1218 already resided on ~18 m.y. old crust and was ~4100 m deep. Site 1219 was on ~32 m.y. old crust and was ~4500 m deep. There was a relative increase in the large diatoms near this boundary in the

siliceous coarse fraction, suggesting increased productivity; however, detailed high-resolution flux rates across this interval have yet to be determined. A well-recovered section on the latest Oligocene Equator near the late Oligocene ridge crest was targeted by Site U1335 and should provide both the resolution and the preservation required to better describe the changes in the equatorial ocean taking place at this time.

#### ***Miocene (Site U1337; 24 Ma crust)***

Site U1337 was proposed for drilling to focus on the paleoceanographic events in the early and middle Miocene. The latest Oligocene through the middle Miocene appears to have been a time of relative warmth comparable to the latest Eocene. However, the variability in the isotopic record of the early to middle Miocene is larger than that of the Eocene and may indicate more variability in climate and global ice volume. The climatic “optimum” at ~15 Ma comes just before the major development of ice sheets on Antarctica and the marked increase in ice-rafted debris in circum-Antarctic sediments. The early Miocene also marks a major evolutionary change from the relatively static Oligocene planktonic foraminifer biota. In the equatorial Pacific, the early Miocene also marks the beginning of abundant diatoms in the stratigraphic record (J. Barron, pers. comm., 2003) and thus may represent a major change in carbon cycling as well.

The only major ocean boundary change proposed for the time near the Oligocene/Miocene boundary was the opening of the Drake Passage to deep flow; however, there is some debate as to the exact timing of this event (Barker, 2001; Pagani et al., 1999; Lawver and Gahagan, 2003; Scher and Martin, 2006) and its direct impact on the tropical ocean is uncertain. It may be that, as in the Eocene/Oligocene boundary section, the link lies in the shallow intermediate waters that provide nutrients to lower latitude upwelling regions. For the equatorial region, an even more pertinent question is “What changes were occurring in the Miocene tropical ocean that led to this burst of Miocene evolution?”

#### ***Early and middle Miocene (Site U1338; ~18 Ma crust)***

In principle, the age transect strategy of this proposal would not be complete without data from the Pliocene–Pleistocene. However, in addition to logistical reasons of cruise length, near-paleoequatorial records have already been targeted by ODP Legs 138 (Pisias, Mayer, Janecek, Palmer-Julson, and van Andel, 1995) and 202 (Mix, Tiedemann, Blum, et al., 2003), which provide information about the development of

Northern Hemisphere glaciation. Our last site (U1338) focuses instead on the interesting events following a middle Miocene maximum in deposition (van Andel, 1975).

Site U1338 was proposed for drilling to focus on the paleoceanographic events following a middle Miocene maximum in deposition (van Andel, 1975). In addition, large changes in the glaciation state and frequency have recently been described in the late early and middle Miocene (Holbourn et al., 2005; Abels et al., 2005; Raffi et al., 2006), in the interval following ~14 Ma. There is a wide latitude range of CaCO<sub>3</sub> deposition during the earliest Neogene, with a relatively sharp transition to a narrower CaCO<sub>3</sub> belt after 20 Ma (Lyle, 2003). CaCO<sub>3</sub> mass accumulation rates in the central equatorial Pacific recovered from the 18–19 Ma “famine” and in the period between 14 and 16 Ma reached a second maximum in carbonate deposition, which is also evident in the seismic stratigraphy of the equatorial sediment bulge (Knappenberger, 2000; Mitchell et al., 2003). We designed Site U1338 to recover an equatorial record at the early middle Miocene sedimentation maximum.

## Results and highlights

Two major Neogene equatorial Pacific sediment sections were recovered during Expedition 321 by drilling seven holes at two sites (Holes U1337A–U1337D and Holes U1338A–U1338C). One additional hole (U1338D) was drilled at Site U1338 to provide sediment cores for the upcoming Bering Sea Expedition 323 to practice on. Expedition 320 drilled three other sites that also define Neogene sedimentation in the equatorial Pacific (Sites U1134–U1136). In this section, we synthesize our observations about the Neogene equatorial Pacific primarily from the Expedition 321 drilling but also include appropriate sites from Expedition 320. The cores recovered from Expedition 320/321 provide the raw material to address Neogene PEAT objectives for the equatorial Pacific megasplice. Shipboard research has provided the framework of studies to define the lithology, show continuity of the sediment section, and define the basic time framework. Shorebased work will refine the chronostratigraphy through orbital tuning and will measure proxies of surface and deep water change and paleoproductivity/carbon cycles to show how the modern equatorial Pacific developed as the icehouse world developed.

For the PEAT program, only Sites U1337 and U1338 recovered sedimentary sections of the late Miocene-Holocene with relatively high sedimentation rates and preserved carbonate (~15 m/m.y.) (Fig. F12). Sites further west and north on older crust (Sites

U1331–U1336) suffer from low sedimentation rates or hiatuses in the younger section because they are farther from the modern equatorial productivity zone and on deeper (older) ocean crust where depth-dependent carbonate dissolution has become strong. Of the older sites, the best higher sedimentation-rate sediment sections for the middle Miocene through late Oligocene are found at Sites U1334–U1336.

One of the important accomplishments of Expedition 321 was to recover two continuous essentially complete Neogene sedimentary sections, Site U1338 from 0 to >17 Ma and Site U1337 from 0 to >23 Ma, just beyond the Oligocene/Miocene boundary. These represent the only complete Neogene sections in the equatorial Pacific, possibly for all the tropics, that have high enough sedimentation rates to resolve orbitally forced sediment cycles. Coring during DSDP Legs 8, 9, and 16 was accomplished with the rotary core barrel and the sediments were highly disturbed. During ODP Leg 85 at Site 574, the middle Miocene to present was double APC cored, but sedimentation rates were slow (~5 m/m.y.) from 0 to 10 Ma and the middle Miocene section was never spliced (Mayer et al., 1985). Below the middle Miocene, only one hole was drilled. Similarly, Site 572 had only a single hole drilled through the upper and middle Miocene interval (Mayer et al., 1985). Most Leg 138 sites were drilled on 10 Ma crust and did not contain significant middle and lower Miocene sediments (Mayer, Pisias, Janecek, et al., 1992). Site 846 was drilled on 17 Ma crust on the Nazca plate but experienced poor recovery below 12 Ma. In addition, Site 845 in the Guatemala Basin has a spliced sediment section to only ~12 Ma (Mayer, Pisias, Janecek, et al., 1992), even though it was located on 17 Ma crust. Even in the tropical Atlantic on the Ceara Rise, the middle and early Miocene were discontinuously cored and longer records were spliced between different sites (Shipboard Scientific Party, 1995; Raffi et al., 2006).

## Neogene, Sites U1334–U1338

Neogene sediments of the tropical Pacific are primarily biogenic in origin (Figs. F13, F14). PEAT sites within the equatorial zone in the Neogene (Sites U1335–U1338) are all primarily composed of nannofossil oozes with secondary biosiliceous components. Aluminosilicates are only a small component of the sediments. Most clay is of aeolian origin and is typically in low abundance. Clays become more dominant ~5° north of the Equator, where biogenic carbonate and opal is being dissolved away and sedimentation rates are very low.

Within the equatorial zone ( $\pm 2^\circ$  of the Equator), diatoms, and to a lesser extent radiolarians, are a more important part of the sediments from the upper part of the middle Miocene to the present. An important diatom-rich interval occurs between 10 and 11.5 Ma. This interval is best developed at Site U1337 but can be correlated regionally. These events are discussed more fully in [“Neogene biogenic events and cycles.”](#)

A short lower Miocene biogenic carbonate sediment section was found at the top of Site 1218 on 42 Ma crust (Lyle et al., 2002) below a radiolarian clay interval (Figs. [F13](#), [F14](#)). Site 1218 is representative of the northern edge of Miocene carbonate deposition. Miocene carbonate sediments can only be found in piston cores to  $\sim 10^\circ\text{N}$  (Riedel, 1967). At the PEAT sites, significant but slowly accumulating lower to middle Miocene carbonates were found at Sites U1334 and U1336. The upper parts of Sites 1218, U1334, and U1336 were all either biosiliceous clays or, in the case of Site U1336, a hiatus.

At Sites U1335, U1337, and U1338, sediments have experienced relatively little diagenesis. The lower sections have turned to chalk by compaction and because of mild increases in downcore temperature from geothermal heating (Fig. [F11](#)). The sediment columns of these sites are between 410 and 450 m thick, and at each site most of the sediment column was cored by APC. Site U1335 was cored by APC to 378 m core depth below seafloor, method A (CSF-A), whereas Site U1337 was cored by APC to 267 m CSF-A and Site U1338 was cored by APC to 414 m CSF-A, a new drilling record. The deep APC cores typically had little disturbance, much less than XCB cores taken at the same interval (Fig. [F15](#)). The excellent quality of the cores will make them useful for later high-resolution paleoceanographic studies. For the most part, shipboard correlators were able to splice together continuous sediment columns from the multiple holes drilled at each site, except for some difficulties in the upper to middle Miocene diatom-rich interval (see [“Neogene biogenic events and cycles”](#)).

Site U1336 experienced significantly higher diagenesis than other PEAT sites, perhaps because of higher sediment temperatures and/or fluid flow. The basal 100 m of Site U1336 (upper–lower Oligocene) are barren of siliceous microfossils and have lithified to cherts and chinks even though the sediment column is only  $\sim 300$  m thick. We speculate that faulting parallel to the Clipperton Fracture Zone—Site U1336 is located just north of the fracture zone—may have served to localize fluid flow in the vicinity of the site. Unfortunately, no sediment temperatures were taken during coring at this site.

## New capabilities on the *JOIDES Resolution*

The shipboard laboratories have new capabilities that greatly improve the ability of shipboard scientists and later researchers to study the sediment column. One important capability is a much better capacity to integrate line-scan core images into descriptions and analyses. Figure F16 shows color images from different holes at Site U1337 and how they were joined into the Site U1337 splice. The color images are particularly useful to resolve color banding and cyclic behavior in the multicolored sediment intervals. In the upper parts of all the sites, it is common to find oxidized brown sediments that become green when Fe within the sediments is reduced (Lyle, 1983). Typically this feature has been described in the upper meter of the sediment column. Further west, where the PEAT sites are located, brown colors extend downward for tens of meters. Not all of the color information is stratigraphically useful—redox state and other diagenetic processes can overprint other sediment information. For example, the color change from green to yellow at the base of the Site U1338 sedimentary section cuts across stratigraphic correlations between different holes.

Dark-light color banding, whatever shade of color, is indicative of carbonate content in the equatorial Pacific. Darker layers usually have lower carbonate contents, higher magnetic susceptibility, higher natural gamma activity, and lower bulk density. Different scales of carbonate cycles are found in the core images. Because many of the low-carbonate events are chronostratigraphic, they can be used to correlate between cores. At the larger scale, the dark-light color banding can be used to correlate between sites.

Another new instrument on the *JOIDES Resolution* is the whole-round natural gamma detector. The instrument is much more sensitive than the ODP natural gamma detector and can be used as part of the normal core-flow measurements. Biogenic sediments of the equatorial Pacific are not ideal for natural gamma activity studies—they only have low levels of natural radioactivity. Nevertheless, the new detector was able to reliably detect natural gamma ray activity variations of <1 cps. Small natural gamma activity highs correlated with dark sediment layers. One of the objectives for the natural gamma ray measurement on cores is to produce a record that can be correlated with the wireline logging measurements. Unfortunately, the low natural gamma ray activity levels produced inconsistent peaks on repeat passes of the logging tool strings, with the exception of a few intervals.

The seafloor was one interval that consistently had high natural gamma ray activity (Fig. F17). Whereas counts at a distance from the seafloor were <5 cps, seafloor natural radioactivity levels were as high as 160 cps within 1 m of the top of the sediments. Natural gamma ray activity dropped to the typical low count a few meters below the surface. Spectral studies using hour-long counts on the surface cores revealed that natural gamma ray activity at the surface is being produced by high uranium levels, not thorium or potassium. It is not clear yet why uranium is being concentrated only near the sediment/water interface. Because the near-surface sediments have low organic carbon contents, uranium has not been concentrated by reduction and precipitation from seawater. Kunzendorf et al. (1983) instead argues that enrichments of uranium in tropical Pacific sediments result from coprecipitation of seawater uranium with Fe-oxides. This solution still begs the question as to why the level of Fe-oxides might be higher.

## Neogene biogenic events and cycles

The Neogene has significant changes in temperature, glaciation, plankton community, and carbon cycle, including a significant warm interval at ~15–16 Ma, and multiple glaciations first in Antarctica and then in the Northern Hemisphere (Zachos et al., 2001a). There also have been important changes in the CCD. Changes in isotope composition and SST proxies can only be monitored by shore-based geochemical studies. However, shipboard monitoring of changes in plankton composition and relative abundance indicate that dissolution has taken place in the Neogene equatorial Pacific, achieving parts of objectives 2, 3, 4, and 7 listed in “**Scientific objectives.**”

The eastern equatorial Pacific has times of known change in CCD (at ~18 and ~10 Ma) (Lyle et al., 1995; Lyle, 2003). There are also important intervals where biogenic fluxes have changed significantly (Farrell et al., 1995) and important time intervals of high diatom flux (Kemp and Baldauf, 1993). We were able to identify these intervals at Sites U1337 and U1338 and expect that further work will identify new intervals, thereby achieving objective 1 listed in “**Scientific objectives.**”

### *Neogene chronostratigraphy*

One of the major shipboard scientific efforts for every paleoceanographic drilling cruise is to place the depth column into a time framework (objective 3 in “**Scientific objectives**”) (Fig. F12). During Expedition 321 we depended on shipboard biostratigraphy and magnetostratigraphy for the basic time framework. Shipboard biochronostratigraphy is based upon the PEAT timescale developed before the PEAT expeditions

and will be refined postcruise. Depth positions of recognized biostratigraphic zones and microfossil datum levels will be listed in each of the site summaries.

### **Biostratigraphy**

One of the highlights of Expedition 321 was the recovery of well-preserved and diverse assemblages of siliceous radiolarians and diatoms and calcareous planktonic foraminifers and nannofossils for the Neogene. Although the zonation and calibrations of each of these groups has been established and refined over the last 50 y, there are very few locations with both well-preserved and abundant siliceous and calcareous microfossils. Leg 199 established a well-defined radiolarian stratigraphy and calibration for the equatorial Pacific Ocean (Nigrini et al., 2006); unfortunately the planktonic foraminifers and calcareous nannofossils were sufficiently preserved to provide robust calibrations only for the Oligocene (Pälike et al., 2006b; Wade et al., 2007).

In spite of well-defined Neogene diatom stratigraphy and calibration for the low-latitude Pacific (Baldauf, 1985; Baldauf and Iwai, 1995; Barron, 1985), it is clear from Sites U1337 and U1338 that the presence of some of the diatoms used in the diatom stratigraphy is discontinuous in the expanded Miocene section at both drill sites. This has been noticed in sediments recovered during Leg 138 (Baldauf and Iwai, 1995). The discontinuous occurrences may reflect large variations in the abundances of these species with time and changing ecologic conditions. However, there is also the possibility that some of these intermittent disappearances of a species may reflect genetic changes in the lineage that give rise to either “iterative evolution” or changing ecological preferences (objective 7 in “**Scientific objectives**”).

The diatom, radiolarian, calcareous nannofossil, and planktonic foraminifer stratigraphies at Sites U1337 and U1338 all generally agree, with some minor discrepancies. The fully integrated biostratigraphies coupled with the cyclostratigraphy and paleomagnetostratigraphy will lead to an integrated magneto-, astro-, and biochronology of all four microfossil groups for the equatorial Pacific Ocean (objective 3 in “**Scientific objectives**”).

### **Magnetostratigraphy**

Paleomagnetism and magnetostratigraphic studies are essential observations to obtain a well-intercalibrated Cenozoic megasplite and to constrain the tectonic motion of the Pacific plate (objectives 3 and 5 in “**Scientific objectives**”). Shipboard magnetostratigraphy (Fig. **F18**) was used as a Neogene chronostratigraphic tool. Unlike the

Paleogene, significant parts of the sedimentary section have low magnetic intensity and do not retain a strong paleomagnetic signal. These intervals of weak magnetic intensity correlate in part to the “green” sediment intervals, but not entirely.

The magnetic polarity stratigraphy of the entire middle Eocene to Quaternary interval was resolved at the eight sites occupied during Expedition 320/321. The middle Eocene and Oligocene interval was well documented at Sites U1332 and U1333. At Site U1332, mean sedimentation rates in this interval range from 3 to 8 m/m.y., and at Site U1333 the mean sedimentation rates reach ~12 m/m.y. in the lower Oligocene. At Site U1334 the upper Oligocene and lower Miocene magnetic stratigraphy was well resolved with mean sedimentation rates of 12 m/m.y. in the lower part of the interval and 4 m/m.y. in the upper part. At Site U1335, the upper Miocene and Quaternary magnetic stratigraphy was well resolved at sedimentation rates of ~6 m/m.y., and below these sediments lies an interval of upper middle Miocene where the magnetic stratigraphy is not resolved because of weak magnetization intensities. This ~20 m long unresolved interval is underlain by sediments that carry a magnetic stratigraphy of part of the middle and lower Miocene, although the interval is interspersed with turbidites and evidence of reworking. At Site U1336, the magnetic stratigraphy of part of the middle and lower Miocene is resolved in the 0–80 m CSF-A interval at mean sedimentation rates of ~10 m/m.y.; however, below ~80 m CSF-A magnetization intensities are too low for resolvable magnetization directions. At Site U1337, although the magnetic polarity stratigraphy is interpretable for the upper Miocene to Quaternary, data quality is poor for the upper Miocene. At Site U1338, the magnetic stratigraphy is resolvable in three intervals: part of the Pliocene–Pleistocene (0–4 Ma), part of the late Miocene (8.7–11 Ma), and part of the middle Miocene (12.7–16 Ma). These three intervals at Site U1338 are separated by intervals of low magnetization intensities where the magnetic stratigraphy was not resolvable.

### ***Biotic response to climatic change***

The phytoplankton, zooplankton, and benthic foraminifers at these sites provide an excellent opportunity to document the biotic response to intervals of rapid climatic change in both the surface and deep ocean, addressing PEAT objectives 1, 2, 4, and 7 (see “[Scientific objectives](#)”).

Planktonic foraminifer assemblages are generally well preserved. As with other microfossil groups, distinct changes in assemblage composition reflect preservational and evolutionary changes, fluctuations in the water column structure, and the position of each site relative to the paleoequator (Fig. [F19](#)). Globoquadrinids and dentoglobiger-

inids dominate the assemblages from the Oligocene to middle–late Miocene. This interval is also associated with extremely abundant and diverse paragloborotaliids. These taxa are considered to occupy the thermocline and prefer nutrient rich environments (Wade et al., 2007). The decrease in globoquadrinids and dentoglobigerinids is associated with an increase in *Globigerinoides*, which increases in abundance from the middle Miocene. Keeled globorotaliids dominate the Pleistocene assemblages. Peak abundances of *Globigerinoides* spp. occur within the late Miocene.

There appears to be a relationship between the diversity in the planktonic foraminifers and climatic change. At Site U1338, a high diversity of planktonic foraminifers are recorded in Zone M5, with many microperforate taxa (*Globigerinita*, *Globigerinella*, *Mutabella*, and *Tenuitella*). The diversity of this group is particularly high through the early middle Miocene. These taxa occupied the warmer mixed layer (Pearson et al., 2001b; Majewski, 2003), and the high diversity may be related to higher SSTs and increased stratification associated with the Middle Miocene Climatic Optimum (MMCO).

Planktonic foraminifers, because they dissolve more easily than benthic foraminifers or nannofossils, are useful to evaluate the degree of dissolution in calcareous biogenic sediments (objective 1 in “**Scientific objectives**”) (Fig. F20). Intervals of enhanced dissolution have been detected at Sites U1337 and U1338 and are associated with laminated diatom oozes between 11.5 and 9 Ma, the “carbonate crash” interval. Another short interval is barren of planktonic foraminifers and marked by a high benthic/planktonic foraminifer ratio at ~17 Ma at Site U1337.

Much like the planktonic foraminifers, calcareous nannofossil assemblages reflect global and regional oceanographic changes. Neogene placolith diversity peaks in the early to middle Miocene, during the MMCO. At ~14 Ma, nannofossil assemblages begin to fluctuate, indicating changes in productivity. At Site U1338 there are several instances when assemblages are dominated by very small (<3 µm) *Dictyococcites* species, here interpreted as bloomlike episodes. These events are also present at Site U1337, but in limited quantity, suggesting that Site U1338 was located under a more intense upwelling regime. Another indication that Site U1338 records a higher productivity signal is the exclusion of multiple taxa, such as the marker species *Helicosphaera ampliapertura* and *Catinaster coalitus*, both of which are rare but present at Site U1337.

Lower bathyal to abyssal benthic foraminifers occur throughout the early Miocene to Pleistocene in Sites U1337 and U1338 and show relatively good preservation. Marked variations in downcore abundance and assemblage composition relate to fundamental changes in global climate, major ice-volume fluctuations, and reorganizations in oceanic circulation during the Neogene. Organic flux-sensitive taxa track substantial changes in equatorial Pacific Ocean surface productivity throughout the latest Miocene to Pleistocene. Impoverished assemblages and high benthic/planktonic ratios prominently mark the late Miocene “carbonate crash” (Fig. F20), whereas diversified assemblages, including high numbers of epifaunal or near surface dwellers such as *Cibicidoides*, signal a marked improvement in deep ocean ventilation following middle Miocene high-latitude ice sheet expansion. Early to early middle Miocene assemblages exhibit significant fluctuations in abundance and diversity, hinting at major changes in upper ocean structure and deep water ventilation at the onset of and during the Miocene climate optimum.

#### ***Diatoms and diatom mat intervals in the Miocene and Pliocene***

Diatoms are well represented at Sites U1337 and U1338 between ~0 and 18 Ma. Diatoms are a less common part of the equatorial Pacific plankton before this time. Based on smear slides, diatoms comprised <15% of the total plankton assemblage in the early Miocene but are often >25% of the plankton after 15 Ma (Fig. F21). In spite of minor differences in the qualitative composition of the assemblages, the diatom community preserved at Sites U1337 and U1338 mostly consists of Neogene species typical of the low-latitude eastern equatorial Pacific Ocean (Baldauf, 1985; Baldauf and Iwai, 1995; Barron, 1985).

A striking feature of Site U1337 sediments is the occurrence of thick sequences of laminated diatom oozes (diatom mats) (Fig. F22). These diatom mats are mainly composed of the needle-shaped diatom *Thalassiothrix* and are deposits that record unusual oceanographic conditions that repeated a few times in the eastern equatorial Pacific region in the middle to late Miocene and early Pliocene (Fig. F23) (Kemp and Baldauf, 1993). A diatom mat interval is made up of essentially pure diatoms and macroscopically has the appearance of layers of wet paper. One of the unsolved questions of Expedition 321 is why the mats were prominent at Site U1337, whereas at Site U1338 the same time intervals were marked by diatom-rich sediments but only rarely mats. Site U1338 was closer to the Equator during the mat-forming interval, being at the Equator during the major interval at 10.3–11.3 Ma, whereas Site U1337 was at 1°N.

Kemp and Baldauf (1993) proposed that the mats record extraordinarily high open ocean sedimentation rates and represent vast sinks of silica and carbon. However, at the coarse resolution of shipboard biostratigraphy we could detect no change in sedimentation rate through this interval and could easily correlate the bulk density profiles between Site U1337 with extensive mats to Site U1338 without them. Postcruise work will be important to determine how fast the diatom mats deposited.

Within the mat interval, the alternation between the *Thalassiothrix* and mixed-sediment laminae could reflect the periodic movement of the frontal zone in the eastern equatorial Pacific Ocean. An improved insight into *Thalassiothrix* mats from Site U1337 will be an important prerequisite for enhancing our understanding of the marine biogeochemical cycling and for assessing the impacts of rapid climate change on ocean export production in the low-latitude eastern Pacific Ocean (objectives 1, 2, 4, and 7 in “[Scientific objectives](#)”).

### ***Late Miocene carbonate crash and middle Miocene glaciation***

Sites U1337 and U1338 recovered a full suite of Pleistocene to earliest Miocene calcareous and siliceous microfossils. All groups exhibit prominent downcore variations in preservation and abundance that appear related to major changes in primary production, export flux, and water-column and seafloor dissolution, thus reflecting fundamental changes in global climate. The carbonate crash, an extended period of low carbonate deposition widely recorded throughout the eastern Pacific Ocean at ~9–11 Ma (Lyle et al., 1995; Farrell et al., 1995), is strikingly expressed at Sites U1337 and U1338 by sharp decreases or the disappearance of planktonic foraminifers, high benthic to planktonic foraminifer ratios, and generally impoverished benthic foraminifer assemblages (Fig. [F20](#)). Calcareous and siliceous microfossils indicate that this prominent dissolution event was less intense and of shorter duration at Site U1338 than at Site U1337 (Fig. [F20](#)), probably because it is located on younger oceanic crust and in closer proximity to the Equator during this time window. Site U1338 was ~200 m shallower than Site U1337 and essentially at the Equator during the carbonate crash interval.

During episodic expansion of the Antarctic ice sheet at ~14–15 Ma, calcareous microfossils exhibit overall good preservation and relatively high diversity, suggesting a vigorous Pacific Ocean circulation and deep CCD. In contrast, the preceding prolonged period of global warmth, often referred to as the MMCO, appears marked by transient changes in CCD. Postcruise studies and integration of paleontological data will provide an opportunity to further investigate temporal and spatial variations in micro-

fossil distribution across the equatorial Pacific Ocean and to unravel links with global climatic and oceanographic events during the Neogene (objectives 1 and 9 in “**Scientific objectives**”).

## **Orbital cycles, physical properties, and site correlation**

The equatorial Pacific is a classic “binary” sediment system, with variable amounts of biogenic calcium carbonate and biosiliceous sediment components but very little clay. It is also well known that carbonate contents of equatorial Pacific sediments can be estimated from the bulk density because the carbonates have lower porosity and higher grain density than biosiliceous sediments (Mayer, 1991). Consequently, physical property records contain meter-scale cyclicity that will ultimately be useful for orbital-tuning timescales (objective 3 in “**Scientific objectives**”).

On longer depth scales, physical property records are useful to correlate between sites. Figure F24 shows the two high-resolution density logs at Sites U1337 and U1338 and illustrates the high degree of correlation between the two sites that are separated by ~600 km. Lines on the figure represent equivalent nannofossil biostratigraphic datum levels. The two records are aligned such that the top peaks line up. The depth scale for Site U1338 is compressed so that the bottom event also lines up. Density events can easily be correlated between the sites even though they are separated by >600 km.

Mayer et al. (1985) developed a seismic stratigraphy for the central Pacific at Site 574 during Leg 85. They noted that major seismic horizons were caused by density variations associated with low-carbonate intervals. They proposed that these intervals were chronostratigraphic because they were caused by paleoceanographic changes in deposition and/or dissolution of calcium carbonate.

Unfortunately, Mayer et al. (1985) did not have logs to measure in situ velocities. One of the important experiments of Expedition 321 was to use logging as well as cores to check this conclusion and to better constrain the age of the equatorial Pacific seismic horizons. For this reason, we planned a vertical seismic profile (VSP) experiment at one of the Neogene PEAT sites (objective 6 in “**Scientific objectives**”). We were able to run the VSP log at both Site U1337 (Fig. F25) and U1338. Figure F25 is an initial comparison between the Site 574 seismic stratigraphy of Mayer et al. (1985) and the initial results for Site U1337. The events appear to correlate in age, as would be predicted by Mayer et al. (1985). Site 574 is at essentially the same latitude as Site U1337 but >1000 km to the west. The length scale of the correlatable seismic horizons across

the Pacific helps to define the length scale of the paleoceanographic events with which they are associated. Postcruise studies will focus on better defining the seismic stratigraphy at both Sites U1337 and U1338, allowing new tie points for the seismic stratigraphic study of the equatorial Pacific sediment bulge (Mitchell et al., 2003).

### ***Cherts in the Neogene sediment section***

Chert intervals were found at Sites U1336–U1338. At Site U1336, a chert interval was found in unlithified early Miocene sediments at ~130 m CSF-A. The section below 200 m CSF-A also had significant numbers of chert intervals and the carbonates had been turned to limestone, suggesting significant higher temperature diagenesis.

At Sites U1337 and U1338, only one cherty interval was found—what we referred to as the “baby chert” interval. At both sites the cherty interval hampered recovery around it, but it was easily penetrated by drilling. Interestingly, its position appears to be chronostratigraphic, at ~12 Ma in the upper middle Miocene (~240 m CSF-A at Site U1337 and ~282 m CSF-A at Site U1338). It was located in a diatom mat interval at Site U1337 and a diatom-rich interval at Site U1338. The interval was well-imaged by Formation MicroScanner (FMS) logging and shows that the chert interval is 40 cm thick at Site U1337 and about one-quarter of the way up from the base of the low resistivity diatom-rich interval (Fig. F26). At Site U1338 the baby chert interval was only 16 cm thick but also about one-quarter of the way through the low resistivity interval. The logs allowed us to estimate the amount of disturbed and missing section in the cored sediments—there is only a small loss of material (<1 m) around the chert.

At Site U1337 it was clear from interstitial water profiles that the baby chert interval is a barrier to diffusion. There were offsets in Li, Sr, and SO<sub>4</sub> in interstitial waters immediately below and above the baby chert interval. It is unclear why the chert formed in this interval alone at both sites. There were additional diatom-rich intervals below the baby chert that were unaffected, and the temperature gradients at both sites are not large. The more extensive chert layer at Site U1337 is actually formed ~30 m shallower (250 m CSF-A) than the interval at Site U1338 (280 m CSF-A). Postcruise research focused on diagenesis and fluid flow may provide insight into chert formation with these diatom-rich intervals.

### ***Color banding and redox at the Neogene PEAT drill sites***

The Expedition 320 scientific party noted a strong signal of magnetic susceptibility, brown-green color change, and Mn and Fe contents in interstitial waters at Sites U1334–U1336. The results are not as clear cut at Sites U1337 and U1338 (Fig. F27).

All sites have significant dissolved manganese peaks in the upper sediment column. The low-latitude younger sites (U1335, U1337, and U1338) have the Mn peak very near the sediment/water interface, whereas the dissolved manganese peak in the older, more northerly sites is found tens of meters into the sediment column. The dissolved Mn peaks in Site U1337 and U1338 sediments are about a factor of 30 higher than those found in the other sites, however, perhaps because of higher water-column scavenging of Mn to the sediments. The dissolved-Fe peak does not clearly match the green intervals, especially at Site U1338. Although not plotted on the paleolatitude graph, green sediments appear when Sites U1337 and U1338 are near or within the equatorial zone, showing a sedimentary “memory” of the equatorial productivity zone.

### ***Organic carbon and carbonate burial***

Both total organic carbon (TOC) and  $\text{CaCO}_3$  (estimated from evolved  $\text{CO}_2$ ) were measured as part of the shipboard geochemical program during Expedition 321. TOC was measured by acidification of the bulk sediment to remove carbonate and analysis by the CHN analyzer during Expedition 321. Carbonate was measured using a coulometer with an acidification module. Trends in carbonate match with Neogene dissolution intervals, whereas TOC increases from low levels at the base of the sedimentary section to higher levels upcore. Postcruise research will focus upon measuring alkenones, other biomarkers, and productivity proxies to better understand the variations in TOC and productivity (objectives 2, 4, and 9 in “[Scientific objectives](#)”).

Figure [F28](#) shows the TOC and carbonate profiles versus age at Sites U1336–U1338. None of these sites were ever below the CCD, although Site U1337 briefly approached zero carbonate levels during the 9–11 Ma carbonate crash interval. We can date other carbonate minima between 16 and 18 Ma and 3 and 4 Ma. The 16–18 Ma minimum correlates with the early Miocene carbonate flux minimum identified by Lyle (2003) but is much better defined at Site U1337. It reaches its minimum at 17.2 Ma. The 3–4 Ma carbonate minimum is not well identified in Leg 138 sediments, perhaps because these sites are on younger, shallower crust.

TOC profiles identify a trend from lower to higher TOC from the base of the cores and small intervals of high TOC that were not resolved well at the very coarse shipboard sample interval. High TOC was found in high-biosiliceous intervals to levels as high as 0.7%. The distribution of high TOC deserves more study postcruise to determine how these short events have affected TOC burial fluxes. The base of each site had TOC contents of ~0.1% or below, whereas younger sediments have values of 0.2% or

higher. Site U1336, which has a hiatus at 12 Ma, has low TOC values to the surface of the core. Earlier drilling did not find trends in TOC because the standard technique to measure TOC on ODP and DSDP legs (assigning the difference between total carbon and carbonate carbon to TOC) has very high errors in carbonate-rich sediments like the equatorial Pacific.

The longer TOC trend could be the result of age and long-term degradation or the strength of early diagenetic degradation, or it could result from changes in TOC particulate rain (“productivity”) through time. Distinguishing between these alternatives will require postcruise study of mass accumulation rates and abundances of different biomarkers.

## Site U1336

Two holes were cored at Site U1336 (proposed Site PEAT-5C; 7°42.067'N, 128°15.253'W; 4286 m water depth) targeting paleoceanographic events in the late Oligocene and into the Miocene, including a focus on the Oligocene–Miocene transition and the recovery of the Mi-1 glaciation event (Zachos et al., 2001b; Pälike et al., 2006a). In conjunction with Sites U1335 and U1337 it was also designed to provide a latitudinal transect for early Miocene age slices. Site U1336 provides data toward a depth transect across the late Oligocene and Miocene that allow us to verify and apply a previous astronomical age calibration from Site 1218 (Pälike et al., 2006b).

At Site U1336, APC cores were taken from the seafloor to 184.8 m (Cores 321-U1336A-1H through 21H) and 173.6 m (Cores 321-U1336B-1H through 20H). Nonmagnetic core barrels were used for Cores 321-U1336A-1H through 16H and Cores 321-U1336B-1H through 16H and steel barrels were used for all other cores. Two hard layers, one at ~121 m CSF-A (Cores 321-U1336A-14H and 321-U1336B-14H) and one at ~135 m CSF-A (Core 321-U1336B-16H) caused core loss and prevented the development of a continuous sediment section. XCB cores (321-U1336A-22X through 35X) were taken from 184.8 to 302.9 m CFS-A at Hole U1336A. We stopped coring before reaching the basement objective because of decreasing rates of penetration, relatively low recovery, and the possibility of obtaining a stratigraphically complete Miocene section.

At Site U1336, ~300 m of pelagic sediments are divided into three major lithologic units (Fig. F29). The sediments are composed mainly of nannofossil oozes, nannofossil chalks, and chert. The early to middle Miocene sedimentary sequence of Unit I (0–

74.54 m CSF-A) contains more radiolarians, clay, foraminifers, and diatoms relative to the early Miocene to early Oligocene sediments below ~70 m CSF-A. Subtle changes in the relative proportions of these minor components produce meter-scale dark-light color cycles and two diatom rich layers. Numerous rounded fragments of pumice occur throughout this unit.

Unit II (74.50–189.50 m CSF-A) is dominated by nannofossil ooze. Sediment color changes occur downhole from pale yellow to light greenish gray at 92 m CSF-A. Below this boundary, the color of Unit II alternates between light greenish gray and white to 184.80 m CSF-A. The oxidation-reduction reactions responsible for the observed vivid colors and pore water chemistry changes are likely fueled by enhanced availability of organic carbon relative to overlying and underlying sediments. Occasional thin chert layers were encountered below 120 m CSF-A in Unit II. Mainly broken chert fragments were recovered except for a small in situ chert fragment at 159.6 m CSF-A in Section 320-U1336B-18H-4, 106 cm. More abundant chert layers are common in the lower third of the recovered sequence.

Unit III (189.5–299.6 m CSF-A) was only recovered in Hole U1336A. The dominant lithologies of this unit are light greenish gray and white nannofossil chalk with light greenish gray millimeter-scale color banding and chert layers. The chert shows many different colors including black, dark greenish gray, very dark greenish gray, dark gray, olive yellow, dark brown, and pink. The Unit II–III transition is identified by the uppermost common occurrence of chert. Below 289 m CSF-A, nannofossil chalk contains increasing amounts of micrite and the cherts vary in color. The lowermost cherts are olive yellow, then pink, and, finally, dark brown at the base. The chalk changes color to white below 298.54 m CSF-A. CaCO<sub>3</sub> contents remain >88% in the chalk layers. Igneous basement was not recovered at Site U1336.

All major microfossil groups have been found in sediments from Site U1336, representing a complete biostratigraphic succession at the shipboard sample resolution level of middle Miocene to early Oligocene sediments. They provide a coherent, high-resolution biochronology through a complete sequence (Fig. F29). Calcareous nannofossils are moderately to poorly preserved throughout the succession. There appears to be a complete sequence of nannofossil zones from Zone NN6 (middle Miocene) through NP22 (lower Oligocene), except for Zone NN3, which could not be resolved. Planktonic foraminifers are present throughout the succession ranging from Zones N12 through O1. They are moderately well preserved in the Miocene and less well preserved in the Oligocene. The radiolarian stratigraphy at Site U1336 spans the in-

terval from just above the RN6/RN5 boundary (middle Miocene) to the upper part of RP22 (upper Oligocene) at ~170 m CSF-A. Below this level the sediments are barren of radiolarians. Above this level the assemblages tend to have good to moderate preservation with intermittent intervals of good preservation in RN3 and RN4 (lower to middle Miocene). The downsection decrease in preservation and ultimate disappearance of the radiolarians below Core 320-U1336A-19H appears to be associated with dissolution and reprecipitation of the biogenic silica as intergranular cement and as chert.

Diatom stratigraphy in Hole U1336B spans the interval from just above the *Cestodiscus peplum* zone (middle Miocene) in Core 320-U1336B-1H to the lowermost part of the *Crucidentricula nicobarica* zone (upper lower Miocene) in Core 320-U1336B-7H. Below Sample 320-U1336B-7H-CC, the sediments are barren of diatoms. Above this level the valves tend to be mostly poorly preserved. Sample 320-U1336B-1H-CC contains the highest diversity with *Cestodiscus pulchellus* as dominant component, accompanied by *Synedra jouseana* and *Thalassiosira yabei*. Fragments of the large centric diatom *Ethmodiscus* are present in the upper part of Hole U1336B.

Benthic foraminifers are present throughout the section, although abundances are overall quite low. The preservation of tests is moderate in the upper part of Site U1336 (Sections 320-U1336A-1H-CC through 19H-CC, 8.22–170.63 m CSF-A, and 320-U1336B-1H-CC through 20H-CC, 1.68–174.01 m CSF-A) but deteriorates below this level. The Oligocene to middle Miocene benthic foraminifer assemblage is relatively diverse and indicates oligotrophic lower bathyal to abyssal paleodepths.

The Oligocene/Miocene boundary is placed between the bioevent base *Paragloborotalia kugleri* (23.0 Ma) and top *Sphenolithus delphix* (23.1 Ma). The base of planktonic foraminifer *P. kugleri* (23.0 Ma) occurs between Section 320-U1336A-16H-CC and Sample 320-U1336A-17H-2, 38–40 cm (142.96 m CSF-A) and Samples 320-U1336B-16H-1, 52–54 cm, and 17H-3, 80–82 cm (137.72 m CSF-A). Calcareous nannofossil event top *S. delphix* is recognized between Samples 320-U1336A-17X-2, 90 cm, and 17X-4, 90 cm (145.9 m CSF-A), and between Section 320-U1336B-16H-CC and Sample 320-U1336B-17H-1, 150 cm (137.56 m CSF-A).

Paleomagnetic measurements were conducted on archive-half sections of 21 APC cores from Hole U1336A and 20 APC cores from Hole U1336B. Measurements of natural remanent magnetization (NRM) above ~80 m CSF-A in Holes U1336A and U1336B indicate moderate magnetization intensities ( $1 \times 10^{-3}$  A/m) with a patchy but

generally weak viscous remanent magnetization (VRM) or isothermal remanent magnetization (IRM) coring overprint, and polarity reversal sequences are clearly recognized in general (Fig. F29). Demagnetization data from discrete samples above ~ 80 m CSF-A indicate that the characteristic remanent magnetization of the sediments is identified at the 10–20 mT demagnetization steps.

Below ~80 m CSF-A, a zone of diagenetic alteration involving dissolution of remanence carriers reduces remanence intensities after alternating-field (AF) demagnetization of 20 mT to values close to magnetometer noise level in the shipboard environment ( $\sim 1 \times 10^{-5}$  A/m). In this zone, sediment magnetizations have been partly or entirely overprinted during the coring process and remanence inclinations are sometimes steep after AF demagnetization at peak fields of 20 mT. At ~130–140 m CSF-A (Cores 320-U1336A-15H through 16H and 320-U1336B-15H) and below ~160 m CSF-A (Cores 320-U1336A-19H through 21H and 320-U1336B-18H through 20H), polarity reversals are apparently present but the inclinations are steep (up to 80°), indicating that the drilling overprint has not been effectively removed during shipboard demagnetization.

Biostratigraphic datums and magnetostratigraphic results allow the calculation of average linear sedimentation rates (LSRs) that are 9 m/m.y. for the upper 74 m of the section on the corrected CCSF-A depth scale. The LSRs of Site U1336 increase from 12 m/m.y. in the lower Miocene and to 15 m/m.y. in the Oligocene. There are no apparent hiatuses at the shipboard biostratigraphic resolution.

A complete physical property program was conducted on whole cores, split cores, and discrete samples. Physical properties measurements on whole-round sections and samples from split cores reflect the differences among lithologies drilled at Site U1336 (Fig. F29). Nannofossil ooze with varying amounts of clay, radiolarians, and diatoms makes up lithologic Unit I and is characterized by high-amplitude and high-frequency variations in bulk density, magnetic susceptibility, natural gamma radiation (NGR), and color reflectance. Magnetic susceptibility is highest in Unit I, with values ranging from  $5 \times 10^{-5}$  to  $30 \times 10^{-5}$  SI. Natural gamma radiation is also high in this unit, with values to 56 cps near the seafloor. Wet-bulk densities are lowest in Unit I, with values ranging from 1.4 to 1.7 g/cm<sup>3</sup>. Porosity is highest in this interval, ranging from 65% to 80%. The grain density of most of the sediments of Unit I, as well as Units II and III, range from 2.6 to 2.9 g/cm<sup>3</sup>, reflecting the dominance of carbonate constituents at Site U1336. The sediment velocity in Unit I is low, averaging 1500 m/s. The

color reflectance of Unit I is marked by luminance ( $L^*$ ) values that are slightly lower and more variable than values determined for sediments in Units II and III.

Below Unit I, a more uniform increase in wet bulk density and decrease in porosity in Units II and III reflect the increasing compaction of the sediments. A slight step increase in wet bulk density marks the transition between Units II and III. In Unit III wet bulk density and porosity average  $1.9 \text{ g/cm}^3$  and 51%, respectively. Magnetic susceptibility and NGR are low and nearly uniform in Units II and III. Magnetic susceptibility typically is below  $5 \times 10^{-5}$  SI, and NGR is  $\sim 2$  cps. Lower clay abundance in Unit II is marked by an increase in  $L^*$  at the boundary between Units I and II. At 92 m CFS-A, within Unit II, sharp decreases in the  $a^*$  and  $b^*$  reflectance parameters mark the change in sediment color from pale yellow to greenish gray. One of the most pronounced changes in physical properties at Site U1336 is the sharp increase in velocity that accompanies the change from nannofossil ooze to nannofossil chalk at the boundary between Units II and III. The velocity at the base of Unit II is  $\sim 1700$  m/s. Below 190 m CFS-A, in Unit III, the rate at which velocity increases with depth increases, ultimately reaching  $\sim 2200$  m/s at 290 m CFS-A, near the base of Hole U1336A.

Special Task Multi Sensor Logger (STMSL) data were collected at 5 cm intervals from Hole U1336B and compared to the Whole-Round MultiSensor Logger WRMSL data obtained at 2.5 cm resolution from Hole U1336A during Expedition 320. Features in the magnetic susceptibility and gamma ray attenuation density are well aligned between Holes U1336A and U1336B down to a depth of  $\sim 94$  m CCSF-A. Below 94 m CCSF-A the magnetic susceptibility signal drops to very low values but the density data are good enough to sustain a correlation to interval U1334B-14H-4, 122 cm. At this point (138.50 m CCSF-A) sediments recovered in both holes are disturbed.

Paleomagnetic reversals were used to calculate the average LSRs for the upper 74 m of the section at Site U1336 on the corrected CCSF-A depth scale. Below 74 m CSF-A only biostratigraphic datums were used to calculate the average LSRs. The LSR at Site U1336 decreases from 15 m/m.y. in the upper Oligocene to 12 m/m.y. in the lower Miocene and stays relatively constant at 9 m/m.y. in the remainder of the section.

A standard geochemical analysis of pore water and organic and inorganic properties was undertaken on Site U1336 sediments. Twenty two interstitial whole-round water samples from Hole 1336B were analyzed. Chlorinity values distinctly increase from  $\sim 555$  to  $\sim 570$  mM in the uppermost 40 m CSF-A, potentially reflecting the boundary condition change from the more saline ocean at the last glacial maximum to the pres-

ent. Alkalinity is relatively constant at values  $>2.5$  mM in the upper 110 m CSF-A, with a pronounced decline to 1 mM by 170 m CSF-A. Sulfate concentrations decrease with depth to values as low as 22 mM. Dissolved phosphate concentrations are  $\sim 5$   $\mu\text{M}$  at  $\sim 9$  m CSF-A, decreasing to values of  $\sim 1$   $\mu\text{M}$  by  $\sim 15$  m CSF-A. Dissolved manganese has a broad peak in the depth range from  $\sim 25$ – $120$  m CSF-A, and dissolved iron appears then peaks below 100 m CSF-A. The increase of dissolved Fe occurs where Mn decreases downhole. Concentrations of dissolved silicate increase with depth from  $<400$  to 800  $\mu\text{M}$ .

### ***Highlights***

#### **Miocene sedimentary section and cyclic sedimentations**

One of the highlights from Site U1336 is the recovery of a thick Miocene carbonate section from the central equatorial Pacific, one of the high priority objectives of the PEAT program. We recovered the complete early Miocene sequence ( $\sim 9$  m.y. duration) in a  $\sim 110$  m thick section, with a sedimentation rate of 12 m/m.y. and the middle Miocene sequence (4.5 m.y. duration) in a  $\sim 45$  m thick with a sedimentation rate of  $\sim 21$  m/m.y. These high sedimentation rates will facilitate the study of paleoceanographic processes at unprecedented resolution for the equatorial Pacific.

The obvious variations of both color and biogenic composition within nannofossil oozes represent cyclically changing fluctuations of CCD and upwelling intensity during the middle Miocene through early Miocene. The variable lithology also results in the variations of many petrophysical signals of physical properties including  $L^*$ ,  $b^*$ , magnetic susceptibility, NGR, and gamma ray attenuation (GRA) bulk density. These high sedimentation–rate cyclically deposited sediments will facilitate the study of paleoceanographic processes at unprecedented resolution for the equatorial Pacific.

#### **Oligocene–Miocene transitions and depth transects**

Site U1336 was planned as part of a latitudinal transect for early Miocene age slices and the PEAT Oligocene–Miocene depth transect in conjunction with Sites U1335 and U1337. The Miocene sequence at these sites includes the critical intervals of the Mi-1 glaciation and middle Miocene ice sheet expansion (Holbourn et al., 2005; Zachos et al., 2001b; Pälike et al., 2006a). The dominant lithologies of nannofossil ooze and chalk at Sites U1336 and U1335, with better preservation of calcareous microfossils than any other site drilled during Expedition 320, will allow us to achieve the prime objective for this coring site.

The Oligocene–Miocene transition in Hole U1336A occurs in homogeneous nanofossil ooze within the alternations of white and light greenish gray ooze. The same alternating sequence is observed above the Oligocene–Miocene transition at Site U1334. Biostratigraphy reveals that the Oligocene/Miocene boundary exists between 142.96 and 145.9 m CSF-A at Site U1336; this will allow the high-resolution study of this critical interval.

### **Geochemical front**

Site U1336 recovered an interval of greenish gray carbonates that exhibit a distinct Mn increase and elevated Fe pore water concentrations with similar characteristics as geochemical alteration fronts at Sites U1334 and U1335. At Site U1336, this zone is ~200 m thick. The paleomagnetic signal is very weak in most parts of this section (80–160 m CSF-A). High amounts of dissolved Fe and Mn in pore water is probably caused by changes in the oxidation state in the sediments. The oxidation-reduction reactions are likely fueled by enhanced availability of organic carbon in overlying and underlying sediments. This site may provide the opportunity to study organic matter degradation.

Site U1336 migrated from south to north through the equatorial belt of high productivity. Based on paleolatitude reconstructions these geochemical alteration fronts can be mapped to similar equatorial positions between Sites U1334 and U1335, roughly between the Equator and ~4°N.

### **Chert formation in the early Oligocene**

The sequence at Site U1336 includes barren intervals of radiolarian fossils and many thin intercalated chert layers and fragments. The radiolarians decrease in preservation downsection and disappear below Core 320-U1336A-19H. Instead, the sediments contain several chert fragments. Some inferred chert layers occur at ~120–140 m CSF-A and blocked APC penetration. Below ~190 m CSF-A, various colored chert layers and fragments occurred within the cores. The chert frequently contains foraminifer tests, reflecting diagenetic process of dissolution and reprecipitation of the biogenic silica.

The dissolution of biogenic silica is the source of porcellanite and chert and, on crust younger than 65 Ma, almost all cherts in the Pacific Ocean lie <150 m above basement. Although we did not recover basement rocks at this site, the sediments became hard, lithified limestones and the drilled section is probably close to basement. The

dissolution of silica in the basal sedimentary section is likely associated with the circulation of warm hydrothermal waters in the upper oceanic crust that extend into the lower sediments where they are cut by fractures and faults (Moore, 2008a, 2008b). This site will provide information on chert formation in the equatorial Pacific regions.

## Site U1337

### *Science summary*

The latest Oligocene through the middle Miocene appears to have been a time of relative warmth comparable to the latest Eocene. However, variability in the isotopic record of the early to middle Miocene is larger than that of the Eocene and may indicate more variability in climate and global ice volume. Site U1337 (proposed Site PEAT-7C; 3°50.009'N, 123°12.352'W; 4463 m water depth) was targeted to collect an early middle Miocene segment of the PEAT equatorial megasplice on ~24 Ma crust between the Galapagos and Clipperton Fracture Zones, ~390 km southeast of Site U1335. In conjunction with Sites U1335 and U1336, it was also designed to provide a latitudinal transect for early Miocene age slices. The recovered sediment column at Site U1337 represents a nearly complete and continuous Neogene sedimentary section.

### *Operations*

Four holes were cored at Site U1337. At Hole U1337A, APC cores were taken from the seafloor to 195.5 m drilling depth below seafloor (DSF) (Cores 321-U1337A-1H through 21H). Nonmagnetic core barrels were used for all APC cores except for Core 321-U1337A-21H. FlexIt core orientation was conducted for all cores except 321-U1337A-1H. In addition, five successful advanced piston corer temperature tool (APCT-3) temperature measurements were taken with Cores 321-U1337A-5H, 7H, 9H, 11H, and 13H. XCB coring continued with Cores 321-U1337A-22X through 48X. The sediment/basement contact was recovered at the base of Core 321-U1337A-48X. Three logging strings (triple combination [triple combo], vertical seismic imager (VSI), and FMS-sonic) were deployed in Hole U1337A.

In Hole U1337B, APC cores were taken from the seafloor to 245.2 m DSF (Cores 321-U1337B-1H through 27H). Nonmagnetic core barrels were used through Core 321-U1337B-20H. The FlexIt core orientation system was deployed successfully for all but two APC cores (321-U1337B-17H and 18H). FlexIt and steel core barrels were used through Core 321-U1337B-27H. APCT-3 temperature measurements were obtained

with Cores 321-U1337B-15H, 17H, and 19H. Coring continued with a single XCB core (321-U1337B-28X) to 251.9 m DSF; however, this barrel could not be recovered and Hole U1337B was abandoned prematurely.

Hole U1337C was cored to recover sections that were missing from Holes U1337A and U1337B. APC cores were taken from the seafloor to 11.4 m DSF (Cores 321-U1337C-1H through 2H) using nonmagnetic core barrels and the FlexIt core orientation system. A wash barrel (Core 321-U1337C-3W) was then deployed, and the hole was washed to a depth of 169.4 m DSF. APC coring resumed at that depth and continued through Core 321-U1337C-9H to 221.3 m DSF and then switched to steel core barrels. Coring with the XCB system continued with Cores 321-U1337C-10X through 33X. Basement was recovered in Core 321-U1337C-33X.

Hole U1337D was planned to target the few remaining areas that had yet to be fully recovered and to duplicate recovery through those sections of the formation already recovered to provide additional sample material. The most troublesome material encountered in the previous holes was the large diatom mats located directly above and below a hard ~0.4 m thick porcellanite (baby chert) layer. In Hole U1337D, APC cores were taken from the seafloor to 237.7 m DSF (Cores 321-U1337D-1H to 26H). Nonmagnetic core barrels were used through Core 321-U1337D-20H. The first XCB core (321-U1337D-27X) was designed to only core through the hard ~0.4 m thick baby chert layer. The APC was once again deployed and cored to 267.0 m DSF (Cores 321-U1337D-28H through 30H). At this point the XCB coring system was once again deployed for Cores 321-U1337D-31X through 49X to a total depth of 442.9 m DSF. The FlexIt core orientation system was deployed successfully with all APC cores. The Sediment Temperature Tool (SET) was deployed for the first time from the *JOIDES Resolution* after Core 321-U1337D-17X at 298.1 m DSF.

### **Lithostratigraphy**

At Site U1337, latest Oligocene seafloor basalt is overlain by ~450 m of nannofossil and biosiliceous oozes and nannofossil chinks that are divided into four lithologic units (Fig. F30). The Pleistocene through uppermost Miocene sediments of Unit I are characterized by multicolored (various hues of white, brown, green, and gray) nannofossil oozes, diatom oozes, and radiolarian oozes that alternate on meter scales with a general downsection increase in siliceous microfossils relative to nannofossils. Green and gray biosiliceous lithologies, interbedded on meter scales with white and light greenish gray nannofossil ooze, comprise the dominant sedimentary constituents in the uppermost Miocene to middle Miocene Unit II, which includes regular di-

atom mat deposits. Meter-scale color alternations in Units I and II are associated with variations in lithology and physical properties. However, similar to the common millimeter- and centimeter-scale color banding that do not mark compositional changes, they are likely associated with sediment redox conditions. White, pale yellow, and pale green nannofossil oozes and chalks dominate the sediments of middle Miocene to latest Oligocene age, although diatoms and radiolarians remain present in low abundances. Latest Oligocene seafloor basalt (Unit IV) was recovered at the base of the sedimentary section.

### Biostratigraphy

All major microfossil groups have been found in the sediments recovered at Site U1337. Planktonic foraminifers at Site U1337 are rare to abundant with poor to good preservation throughout most of the succession but are absent or extremely rare in some intervals of the late Miocene and early Miocene. Biozones PT1b to O6 are recognized, with the exception of Zones PL4, M12, and M3 (Fig. F30). Calcareous nannofossils at Site U1337 are moderately to poorly preserved and some samples with high silica content are barren. Nannofossil Zones NN1 to NN21 are present, indicating an apparently complete sequence. The radiolarian stratigraphy at Site U1337 spans the interval from the uppermost part of Zone RN16-17 (upper Pleistocene) to RN1 (lower Miocene). The radiolarian assemblages of Pleistocene to upper Miocene age tend to have good preservation, whereas middle to lower Miocene assemblages show moderate preservation. In the lowermost part of the section, above the basement, sediments are barren of radiolarians. The high-resolution diatom stratigraphy at Site U1337 spans the interval from the *Fragilariopsis (Pseudoeunotia) doliolus* zone (upper Pleistocene) to the lowermost part of the *Craspedodiscus elegans* zone (lower Miocene). The diatom assemblage is generally well to moderately preserved throughout the recovered section; however, there are several intervals in which valve preservation becomes moderate to poor. The base of the sediment column is barren of diatoms. The nannofossil, foraminifer, radiolarian, and diatom datums and zonal schemes generally agree, though some discrepancies occur in the lowest part of the core. Benthic foraminifers occur continuously throughout the succession recovered in Hole U1337A and show good to moderate preservation. The overall assemblage composition indicates lower bathyal to abyssal paleodepths. Marked variations in downcore abundance and species distribution reflect major changes in global climate linked to fluctuations in ice volume and reorganization of Pacific circulation during the Neogene.

### Stratigraphic correlation

Stratigraphic correlation provided a complete spliced record to ~220 m CCSF-A. Several gaps (perhaps three) were encountered over the next 50 m CCSF-A. Comparison of GRA density records with well logging density data suggest that no more than 1 m of section was lost in any of the gaps. Correlation between the holes was broken again several times between 440 m CCSF-A and basement at 490 m CCSF-A. Growth factor for the correlation was 1.12. The linear sedimentation rate decreases from ~21 m/m.y. in the middle Miocene to 17 m/m.y. in the late Miocene.

### Paleomagnetism

Paleomagnetic measurements were conducted on archive-half sections of 20 APC cores and 14 XCB cores from Hole U1337A, 27 APC cores from Hole U1337B, 8 APC cores from Hole 1337C, and 30 APC cores from Hole 1337D. The FlexIt core orientation tool was deployed in conjunction with all APC cores, and we conclude that the FlexIt orientation data are generally reliable. Measurements of NRM above ~93 m CSF-A indicate moderate magnetization intensities (on the order of  $10^{-3}$  A/m) with a patchy but generally weak VRM or IRM coring overprint, and polarity reversal sequences from the Brunhes to the bottom of the Gilbert Chron are recognized. Below ~93 m CSF-A, remanence intensities after AF demagnetization of 20 mT are reduced to values close to magnetometer noise level in the shipboard environment ( $\sim 1 \times 10^{-5}$  A/m). In this zone, sediment magnetizations have been partly overprinted during the coring process, and remanence inclinations are occasionally steep after AF demagnetization at peak fields of 20 mT. Nonetheless, polarity reversals are apparently recorded to ~200 m CSF-A and are provisionally correlated to the geomagnetic polarity timescale (GPTS) from Chron C3An to C5n (~6–11 Ma) (Fig. F30). Magnetic polarity interpretation was impossible for APC cores taken with steel core barrels and XCB cores because of severe magnetic overprint during coring.

### Physical properties

Physical property measurements on whole-round sections and samples from split cores display a strong lithology-dependent variation at Site U1337 (Fig. F30). Variations in the abundances of nannofossils, radiolarians, diatoms, and clay in Unit I account for high-amplitude, high-frequency variations of all physical properties. Intervals enriched in biogenic silica and clay generally display lower grain density and bulk density and higher porosity, magnetic susceptibility, and NGR. Velocity is generally directly related to bulk density; however, it is commonly higher in low-den-

sity siliceous-rich sediments than it is in more calcareous intervals. Wet bulk density is low in Unit I, ranging from 1.12 to 1.46 g/cm<sup>3</sup>. Porosity is as high as 92% in this unit. Velocity also is low, averaging 1525 m/s. The natural gamma record, as at previous Expedition 320/321 sites, is marked by an anomalously high near-surface peak (~65 cps). Magnetic susceptibility varies between  $4 \times 10^{-5}$  and  $18 \times 10^{-5}$  SI. The color of Unit I is characterized by the lowest L\* and high and variable a\* and b\* values. Unit II is characterized by a continued high variability in grain density. Together, the grain density in Units I and II averages 2.51 g/cm<sup>3</sup> and ranges from 2.17 to 2.85 g/cm<sup>3</sup>. All other physical properties display less variability in Unit II than in Unit I, reflecting a less variable lithology. Wet bulk density increases and porosity decreases with depth in Unit II; however, in Units II and III these trends are interrupted by low-density, high-porosity diatom- and radiolarian-rich intervals. Unit II is slightly lighter colored (lower L\*) and distinctly more blue (lower a\*) and green (lower b\*) than Unit I. Unit III is characterized by more uniform physical properties that accompany the high and uniform carbonate composition of the unit. The nannofossil oozes and chinks of this unit are characterized by a uniform grain density that averages 2.67 g/cm<sup>3</sup>. The bulk density and porosity trends of Unit II continue in Unit III. The transition from ooze to chalk is marked by a change in gradient of these properties to a more rapid decrease in wet bulk density and an increase in porosity with depth. Wet bulk density and porosity at the base of the sediment section are 1.95 g/cm<sup>3</sup> and 47%, respectively. The increase in velocity with depth also changes to a higher gradient in Unit III, with values increasing from 1510 m/s at ~340 m CSF-A to ~1800 m/s near the base of the hole. Magnetic susceptibility and NGR values remain low in Unit III but do vary in response to small changes in lithology. The sharp color change from greenish gray to pale yellow at ~410 m CSF-A is marked by a sharp increase in a\* and b\*. The change in color to pale brown chalk immediately above basement is marked by an increase in both a\* and b\* and a decrease in L\*.

### **Downhole logging**

Downhole logging consisted of deploying three tool strings in Hole U1337A. Two tool strings took downhole measurements of natural gamma ray radioactivity, bulk density, electrical resistivity, elastic wave velocity, and borehole resistivity images in the 77–442 m wireline log depth below seafloor (WSF) depth interval. The third tool string measured seismic waveforms in a VSP experiment in the 214–439 m WSF depth interval. Measurement depths were adjusted to match across different logging runs, obtaining a wireline log matched depth below seafloor (WMSF) depth scale. The downhole log measurements were used to define three logging units. Unit I (77–212

m WMSF) and Unit II (212–339 m WMSF) have average densities of  $\sim 1.3$  and  $\sim 1.6$  g/cm<sup>3</sup>, respectively, that do not show any trend with depth, whereas Unit III (339–442 m WMSF) density increases with depth reaching 1.85 g/cm<sup>3</sup> at the base of the hole (Fig. F31). Resistivity and *P*-wave velocity follow a pattern similar to that of density, suggesting that the major control on these physical properties are variations in sediment porosity. Natural gamma ray measurements are low throughout the logged interval ( $\sim 5^\circ$  gAPI), except for two pronounced peaks caused by uranium, one at the seafloor and the other at 240 m WMSF. The gamma ray peak at 240 m WMSF corresponds to the  $\sim 40$  cm thick baby chert layer that has only been recovered as rubble in the cores but can be clearly identified in the downhole logs and borehole images as an interval of high density and resistivity. VSP logging measured arrival time of the seismic pulse from the sea surface at 16 stations. Together with the traveltime to the seafloor, VSP measurements are the basis for a traveltime-depth conversion that allows seismic reflectors to be correlated to stratigraphic events. Downhole temperature measurements and thermal conductivities of core samples were combined to estimate a geothermal gradient of 32.4°C/km and a heat flow of 28.4 mW/m<sup>2</sup> at Site U1337.

### Geochemistry

A total of 85 interstitial water samples were collected from Hole U1337A, 49 using the whole-round squeezing approach across the entire hole and 36 in the upper 100 m by Rhizon sampling. Chloride ion concentration (not corrected for Br contribution) varies slightly with depth and ranges from 554 to 566 mM. Alkalinity increases slightly downhole from  $\sim 2.7$  mM in the upper 100 m to values scattered around 3.8 mM below 300 m CSF-A. Sulfate concentrations vary between 26 and 29 mM, with slightly decreasing values with depth. An enormous dissolved manganese peak of  $\sim 150$  mM at 13 m CSF-A is captured by the high-resolution interstitial water sampling. Dissolved iron is sporadically detectable in the upper 200 m and then increases to a peak of  $\sim 5$  mM between 275 and 300 m CSF-A before becoming undetectable again below 400 m CSF-A. Nitrate concentrations are low and variable except for higher values at the top and bottom of the sediment column. These variations in nitrate, manganese, and iron reflect changes in redox chemistry that also manifest as changes in sediment color. The silicic acid (dissolved silicate) content of the interstitial waters is substantially greater than that of bottom waters (e.g., Peng et al., 1993) and increases with depth from  $\sim 700$   $\mu$ M in the uppermost sediments to peak at  $\sim 1200$   $\mu$ M at  $\sim 350$  m CSF-A before decreasing to  $\sim 900$   $\mu$ M near the basaltic basement. Calcium carbonate and inorganic carbon concentrations were determined on 283 and 28 sediment samples from Holes U1337A and U1337B, respectively. Calcium carbonate concentrations

vary greatly in the upper two lithologic units, ranging from 30% to 90%, reflecting the alternation between calcite and opal producers (Fig. F30). In lithologic Unit III calcium carbonate contents are generally high, scattered around 80%, but a distinctive decrease is observed between 350 and 400 m CCSF-A. The concentration of TOC was determined for 47 sediment samples from Holes U1337A and U1337B. In the upper 235 m CCSF-A, TOC content ranges between 0.10% and 0.34% except for the high value of 0.72% in the uppermost sample. TOC content increases at 44.00 m CCSF-A and in the interval from 87.28 to 108.59 m CCSF-A. Below 235 m CCSF-A, TOC values are generally <0.10%.

Shipboard geochemical analyses of interstitial water and bulk sediment samples reflect large variations in sediment composition resulting from shifts in carbonate versus opal primary production. The large-scale redox state and diagenetic processes of the sediment column are related to overall changes in sediment composition. Interstitial water chemistry is also influenced by the baby chert layer forming a diffusive boundary at ~240 m CSF-A and seawater circulation in the basement. The basement itself appears to exert little influence on the geochemistry of sediments and interstitial waters.

## **Highlights**

### **Diatom mat deposition**

Lithologic Unit II at Site U1337 is mostly composed of biosiliceous lithologies, notably diatoms. The abundance of diatoms in the middle and upper Miocene section at Site U1337 is much higher than encountered in any interval at Sites U1331–U1336. Several decimeter- to meter-scale intervals of diatom ooze are laminated, and smear slide analyses indicate that the diatom assemblage is composed primarily of pennate taxa, with abundant “needlelike” *Thalassiothrix* spp., indicating diatom mat deposition. The lowermost laminated diatom mat is in the upper portion of Unit III at ~15 Ma. Much larger intervals are present in Unit II at roughly 10 Ma and shorter intervals at ~4.5 Ma. Ages of laminated diatom mats at this site are similar to those found at Leg 138 sites farther to the east (Mayer, Pisias, Janecek, et al., 1992), which have been interpreted to reflect regional bursts of export silica production in the eastern equatorial Pacific (Kemp and Baldauf, 1993). No laminated diatom oozes were recorded during Expedition 320 at drill sites farther to the northwest; however, near 10 Ma at Site U1335, drilling recovered clayey diatom ooze and clayey radiolarian ooze containing no carbonate at all, suggesting that dissolution may also play an important role in the deposition of laminated diatom mats.

### **Oligocene–Miocene transition**

The Oligocene/Miocene boundary was recovered in Holes U1337A, U1337C, and U1337D. In Hole U1337A, the Oligocene/Miocene boundary is estimated to fall between Samples 321-U1337A-48X-2, 85–87 cm, and -48X-3, 55 cm (445.56–446.75 m CSF-A; 490.92–492.11 CCSF-A). It occurs in white (2.5Y 8/1) nannofossil chalk with foraminifers, interbedded and heavily mottled with pale yellow (2.5Y 7/4) to very pale brown (10YR 7/4) nannofossil chalk. Abundant millimeter-scale dendritic manganese grains composed of manganese oxide occur throughout this interval. The lower 15 cm of the core catcher of this core represents basement. No prominent change in lithology, GRA bulk density, reflectance, or magnetic susceptibility is seen through the Oligocene–Miocene transition.

### **Neogene carbonate dissolution**

The CCD of the Neogene is much more stable than that of the Eocene, but there are intervals of lower carbonate deposition at Site U1337 that probably represent significant changes of the Neogene CCD. In the early Miocene, a significant carbonate low reaches its minimum at ~17 Ma (340 m CSF-A in Hole U1337A), when the site was at a depth of ~3500 meters below sea level. This early Miocene interval marks a strong minimum at Site U1334 as well, on crust with a depth of ~4000 m at that time. Highly variable carbonate is also characteristic of the late/middle Miocene boundary, but the role of carbonate dissolution versus elevated deposition of biosilica needs to be determined.

## **Site U1338**

### ***Science summary***

Site U1338 (proposed Site PEAT-8D; 2°30.469'N, 117°58.178'W; 4200 m water depth) was sited to collect an 3–18 Ma segment of the PEAT equatorial megasplince and is located on ~18 Ma crust just north of the Galapagos Fracture Zone, 324 nmi (600 km) southeast of Site U1337. A seamount (3.7 km water depth) with surrounding moat is found ~25 km to the north-northwest of Site U1338 at the downslope end of the survey area. Originally a site was chosen ~10 km from the seamount (proposed Site PEAT-8C). However, the alternate proposed site was selected and drilled uphill and further away from the seamount to avoid possible turbidites, as were found near seamounts during drilling of Expedition 320 Sites U1331 and U1335. The recovered sediment

column at Site U1338 represents a nearly complete and continuous early Miocene to Holocene sedimentary section.

## Operations

Four holes were cored at Site U1338. From Hole U1338A, APC cores were taken from the seafloor to 221.2 m DSF (Cores 321-U1338A-1H through 24H) using nonmagnetic core barrels and the FlexIt core orientation system installed. FlexIt and steel core barrels were used for Cores 321-U1338A-25H and 26H. In addition, five successful APCT-3 temperature measurements were taken with Cores 321-U1338A-5H, 7H, 9H, 11H, and 13H. XCB coring continued with Cores 321-U1338A-27X through 44X. A small piece of basement was recovered in the core catcher of Core 321-U1338A-44X.

From Hole U1337B, APC cores were taken from the seafloor to 188.1 m DSF (Cores 321-U1338B-1H through 20H) except for a short drilled interval of 2.5 m from 235.6 to 238.1 m DSF to adjust the core breaks. Nonmagnetic core barrels and the FlexIt core orientation system were used through Core 321-U1338B-20H. FlexIt and steel core barrels continued through Core 321-U1338B-42H to 387.4 m DSF. Coring continued with three XCB cores (321-U1338B-43X through 45X) to 416.1 m DSF. Basement contact was recovered in Core 321-U1338B-45X. Three logging strings (triple combo, VSI, and FMS-sonic) were deployed in Hole U1338B.

Hole U1338C was cored to recover sections that were missing from Holes U1338A and U1338B. APC cores were taken from the seafloor to 189.8 m DSF (Cores 321-U1338C-1H through 21H) using nonmagnetic core barrels and the FlexIt core orientation system. FlexIt and steel core barrels were used through Core 321-U1338C-44H to 396.9 m DSF. Coring continued through Core 321-U1338C-47H to a total depth of 414.4 m DSF, setting a new all time depth record for the APC.

Hole U1338D was primarily planned to recover a few “instructional” cores to be used during Expedition 323. Three APC cores were cut to 23.9 m DSF.

## Lithostratigraphy

At Site U1338, ~415 m of nannofossil ooze and chalk with varying concentrations of diatoms and radiolarians overlie early Miocene seafloor basalt and are divided into four lithologic units (Fig. F32). Pleistocene through middle Pliocene sediments of Unit I are characterized by multicolored (various hues of white, brown, green, and gray) nannofossil ooze, diatom nannofossil ooze, and radiolarian nannofossil ooze that alternate on a decimeter- to meter-scale. Light green and light gray nannofossil

ooze with occasional darker intervals with abundant siliceous microfossils, notably diatoms, comprise the upper Miocene to middle Pliocene Unit II. Decimeter-, meter- and tens of meters-scale color alternations in Units I and II are associated with variations in lithology and physical properties. Some of these color changes, as well as common millimeter- and centimeter-scale color banding, are not associated with compositional changes and likely reflect variations in sediment redox state. White, pale yellow, light greenish gray, and very pale brown nannofossil oozes and chalks dominate Unit III of lower to upper Miocene, although slightly darker green and gray intervals with larger amounts of siliceous microfossils remain present. Lower Miocene seafloor basalt (Unit IV) was recovered at the base of the sedimentary section.

### Biostratigraphy

All major microfossil groups have been found in the ~415 m thick succession of Holocene to lower Miocene sediment bulge recovered from Site U1338. Calcareous nannofossils at Site U1338 are in general moderately preserved, but there are some intervals in which the preservation is good or poor. Nannofossil Zones NN4 to NN21 are present, indicating an apparently complete sequence. Planktonic foraminifers vary from rare to abundant, with moderate to good preservation throughout most of the succession, but are absent or rare in a short interval in the late Miocene. Planktonic foraminifer Zones PT1b (late Pleistocene) to M2 (early Miocene) are documented, with the exception of Zones PL4, M12, and M6. The radiolarian stratigraphy spans the interval from the uppermost part of Zone RN16–17 (late Pleistocene) to the uppermost part of Zone RN3 (early Miocene). Radiolarian assemblages show good to moderate preservation except in the lowermost portion (early Miocene), which is barren of radiolarians. The high resolution diatom stratigraphy spans the interval from the *Fragilariopsis (Pseudoeunotia) doliolus* zone (late Pleistocene) to the lowermost part of the *Craspedodiscus elegans* zone (early Miocene). The diatom assemblage is generally well to moderately preserved throughout the recovered section; however, there are several intervals in which valve preservation becomes moderate to poor. The nannofossil, foraminifer, radiolarian, and diatom datums and zonal schemes generally agree, with some inconsistencies (Fig. F32). Benthic foraminifers occur continuously throughout the succession recovered in Hole U1338A and show generally good preservation. The overall assemblage composition indicates lower bathyal to abyssal paleodepths. Marked variations in downcore abundance and species distribution reflect major changes in global climate linked to fluctuations in ice volume and reorganization of Pacific Ocean circulation during the Neogene.

### Stratigraphic correlation

Stratigraphic correlation provided a complete spliced record to a depth of ~260 m CCSF-A. Several gaps were seen between 280 and 360 m CCSF-A. Comparison of GRA density records with well logging density data suggests that no more than 1 m of section was lost in any of the gaps. Correlation between the holes was broken again several times between 435 m CCSF-A and basement at 460 m CCSF-A. Growth factor for the correlation was 1.11. The linear sedimentation rate decreases from ~29 m/m.y. in the Miocene to 13 m/m.y. in the Pliocene-Pleistocene.

### Paleomagnetism

Paleomagnetic measurements were conducted on archive-half sections of 26 APC cores from Hole U1338A, 42 APC cores from Hole U1338B, and 47 APC cores from Hole U1338C. The FlexIt core orientation system was deployed in conjunction with all APC cores except for the deepest three cores of Hole U1338C, and we conclude that the FlexIt orientation data are generally reliable. NRM measurements indicate moderate magnetization intensities (on the order of  $10^{-3}$  A/m) for depth intervals 0–50, 280–225, and 295–395 m CSF-A. Polarity reversal sequences of these intervals are provisionally correlated to the Brunhes to the upper part of the Gilbert Chron (0 to ~4 Ma), Chron C4An to C5n (~9–11 Ma), and Chron C5r to C5Br (~12–16 Ma) of the GPTS, respectively (Fig. F32). Except for these intervals, remanence intensities after AF demagnetization of 20 mT are reduced to values close to magnetometer noise level in the shipboard environment ( $\sim 1 \times 10^{-5}$  A/m). Magnetization directions are dispersed and not interpretable there. Sedimentation rates increase downcore from ~12 m/m.y. at the top to ~30 m/m.y. near the bottom.

### Physical properties

Physical properties measurements on whole-round sections and samples from split cores display a variation strongly dependent on the relative abundance of biosiliceous and calcareous sediment components at Site U1338. As at Site U1337, intervals enriched in siliceous microfossils and clay generally display darker colors, lower grain density and bulk density, and higher porosity, magnetic susceptibility, and NGR. The variation of velocity is more complex in that it is dependent on both the wet bulk density and the sediment rigidity. These parameters vary independently with the variation in abundance of biosiliceous and calcareous components. The physical properties at Site U1338 also display cyclicity on multiple scales, a decimeter to meter scale and a scale with a spacing on the order of tens of meters.

Lithologic Unit I at Site U1338 is characterized by low wet bulk density that decreases from 1.4 g/cm<sup>3</sup> near the seafloor to 1.2 g/cm<sup>3</sup> at the base of the unit as a result of an increasing abundance of radiolarians and diatoms with depth. The grain density in Units I and II displays a greater variability than is found deeper at the site as a result of the greater variability in the abundance of biosiliceous and calcareous components. The average grain density for Units I and II is relatively low, at 2.59 g/cm<sup>3</sup>. The NGR signal at Site U1338 is characterized by a near-seafloor peak that is somewhat lower than those recorded at the other PEAT drill sites but extends deeper and is marked by a double peak. Spectral reflectance measurements show that Unit I is characterized by lower L\* and higher a\* and b\* values in the upper 25 m of Unit I (Fig. F32). Below 25 m CSF-A, the sediment becomes lighter colored (L\* increases) and more bluish green (a\* and b\* decrease).

Unit II is characterized by increasing wet bulk density with depth to ~175 m CSF-A. Below this depth, an increase in the abundance of siliceous microfossils produces a broad density minimum. Magnetic susceptibility and NGR signals are low in Unit II to the depth at which the biosiliceous material increases in abundance. The interval of the broad density minimum is characterized by higher magnetic susceptibility values that are roughly equal to those in the upper 25 m of Unit I. Unit II is lighter colored than Unit I (higher L\*) and more blue (lower b\*).

Unit III at Site U1338 is characterized by a higher and more uniform carbonate content and, as a result, more uniform physical properties. Wet bulk density increases from ~1.5 g/cm<sup>3</sup> at the top of Unit III to 1.7 g/cm<sup>3</sup> at the base of the unit. Grain density varies over a narrower range in Unit III than it does in Units I and II and displays an average (2.64 g/cm<sup>3</sup>) nearer to that of calcite. Velocity, which through much of Units I and II is close to the velocity of water, displays a regular increase in Unit III, from ~1620 m/s at the top to ~1820 m/s near the base of the unit. Velocity gradient increases near the base of Unit III accompanying the transition from nannofossil ooze to chalk. Magnetic susceptibility is low from the boundary between Units II and III, at ~245 m CSF-A, to 300 m CSF-A. Below 300 m CSF-A, susceptibility again increases to values comparable to those in the upper part of Unit I. NGR variability is lower in Unit III than in Unit II and remains uniformly low throughout the unit. Overall, Unit III is the lightest colored (highest L\* values) unit at Site U1338. The transition from greenish gray to pale yellow is marked at ~385 m CSF-A by a shift to higher values of both a\* and b\*.

## Downhole logging

Downhole logging of Hole U1338B began after the end of APC/XCB coring to a total depth of 416.1 m DSF. Three tool strings were deployed in Hole U1338B: a modified triple combo (that did not include a neutron porosity measurement), a FMS-sonic combination, and a VSI seismic tool with a Scintillation Gamma Ray (SGT-N) sonde. The modified triple combo and FMS-sonic tool strings took downhole measurements of natural gamma ray radioactivity, bulk density, electrical resistivity, elastic wave velocity, and borehole resistivity images in the 125–413 m WSF depth interval. The VSI seismic tool string measured seismic waveforms in a VSP experiment that covered the 189.5–414.5 m WSF depth interval. Measurement depths were adjusted to match across different logging runs, obtaining the WMSF depth scale.

Downhole log measurements were used to define three logging units: Unit I (139–244 m WMSF) and Unit II (244–380 m WMSF) have average densities of  $\sim 1.45$  and  $\sim 1.6$  g/cm<sup>3</sup>, respectively, that do not show any trend with depth, whereas in Unit III (from 380 m WMSF) density increases with depth, reaching 1.7 g/cm<sup>3</sup> at the base of the hole (Fig. F33). Resistivity and *P*-wave velocity follow a pattern similar to that of density throughout the logged interval, suggesting that the major control on these physical properties are variations in sediment porosity. Both resistivity and density measurements show a small-scale peak at 280 m WMSF. This peak at 280 m WMSF is clearly visible in the borehole resistivity images as a high-resistivity layer 16 cm thick, and it corresponds to a chert layer that has only been recovered as rubble in the cores. Natural gamma ray measurements are low throughout ( $\sim 4^\circ$  gAPI) but do show a pronounced high at the seafloor caused by a local increase in uranium concentration.

In the VSP experiment, the arrival time of a seismic pulse was measured from the sea surface at 14 stations. Together with the traveltime to the seafloor, the VSP measurements are the basis for a traveltime-depth conversion that allows seismic reflectors to be correlated to stratigraphic events. Downhole temperature measurements and thermal conductivities of core samples were combined to estimate a geothermal gradient of 34.4°C/km and a heat flow of 33.6 mW/m<sup>2</sup> at Site U1338.

## Geochemistry

A total of 118 interstitial water samples were collected from Holes U1338A and U1338B, 43 using the whole-round squeezing approach and 75 by Rhizon sampling. Chloride ion concentration (not corrected for Br contribution) varies slightly with depth and is generally within 555 to 565 mM. Alkalinity increases slightly downhole

from ~2.7 mM at the sediment–water interface to peak slightly above 4 mM at 140 m CSF-A. A monstrous dissolved manganese peak of 150 mM at 10 m CSF-A is captured by the high-resolution interstitial water sampling and is remarkably similar to that observed at Site U1337. These peaks are >10 times greater than the highest dissolved-manganese concentrations encountered during Expedition 320. Lithium concentrations decrease from ~26  $\mu\text{M}$  at the surface to a minimum of ~ 3  $\mu\text{M}$  at ~250 m CSF-A before increasing sharply with depth to seawater values at the base of the section. The interstitial water strontium profile is a mirror image to that of lithium except the decrease from the peak of 400  $\mu\text{M}$  at 200 m CSF-A is punctuated by a sharp drop of >100  $\mu\text{M}$  between ~260 and 290 m CSF-A. The lithium and strontium profiles indicate seawater circulation in the basement as their values tend toward seawater values near the basement.

Calcium carbonate concentrations range between 26% and 88% with substantial variability in the upper 273.31 m CCSF-A, corresponding to the alternation between calcite and opal production in the upper two lithologic units. Below 273.31 m CCSF-A (lithologic Unit III), calcium carbonate contents become generally high and stable between 66% and 91% compared with the upper part of the stratigraphic column (Fig. F32). In the upper ~230 m CCSF-A, TOC content is generally high and variable ranging between 0.09% and 0.46%, whereas below ~230 m CCSF-A, TOC content is <0.09%. Downhole TOC variability is most likely related to lithologic changes, with higher TOC being found in the more biosiliceous intervals.

Interstitial water and bulk sediment samples reflect large variations in sediment composition resulting from shifts in carbonate versus opal primary production. The large-scale redox state and diagenetic processes of the sediment column are related to overall changes in sediment composition. Interstitial water chemistry points to seawater circulation in the basement, although the basement itself appears to exert little influence on the geochemistry of the sediments and interstitial waters.

## ***Highlights***

### **Color changes, lithology, and redox state**

Smear slide analyses and visual core descriptions show that many of the decimeter-, meter-, and tens of meters-scale color variations in lithologic Units I and II to some extent relate to changes in lithology (e.g., Fig. F32). We suspect, however, that some of these color variations, notably the transitions between pale green and pale yellow

lithologies, are controlled by sediment redox state, similar to those recorded at Sites U1331–U1337 and earlier work in the equatorial Pacific Ocean (e.g., Lyle, 1983).

Magnetic susceptibility is relatively low in the light gray and light brown intervals in Unit I and most of Unit II (Fig. F32). A significant decrease in the intensity of the magnetic signal in Unit II suggests dissolution of magnetite resulting from intensified microbial Fe reduction. In the lower part of Unit III, a sharp downcore transition from green to yellow is not associated with any other lithologic change, does not occur at the same stratigraphic level between holes, and thus should not be considered as an equivalent time horizon. Although pore water Fe concentrations reach 6 to 7  $\mu\text{M/L}$  in the green interval, Fe is absent below the transition to yellow and brown. Although some of this signal may be affected by seawater contamination during XCB drilling in Hole U1338A, all available information suggests that the lowermost color change represents a redox front.

#### Occurrence of diatom rich layers

Lithologic Unit II at Site U1338 is mainly composed of nannofossil ooze with relatively high abundances of biosiliceous components, notably diatoms (Fig. F32). The relative abundance of diatoms is lower than that at Site U1337, and the record lacks laminated diatom ooze intervals (diatom mats) such as those observed at Site U1337. However, centimeter to sometimes 1–2 m thick diatom nannofossil ooze layers containing abundant specimens of *Thalassiothrix* spp. are occasionally interbedded with nannofossil ooze (e.g., ~126.2–127.1 and ~231.8–234.3 m CSF-A in Hole U1338A and ~127.3–128.0 and ~233.8–234.8 m CSF-A in Hole U1338C). Units II and III also contain significant amounts of pyrite, particularly in diatom-rich intervals in Unit II (e.g., Cores 321-U1338B-14H, 19H through 21H, 26H, 28H, 29H, and 32H through 41H). In addition, the middle part of Unit III contains thin intervals of abundant pyrite-filled siliceous microfossils (e.g., intervals 321-U1338B-33H-4, 58–66 cm, and 35H-5, 76–82 cm). These diatom-rich layers, pyrite nodule occurrences, and pyrite-rich siliceous microfossil layers in Units II and III are associated with high TOC content, suggesting a relation between the abundance of diatoms in the sediments, sediment redox state, and the production or preservation of organic carbon.

## Operations

Expedition 321 was the second of two expeditions that comprise the PEAT science program. Expedition 321 began in Honolulu, Hawaii, and drilled eight holes at two sites (U1337 and U1338) (Table T1) before returning to San Diego, California.

### Honolulu port call

Expedition 321 officially began at 0736 h on 4 May 2009, with the first line ashore Pier 2B in Honolulu. The R/V *JOIDES Resolution* arrived a full day early, having been scheduled in at 0700 h 5 May. The early arrival added a bonus day to a schedule that already was planned as a four-day port call.

The ship arrived with two propulsion motors out of service, requiring field coil replacement. This was the first priority activity upon arrival. The first day also included offloading of all refrigerated core samples and replacement of the logging winch transmission. During port call, vendor representatives were aboard to replace the elevator mechanical interlocks with a solenoid actuated variety, balance the HVAC system, and repair and calibrate the Rigwatch rig instrumentation system (RIS). Normal on- and offloading activities took place, including loading of 10 short tons of attapulgite drilling mud left over from the Honolulu 1 port call, and 1537 metric tons of marine gas oil were bunkered. Training was conducted on the Rigwatch RIS and on operation of the Schlumberger logging line winch and wireline heave compensator systems. Other activities included a Det Norske Veritas International Safety Management audit of the ship and the arrival of Center for Deep Earth Exploration engineers to discuss the *JOIDES Resolution's* core winch regenerative braking system and coring tools.

Public relation activities were conducted dockside at the Pier 2B cruise ship terminal, the Waikiki Aquarium, and the Marriott Hotel Waikiki. Several high-level dignitaries and other management personnel, including the directors of the National Science Foundation, Ocean Leadership, the University of Hawaii, and Texas A&M University, were in attendance. Ship tours were conducted for dignitaries as well as University of Hawaii faculty and students and high school students and teachers.

The ship departed Honolulu with the last line away from Pier 2B at 0512 h. At ~10 nmi offshore the ship switched from cruise mode to dynamic positioning (DP) control and lowered thrusters. DP trials were conducted for 7 3/4 h to optimize system

performance after changes in the ship profile were made during the Singapore refit. During this period a representative from L3, the Nautronics parent company, collected data and made adjustments to the internal windage modeling program that impacts the anticipatory commands of the system. The vendor was transferred from the *JOIDES Resolution* to the V/L *Karake* at the Honolulu Harbor outer sea buoy. At 1636 h the vessel got underway for Site U1336. Transit speed en route to the first site averaged 10.7 kt over the 79.0 nmi traversed by midnight on 9 May.

## **Transit to Sites U1336 and U1337**

Transit to Site U1336 (proposed Site PEAT-5C) began at 1636 h on 9 May 2009. Transit to the first drill site continued with speed varying considerably as a result of fluctuating currents and eddies surrounding the Hawaiian Islands. Average transit speeds ranged from 9.9 to 10.7 kt with 135 turns on both shafts. One propulsion motor remained offline as field coil replacement continued. On the morning of 11 May, after several days of discussions with the science team, the decision was made to divert our course from Site U1336 to Site U1337 (proposed Site PEAT-7C). The decision was driven by several issues including (1) slower than anticipated transit speeds to date, (2) time spent conducting automated station keeping sea trials took longer than planned, (3) addition of VSI to the suite of wireline logging tools to be deployed at Site U1337, (4) basement projections deepened by 50 m because of results from Expedition 320, and (5) scientific trade-offs in general between completing Site U1336 more thoroughly versus doing a more complete program at Site U1338. During the transit, routine readiness inspections were conducted by the drill crew on all of the drilling equipment. During the inspection it was discovered that the passive heave compensator rod seals were burned up and required replacement. The ship arrived on location the morning of 19 May. The total 2320 nmi transit was accomplished in 9.8 days at an average speed of 10.0 kt.

## **Site U1337**

Although the Global Positioning System (GPS) was the primary positioning reference used for this site, a new-generation acoustic beacon was also deployed at 1250 h on 19 May 2009. The automated station keeping system can be configured to accept position inputs from both the GPS and the seafloor acoustic beacon. Both inputs were used for Expedition 321.

Four holes were drilled at this site using the APC/XCB coring systems. One hole (U1337B) was terminated early when the XCB core barrel became stuck in the bit seal. This necessitated the drilling of the fourth hole. The cause of the stuck barrel was later identified as an errant APC shear pin stub. The first hole was successfully wireline logged using the triple combo, VSI, and FMS-sonic tool strings. Overall recovery for Site U1337, using both APC and XCB coring systems, was 96.0%. The basement contact was recovered in three of the four holes drilled at the site.

### ***Hole U1337A***

Rig floor operations commenced at 1200 h after the ship was stationary over the location coordinates. The pipe trip to the seafloor was slow because of the need for measuring (strapping) and drifting (internal diameter verification) of all tubulars and the picking up of the drill collars from the main deck storage rack. At 0300 h on 20 May, the top drive was picked up; however, the tilt/counter balance feature was not functional. Troubleshooting and repairing the top drive took 4 h before spacing out the drill string and deploying the first APC core barrel. With the bit positioned at 4467.0 m drilling depth below rig floor (DRF) the first APC barrel was pressured up and fired. Upon recovery, the leading edge of the APC cutting shoe was found severely damaged and the core barrel was empty. To confirm the approximate seafloor depth the drill string was lowered and the mudline was “tagged” twice at about the same depth of 4472.0 m DRF. This depth was taken as the official seafloor depth for the hole, the bit was repositioned 1.0 m lower at 4468.0 m DRF, and Hole U1337A was spudded at 1115 h. Core 321-U1337A-1H recovered 0.19 m of core, and once again the APC cutting shoe showed signs of having impacted something very hard. APC coring continued normally from there, however, and was suspended at 195.5 m DSF because of a 90 klb overpull. Nonmagnetic core barrels were used for all cores except Core 321-U1337A-21H. A 60 klb overpull for Core 321-U1337A-20H led to a return to steel core barrels. Average core recovery for the APC was 101.6%. FlexIt core orientation was conducted for all cores except Core 321-U1337A-1H with apparent good success. In addition, five successful APCT-3 temperature measurements were taken with Cores 321-U1337A-5H, 7H, 9H, 11H, and 13H at 43.5, 62.5, 81.5, 100.5, and 119.5 m DSF, respectively. Only one core liner split (Core 321-U1337A-8H), coincidentally the first barrel shot with all three speed control holes open. XCB coring continued with Cores 321-U1337A-22X through 48X, achieving an average recovery of 87.1%. Two split core liners occurred during XCB coring (Cores 321-U1337A-37X and 38X). There was nothing significant noted in the coring parameters for these two cores other than the fact that Core 321-U1337A-38X achieved only 53% recovery compared to Core 321-

U1337A-37X, which had 101% recovery. The sediment/basement contact was recovered at the base of Core 321-U1337A-48X. Total depth of Hole U1337A was 4921.8 m DRF (449.8 m DSF). Overall recovery for the hole using both APC and XCB coring systems was 93.4%. Rig-up for wireline logging began at 1130 h 23 May. Logging was successfully concluded and all logging equipment was rigged down by 0900 h on 25 May. Three logging strings were deployed. The triple combo reached total hole depth of 449.8 m DSF and obtained good-quality logs. The second logging string consisted of the VSI. This tool also reached total hole depth, and shooting stations were conducted at ~15 m stations. VSI logging was conducted during daylight hours to conform with established IODP mammal watch protocols, including a preshooting mammal watch and soft start procedures for the air guns. The third logging string (FMS-sonic) reached a depth of 440.0 m DSF (<10 m off bottom). With the end of pipe positioned at 82.6 m DSF, there were no reported issues with logging tools reentering the pipe. The drill string was pulled back until the bit cleared the seafloor at 0930 h on 25 May, ending operations in Hole U1337A.

### ***Hole U1337B***

The ship was offset 20 m west of Hole U1337A, and the bit was positioned at a depth of 4473.0 m DRF. This was to optimize the core break placement between the two holes, maximizing recovery of a complete section for the formation. The seafloor “tag” depth of 4472.0 m DRF for Hole U1337A was used for Hole U1337B. APC coring continued through Core 321-U1377B-27H to 245.2 m DSF. The FlexIt core orientation system was deployed successfully for all but two APC cores (321-U1377B-17H and 18H). Nonmagnetic core barrels were used through Core 321-U1377B-20H and successful APCT-3 temperature measurements were obtained with Cores 321-U1377B-15H, 17H, and 19H at 143.5, 162.5, and 181.5 m DSF, respectively. Overpull for the APC ranged from 20 to 90 klb and all but five barrels (Cores 321-U1377B-21H, 23H through 25H, and 27H) achieved full stroke. Two cores (321-U1377B-16H and 22H) were recovered with split liners. The first split occurred after recovery with the sectioned cores in the rack. The latter split occurred in the core barrel prior to extraction. Average core recovery for the APC was 99.3%. Coring continued with a single XCB core (321-U1377B-28X) to 251.9 m DSF; however, this barrel could not be recovered, forcing Hole U1337B to be abandoned prematurely. The drill string was recovered and further analysis indicated that an errant shear pin stub from an earlier piston core had caused the XCB core barrel to jam in the bit seal assembly. Operations in Hole U1337B officially ended at 2245 h on 27 May. Total depth achieved was 4723.9 m DRF (251.9

m DSF). Overall recovery for the hole using both APC and XCB coring systems was 96.6%. The lone XCB core (321-U1377B-28X) recovered nothing.

### ***Hole U1337C***

The ship was offset 20 m west from Hole U1337B and, the drill string was tripped to the seafloor. Hole U1337C was spudded with the bit positioned at 4471.0 m DRF. Recovery from APC Core 321-U1377C-1H established a seafloor depth of 4478.6 m DRF. Core 321-U1377C-2H extended the hole to a depth of 11.4 m DSF using nonmagnetic core barrels and the FlexIt core orientation system. A wash barrel was deployed, and the hole was washed to a depth of 169.4 m DSF. APC coring resumed at that depth and continued through Core 321-U1377C-9H to 221.3 m DSF. Steel core barrels were used at this point because of high overpull >70 klb. Full stroke was achieved with all cores except Core 321-U1377C-6H, which was advanced by recovery. Average core recovery for the APC was 102.6%. Coring with the XCB system continued with Cores 321-U1377C-10X through 33X, recovering 95.2% of the section. Total depth of the hole was 4918.9 m DRF (440.3 m DSF), and overall recovery, using both APC and XCB coring systems, was 97.0%. The drill string was pulled clear of the seafloor at 1400 h on 30 May, officially ending operations in Hole U1337C.

### ***Hole U1337D***

The plan for this hole was to duplicate recovery through those sections of the formation already recovered to provide additional sample material. In addition, the goal was to use a more focused coring approach to target once again the few remaining areas that had yet to be fully recovered. The most troublesome material was the large intervals of diatom mats and a porcellanite (baby chert) layer. Hole U1338D was spudded at 1645 h on 30 May. Recovery of APC Core 321-U1377D-1H placed the seafloor depth at 4476.5 m DRF. APC coring continued through Core 321-U1377D-26H to 237.7 m DSF. Nonmagnetic core barrels were used through Core 321-U1377D-20H and Core 321-U1377D-21H was shot with the bit 4.5 m off bottom to set up the first target area of interest. The first XCB core (321-U1377D-27X) was designed to only core through the hard ~0.5 m thick porcellanite (baby chert) layer but not into the material below. The APC was once again deployed, and Cores 321-U1377D-28H through 30H were cut to 267.0 m DSF. At this point the XCB coring system was once again deployed for Cores 321-U1377D-31X through 49X to a total depth of 442.9 m DSF. The FlexIt core orientation system was deployed successfully with all APC cores, and, with the exception of Core 321-U1377D-22H, all barrels fully stroked. Total recovery for the APC in this hole was 102.9%, and recovery with the XCB coring system

was 89.6%. Total recovery for the hole was 97.5%. A much higher incidence of imploded or split liners plagued this hole, and we were unable to identify the reason. The drill string was recovered, the bottom-hole assembly was racked back in the derrick, and the rig floor was secured for transit. Once the bit cleared the seafloor the positioning beacon was recovered and thrusters and hydrophones were raised. At 1625 h on 2 June, control was switched from DP to cruise mode and the ship got underway for the next site.

## **Transit to Site U1338**

The transit to Site U1338 (proposed Site PEAT-8D) began at 1625 h on 2 June 2009, after recovering all thrusters/hydrophones and shifting control to cruise mode on the bridge. The transit to the next site was uneventful, although initially the weather was somewhat dreary. Overcast skies and occasional rain was prevalent for most of the day. In relatively mild seas and moderate wind the vessel made good time, averaging 10.5 kt for the 324 nmi transit. Speed was reduced coming onto location. Thrusters and hydrophones were lowered and at 2320 h on 3 June, and control was switched from bridge cruise mode to DP.

## **Site U1338**

As on the previous site, the position reference was a combination of GPS and an acoustic beacon on the seafloor. At 0005 h on 3 June, the same positioning beacon (FSI BAP-547, SN 1010, 15.0 kHz, 208 dB) used on the previous site was deployed. Four holes were drilled at this site using the APC/XCB coring systems. The last hole (U1338D) was limited to only three cores to be used in the labs for processing demonstrations during the upcoming expedition. Hole U1338B was wireline logged using the triple combo, FMS-sonic, and VSI tool strings. The APCT-3 temperature tool was deployed in Holes U1338A and U1338C. Overall recovery for Site U1338, using both APC and XCB coring systems, was 96.7%. Basement contact was recovered in two of the four holes drilled at the site.

### ***Hole U1338A***

Rig floor operations commenced at 2330 h. The top drive was picked up, and the drill string was spaced out, placing the bit at 4196.0 m DRF or 3.4 m above the “corrected” precision depth recorder depth of 4199.4 m DRF. The first APC barrel was pressured up and fired, but upon recovery it was discovered to have zero recovery (i.e., a “water” core). The bit was lowered an additional 5.0 m to 4201.0 m DRF, and another attempt

for mudline was made. This time the barrel obviously contacted the mudline; however, the small amount of core recovered was completely destroyed by the sloshing of the water column above. For the third attempt, the bit was repositioned an additional 3.0 m lower at 4204.0 m DRF. This time the barrel recovered 2.7 m of core, and an official seafloor depth was established at 4210.8 m DRF. APC coring continued through Core 321-U1338A-24H to 221.2 m DSF using nonmagnetic coring assemblies and the FlexIt core orientation system. Overpull forces of 100 klb and the need to drill over the APC barrel led to the use of steel core barrels beginning with Core 321-U1338A-25H. APC coring was eventually ended with Core 321-U1338A-26H at 240.2 m DSF. All barrels fully stroked; however, the last three cores (321-U1338A-24H, 25H, and 26H) required 100 klb overpull and drill over to extract from the formation. Five successful APCT-3 temperature measurements were obtained with Cores 321-U1338A-5H, 7H, 9H, 11H, and 13H at 40.7, 59.7, 78.7, 97.7, and 116.7 m DSF, respectively. Average core recovery for the APC was 104.5%. XCB coring continued with Cores 321-U1338A-27X through 44X, achieving an average recovery of 55.9%. A small piece of basement was recovered in the core catcher of Core 321-U1338A-44X, defining total depth for Hole U1338A at 4620.8 m DRF (410.0 m DSF.) XCB coring performance was highly variable, with some cores achieving near 100% recovery and others recovering <1% and sometimes zero. In the areas of little or no recovery there were diatom-rich intervals and/or porcellanite (baby chert) found in the surrounding cores. Just as in the earlier holes at Site U1337, these proved to be the troublesome areas for recovery and were targeted in later Holes U1338B and U1338C in an attempt to complete recovery for the section. Overall recovery for Hole U1338A, using both APC and XCB coring systems, was 84.4%. The drill string was pulled clear of the seafloor at 1900 h on 6 June, officially ending operations in the hole.

### ***Hole U1338B***

Operations in Hole U1338B officially began when the drill string cleared the seafloor at 1900 h on 6 June. The drilling line was slipped and cut while the was offset ship 20 m to the west of Hole U1338A. With the drill bit placed at 4208.0 m DRF to optimize the core breaks between holes, the APC was deployed and once again a water core was recovered. After checking the drill string tally it was discovered that the driller was off by a single joint of drill pipe. This single was added to the string, and with the bit positioned at the same depth, the second hole for Site U1338 was spudded at 2330 h on 6 June. Core recovery with APC Core 321-U1338B-1H determined the seafloor depth as 4209.9 m DRF. Except for a short drilled interval of 2.5 m to adjust the core breaks, continuous APC coring continued through Core 321-U1338B-20H to 188.1 m DSF us-

ing the FlexIt core orientation system and nonmagnetic coring assemblies. FlexIt and steel core barrels were then used as APC coring continued through Core 321-U1338B-42H to 387.4 m DSF. Hole U1338B is the second deepest APC hole in ODP and IODP history, surpassing the 378.0 m DSF depth achieved during Expedition 320 in Hole U1335B. APC extraction overpull reached 100 klb on 19 of the 42 cores taken, including the last 11 cores. Full stroke was achieved on all but two cores (321-U1338B-30H and 31H) through the interval from 276.1 to 282.9 m DSF. Coincidentally, the shear pressure for these two cores was inconclusive, so this may have been the reason for the incomplete stroke. Drillover was required on 13 cores, including the last ten. Except for Cores 321-U1338B-30H and 31H, shear pressures were consistent throughout the coring process at 2800 psi. Core liner issues were relatively mild. The Core 321-U1338B-1H liner was broken, the liner for Core 321-U1338B-13H was cracked at the bottom, and the liner in Core 321-U1338B-42H was recovered split. Average core recovery for the APC was 104.1%. Coring continued with three XCB cores (321-U1338B-43X through 45X) to 416.1 m DSF. Basement contact was recovered in Core 321-U1338B-45X. Overall the XCB coring system recovered 57.9% of the interval penetrated. Recovery was problematic with the XCB, and the material that was recovered suffered significantly from the typical “biscuiting” effect. Total depth of Hole U1338B was 4626.0 m DRF (416.1 m DSF). Overall core recovery using both APC and XCB coring systems was 100.9%. The hole was swept clean with 50 bbl of attapulgitic mud. A wiper trip revealed no ledges or bridges, and no fill was identified at total depth. The lockable float valve was locked open, the hole was displaced with heavy 10.5 ppg logging mud, and the end of pipe was placed at 84.7 m DSF. Rig-up for wireline logging began at 2145 h on 9 June. Wireline logging in Hole U1338B was successfully concluded and all logging equipment was rigged down by 1615 h on 11 June. Three logging strings were deployed. The triple combo and the FMS-sonic tool reached total hole depth of 416.1 m DSF. The third and final logging string consisted of the VSI. This tool reached total hole depth and shooting stations were conducted at ~15 m stations. All logging was done during daylight hours to conform with established IODP mammal watch protocols, including a preshooting mammal watch and soft start procedures for the air guns. The drill string was pulled back until the bit cleared the seafloor at 1655 h on 11 June, officially ending operations in Hole U1338B.

### ***Hole U1338C***

Operations in Hole U1338C officially began when the drill string cleared the seafloor at 1655 h on 11 June. The ship was offset 20 m to the west of Hole U1338B. The drill-

ing line was slipped and cut and the Rigwatch drawworks/block position encoder was recalibrated. The drill bit was placed at 4204 m DRF (same as Hole U1338A) to optimize the core breaks between Holes U1338A and U1338B. The APC was deployed, and, for the third time at this site, a water core was recovered. Because 2.7 m of core had been recovered in Hole U1338A with the same bit placement, it was suspected that vessel heave, induced by the large long-period swell train from the south, had impacted bit placement by being on the high side of the swell displacement. The drill string was lowered another 3 m, and the bit was repositioned at 4207.0 m DRF. Hole U1338C was spudded at 2135 h on 11 June. The 3.83 m of core recovery with APC Core 321-U1338C-1H determined the seafloor depth at 4212.7 m DRF. APC coring continued through Core 321-U1338C-21H to 189.8 m DSF using the FlexIt core orientation system and nonmagnetic coring assemblies. FlexIt and steel core barrels were then used as APC coring continued through Core 321-U1338C-44H to 396.9 m DSF. Conditions indicated that Core 321-U1338C-45H fully stroked, and drillover was required to extract it from the formation. Retrieval was delayed because a bent core barrel initially prohibited entry into the drill string. Repeated jarring with the wireline jars eventually sheared the overshot pin. The sinker bar string was recovered, and the FlexIt core orientation tool was removed. The sinker bar assembly was redeployed, and the core barrel was immediately recovered without any further incident. It was deemed prudent at this point to leave the FlexIt tool out of the assembly for the remainder of the coring process. Coring continued through Core 321-U1338C-47H to a total depth of 414.4 m DSF, setting a new all time depth record for the APC. This surpassed the standing ODP record set on 7 August 1992 (Leg 145) when the APC recovered 42 piston cores to a total depth of 398.3 m DSF in Hole 882A. APC extraction overpull reached 100 klb on Cores 321-U1338C-22H through 47H. Drillover prior to removal from the formation was required for 22 cores and full stroke was achieved on all but four cores (321-U1338C-31H and 45H through 47H). Shear pressures were consistent throughout the coring process at 2800 psi. Core liner issues were relatively mild with only two cores recovered with imploded liners (Cores 321-U1338C-10H and 12H), although several barrels were bent during the coring process and several piston rods had to be adjusted and repinned because of overtorqued threads that caused miss-alignment of the rod grooves. Overall core recovery for the APC was 104.4%. The drill string was pulled clear of the seafloor at 2015 h on 14 June, officially ending operations in Hole U1338C.

### ***Hole U1338D***

Operations in Hole U1338D officially began when the drill string cleared the seafloor at 2015 h on 14 June. The ship was offset 20 m to the west of Hole U1338C. This hole was primarily planned to recover a few “instructional” cores for lab demonstrations to be used during Expedition 323. Hole U1338D was spudded at 2150 h on 14 June, and the 4.89 m recovered with Core 321-U1338D-1H established a seafloor depth of 4212.6 m DSF. Three APC cores were cut to 23.9 m DSF. APC core recovery was 103.7%. Official APC/XCB coring totals for Site U1338 include 139 total cores, 1261.9 m penetrated, and 1220.41 m recovered, for 96.7% recovery. The coring tools were secured and the drill string was pulled clear of the seafloor at 0145 h on 15 June. The top drive was set back, the knobby joints were laid out, and the drill string was recovered. Once the drill collars were laid out and the rig floor was secured for transit, control was transferred from DP to the bridge. The ship was placed in cruise mode at 1030 h on 15 for the anticipated 7.6 day (1811 nmi) transit to San Diego.

### **Transit to San Diego**

The vessel departed Site U1338 ~4 1/2 hours ahead of the projected schedule on a northerly course. The 1811 nmi transit from Site U1338 to the San Diego pilot station required 7.3 days at an average speed of 10.5 kt. Expedition 321, the second and final segment of the PEAT program, was officially concluded at 1715 h on 22 June with the first line ashore Berth 10-7 at the Tenth Avenue Marine Terminal, San Diego Harbor.

## References

- Abels, H.A., Hilgen, F.J., Krijgsman, W., Kruk, R.W., Raffi, I., Turco, E., and Zachariasse, W.J., 2005. Long-period orbital control on middle Miocene global cooling: integrated stratigraphy and astronomical tuning of the Blue Clay Formation on Malta. *Paleoceanography*, 20(4):PA4012. doi:10.1029/2004PA001129
- Baldauf, J.G., 1985. A high resolution late Miocene–Pliocene diatom biostratigraphy for the eastern equatorial Pacific. In Mayer, L., Theyer, F., Thomas, E., et al., *Init. Repts. DSDP*, 85: Washington, DC (U.S. Govt. Printing Office), 457–475. doi:10.2973/dsdp.proc.85.109.1985
- Baldauf, J.G., and Iwai, M., 1995. Neogene diatom biostratigraphy for the eastern equatorial Pacific Ocean, Leg 138. In Pisias, N.G., Mayer, L.A., Janecek, T.R., Palmer-Julson, A., and van Andel, T.H. (Eds.), *Proc. ODP, Sci. Results*, 138: College Station, TX (Ocean Drilling Program), 105–128. doi:10.2973/odp.proc.sr.138.107.1995
- Barker, P.F., 2001. Scotia Sea regional tectonic evolution: implications for mantle flow and palaeocirculation. *Earth-Sci. Rev.*, 55(1–2):1–39. doi:10.1016/S0012-8252(01)00055-1
- Barron, J.A., 1985. Late Eocene to Holocene diatom biostratigraphy of the equatorial Pacific Ocean, Deep Sea Drilling Project Leg 85. In Mayer, L., Theyer, F., Thomas, E., et al., *Init. Repts. DSDP*, 85: Washington, DC (U.S. Govt. Printing Office), 413–456. doi:10.2973/dsdp.proc.85.108.1985
- Billups, K., Pälike, H., Channell, J.E.T., Zachos, J.C., and Shackleton, N.J., 2004. Astronomic calibration of the late Oligocene through early Miocene geomagnetic polarity time scale. *Earth Planet. Sci. Lett.*, 224(1–2):33–44. doi:10.1016/j.epsl.2004.05.004
- Bohaty, S.M., Pälike, H., Ridgwell, A., Zachos, J.C., and Lear, C.H., 2008. Timing and significance of a global deep-sea dissolution event during the Eocene–Oligocene transition. *Eos, Trans. Am. Geophys. Union*, 89(53)(Suppl.):PP41D-1487. (Abstract) <http://www.agu.org/meetings/fm08/waisfm08.html>
- Bohaty, S.M., and Zachos, J.C., 2003. Significant Southern Ocean warming event in the late middle Eocene. *Geology*, 31(11):1017–1020. doi:10.1130/G19800.1
- Bohaty, S.M., Zachos, J.C., Florindo, F., and Delaney, M.L., 2009. Coupled greenhouse warming and deep-sea acidification in the middle Eocene. *Paleoceanography*, 24(2):PA2207. doi:10.1029/2008PA001676
- Coxall, H.K., Wilson, P.A., Pälike, H., Lear, C.H., and Backman, J., 2005. Rapid stepwise onset of Antarctic glaciation and deeper calcite compensation in the Pacific Ocean. *Nature (London, U. K.)*, 433(7021):53–57. doi:10.1038/nature03135
- DeConto, R.M., Pollard, D., Wilson, P.A., Pälike, H., Lear, C.H., and Pagani, M., 2008. Thresholds for Cenozoic bipolar glaciation. *Nature (London, U. K.)*, 455(7213):652–656. doi:10.1038/nature07337
- Dore, J.E., Lukas, R., Sadler, D.W., and Karl, D.M., 2003. Climate-driven changes to the atmospheric CO<sub>2</sub> sink in the subtropical North Pacific Ocean. *Nature (London, U. K.)*, 424(6950):754–757. doi:10.1038/nature01885
- Elderfield, H., and Schultz, A., 1996. Mid-ocean ridge hydrothermal fluxes and the chemical composition of the ocean. *Annu. Rev. Earth Planet. Sci.*, 24(1):191–224. doi:10.1146/annurev.earth.24.1.191
- Elderfield, H., Yu, J., Anand, P., Kiefer, T., and Nyland, B., 2006. Calibrations for benthic foraminiferal Mg/Ca paleothermometry and the carbonate ion hypothesis. *Earth Planet. Sci. Lett.*, 250(3–4):633–649. doi:10.1016/j.epsl.2006.07.041

- Engebretson, D.C., Cox, A., and Gordon, R.G., 1985. *Relative Motions between Oceanic and Continental Plates in the Pacific Basin*. Spec. Pap.—Geol. Soc. Am., 206.
- Exon, N.F., Kennett, J.P., Malone, M.J., et al., 2001. *Proc. ODP, Init. Repts.*, 189: College Station, TX (Ocean Drilling Program). [doi:10.2973/odp.proc.ir.189.2001](https://doi.org/10.2973/odp.proc.ir.189.2001)
- Farrell, J.W., Raffi, I., Janecek, T.R., Murray, D.W., Levitan, M., Dadey, K.A., Emeis, K.-C., Lyle, M., Flores, J.-A., and Hovan, S., 1995. Late Neogene sedimentation patterns in the eastern equatorial Pacific Ocean. In Piasias, N.G., Mayer, L.A., Janecek, T.R., Palmer-Julson, A., and van Andel, T.H. (Eds.), *Proc. ODP, Sci. Results*, 138: College Station, TX (Ocean Drilling Program), 717–756. [doi:10.2973/odp.proc.sr.138.143.1995](https://doi.org/10.2973/odp.proc.sr.138.143.1995)
- Gradstein, F.M., Ogg, J.G., and Smith, A. (Eds.), 2004. *A Geologic Time Scale 2004*: Cambridge (Cambridge Univ. Press). <http://www.stratigraphy.org/>
- Holbourn, A., Kuhnt, W., Schulz, M., and Erlenkeuser, H., 2005. Impacts of orbital forcing and atmospheric carbon dioxide on Miocene ice-sheet expansion. *Nature (London, U. K.)*, 438(7067):483–487. [doi:10.1038/nature04123](https://doi.org/10.1038/nature04123)
- Kemp, A.E.S., and Baldauf, J.G., 1993. Vast Neogene laminated diatom mat deposits from the eastern equatorial Pacific Ocean. *Nature (London, U. K.)*, 362(6416):141–144. [doi:10.1038/362141a0](https://doi.org/10.1038/362141a0)
- Kennett, J.P., and Shackleton, N.J., 1976. Oxygen isotopic evidence for the development of the psychrosphere 38 Myr ago. *Nature (London, U. K.)*, 260(5551):513–515. [doi:10.1038/260513a0](https://doi.org/10.1038/260513a0)
- Knappenberger, M., 2000. Sedimentation rates and Pacific plate motion calculated using seismic cross sections of the Neogene equatorial sediment bulge [M.Sc. thesis]. Boise State Univ., Idaho.
- Koppers, A.A.P., Phipps Morgan, J., Morgan, J.W., and Staudigel, H., 2001. Testing the fixed hotspot hypothesis using  $^{40}\text{Ar}/^{39}\text{Ar}$  age progressions along seamount trails. *Earth Planet. Sci. Lett.*, 185(3–4):237–252. [doi:10.1016/S0012-821X\(00\)00387-3](https://doi.org/10.1016/S0012-821X(00)00387-3)
- Kunzendorf, H., Pflüger, W.L., and Friedrich, G.H., 1983. Uranium in Pacific deep-sea sediments and manganese nodules. *J. Geochem. Explor.*, 19(1–3):147–162. [doi:10.1016/0375-6742\(83\)90014-6](https://doi.org/10.1016/0375-6742(83)90014-6)
- Lanci, L., Parés, J.M., Channell, J.E.T., and Kent, D.V., 2004. Miocene magnetostratigraphy from equatorial Pacific sediments (ODP Site 1218, Leg 199). *Earth Planet. Sci. Lett.*, 226(1–2):207–224. [doi:10.1016/j.epsl.2004.07.025](https://doi.org/10.1016/j.epsl.2004.07.025)
- Lanci, L., Parés, J.M., Channell, J.E.T., and Kent, D.V., 2005. Oligocene magnetostratigraphy from equatorial Pacific sediments (ODP Sites 1218 and 1219, Leg 199). *Earth Planet. Sci. Lett.*, 237(3–4):617–634. [doi:10.1016/j.epsl.2005.07.004](https://doi.org/10.1016/j.epsl.2005.07.004)
- Lawver, L.A., and Gahagan, L.M., 2003. Evolution of Cenozoic seaways in the circum-Antarctic region. *Palaeogeogr., Palaeoclimatol., Palaeoecol.*, 198(1–2):11–37. [doi:10.1016/S0031-0182\(03\)00392-4](https://doi.org/10.1016/S0031-0182(03)00392-4)
- Lear, C.H., Bailey, T.R., Pearson, P.N., Coxall, H.K., and Rosenthal, Y., 2008. Cooling and ice growth across the Eocene–Oligocene transition. *Geology*, 36(3):251–254. [doi:10.1130/G24584A.1](https://doi.org/10.1130/G24584A.1)
- Lear, C.H., and Rosenthal, Y., 2006. Benthic foraminiferal Li/Ca: insights into Cenozoic seawater carbonate saturation state. *Geology*, 34(11):985–988. [doi:10.1130/G22792A.1](https://doi.org/10.1130/G22792A.1)
- Lear, C.H., Rosenthal, Y., Coxall, H.K., and Wilson, P.A., 2004. Late Eocene to early Miocene ice sheet dynamics and the global carbon cycle. *Paleoceanography*, 19(4):PA4015. [doi:10.1029/2004PA001039](https://doi.org/10.1029/2004PA001039)

- Liu, Z., Pagani, M., Zinniker, D., DeConto, R., Huber, M., Brinkhuis, H., Shah, S.R., Leckie, R.M., and Pearson, A., 2009. Global cooling during the Eocene–Oligocene climate transition. *Science*, 323(5918):1187–1190. doi:10.1126/science.1166368
- Lowenstein, T.K., and Demicco, R.V., 2007. Elevated Eocene atmospheric CO<sub>2</sub> and subsequent decline. *Science*, 313(5795):1928. doi:10.1126/science.1129555
- Lyle, M., 1983. The brown-green color transition in marine sediments: a marker of the Fe(III)-Fe(II) redox boundary. *Limnol. Oceanogr.*, 28:1026–1033.
- Lyle, M., 2003. Neogene carbonate burial in the Pacific Ocean. *Paleoceanography*, 18(3):1059. doi:10.1029/2002PA000777
- Lyle, M., Dadey, K.A., and Farrell, J.W., 1995. The late Miocene (11–8 Ma) eastern Pacific carbonate crash: evidence for reorganization of deep-water circulation by the closure of the Panama gateway. In Pisias, N.G., Mayer, L.A., Janecek, T.R., Palmer-Julson, A., and van Andel, T.H. (Eds.), *Proc. ODP, Sci. Results*, 138: College Station, TX (Ocean Drilling Program), 821–838. doi:10.2973/odp.proc.sr.138.157.1995
- Lyle, M., Liberty, L., Moore, T.C., Jr., and Rea, D.K., 2002. Development of a seismic stratigraphy for the Paleogene sedimentary section, central tropical Pacific Ocean. In Lyle, M., Wilson, P.A., Janecek, T.R., et al., *Proc. ODP, Init. Repts.*, 199: College Station, TX (Ocean Drilling Program), 1–21. doi:10.2973/odp.proc.ir.199.104.2002
- Lyle, M., Olivarez Lyle, A., Backman, J., and Tripathi, A., 2005. Biogenic sedimentation in the Eocene equatorial Pacific—the stuttering greenhouse and Eocene carbonate compensation depth. In Lyle, M., Wilson, P.A., Janecek, T.R., et al., *Proc. ODP, Init. Repts.*, 199: College Station, TX (Ocean Drilling Program), 1–35. doi:10.2973/odp.proc.sr.199.219.2005
- Lyle, M.W., Pälike, H., Moore, T.C., Mitchell, N., and Backman, J., 2006. *Summary Report of R/V Roger Revelle Site Survey AMAT03 to the IODP Environmental Protection and Safety Panel (EPSP) in Support for Proposal IODP626*: Southampton, U.K. (Univ. Southampton). <http://eprints.soton.ac.uk/45921/>
- Lyle, M., Wilson, P.A., Janecek, T.R., et al., 2002. *Proc. ODP, Init. Repts.*, 199: College Station, TX (Ocean Drilling Program). doi:10.2973/odp.proc.ir.199.2002
- Majewski, W., 2003. Water-depth distribution of Miocene planktonic foraminifera from ODP Site 744, southern Indian Ocean. *J. Foraminiferal Res.*, 33(2):144–154. doi:10.2113/0330144
- Mayer, L., Pisias, N., Janecek, T., et al., 1992. *Proc. ODP, Init. Repts.*, 138: College Station, TX (Ocean Drilling Program). doi:10.2973/odp.proc.sr.138.1995
- Mayer, L.A., 1991. Extraction of high-resolution carbonate data for palaeoclimate reconstruction. *Nature (London, U. K.)*, 352(6331):148–150. doi:10.1038/352148a0
- Mayer, L.A., Shipley, T.H., Theyer, F., Wilkens, R.H., and Winterer, E.L., 1985. Seismic modeling and paleoceanography at Deep Sea Drilling Project Site 574. In Mayer, L., Theyer, F., Thomas, E., et al., *Init. Repts. DSDP*, 85: Washington, DC (U.S. Govt. Printing Office), 947–970. doi:10.2973/dsdp.proc.85.132.1985
- Miller, K.G., Wright, J.D., and Fairbanks, R.G., 1991. Unlocking the ice house: Oligocene–Miocene oxygen isotopes, eustasy, and margin erosion. *J. Geophys. Res.*, 96(B4):6829–6848. doi:10.1029/90JB02015
- Mitchell, N.C., 1998. Modeling Cenozoic sedimentation in the central equatorial Pacific and implications for true polar wander. *J. Geophys. Res., [Solid Earth]*, 103(B8):17749–17766. doi:10.1029/98JB01577
- Mitchell, N.C., and Lyle, M.W., 2005. Patchy deposits of Cenozoic pelagic sediments in the central Pacific. *Geology*, 33(1):49–52. doi:10.1130/G21134.1

- Mitchell, N.C., Lyle, M.W., Knappenberger, M.B., and Liberty, L.M., 2003. Lower Miocene to present stratigraphy of the equatorial Pacific sediment bulge and carbonate dissolution anomalies. *Paleoceanography*, 18(2):1038. doi:10.1029/2002PA000828
- Mix, A.C., Tiedemann, R., Blum, P., et al., 2003. *Proc. ODP, Init. Repts.*, 202: College Station, TX (Ocean Drilling Program). doi:10.2973/odp.proc.ir.202.2003
- Moore, T.C., Rea, D.K., Lyle, M., and Liberty, L.M., 2002. Equatorial ocean circulation in an extreme warm climate. *Paleoceanography*, 17(1):1005. doi:10.1029/2000PA000566
- Moore, T.C., Jr., 2008a. Biogenic silica and chert in the Pacific Ocean. *Geology*, 36(12):975–978. doi:10.1130/G25057A.1
- Moore, T.C., Jr., 2008b. Chert in the Pacific: biogenic silica and hydrothermal circulation. *Palaeogeogr., Palaeoclimatol., Palaeoecol.*, 261(1–2):87–99. doi:10.1016/j.palaeo.2008.01.009
- Moore, T.C., Jr., Backman, J., Raffi, I., Nigrini, C., Sanfilippo, A., Pälike, H., and Lyle, M., 2004. Paleogene tropical Pacific: clues to circulation, productivity, and plate motion. *Paleoceanography*, 19(3):PA3013. doi:10.1029/2003PA000998
- Müller, R.D., Roest, W.R., Royer, J.-Y., Gahagan, L.M., and Sclater, J.G., 1997. Digital isochrons of the world's ocean floor. *J. Geophys. Res.*, 102(B2):3211–3214. doi:10.1029/96JB01781
- Nigrini, C., Sanfilippo, A., and Moore, T.C., Jr., 2006. Cenozoic radiolarian biostratigraphy: a magnetobiostratigraphic chronology of Cenozoic sequences from ODP Sites 1218, 1219, and 1220, equatorial Pacific. In Wilson, P.A., Lyle, M., and Firth, J.V. (Eds.), *Proc. ODP, Sci. Results*, 199: College Station, TX (Ocean Drilling Program), 1–76. doi:10.2973/odp.proc.sr.199.225.2006
- Norris, R.D., and Röhl, U., 1999. Carbon cycling and chronology of climate warming during the Palaeocene/Eocene transition. *Nature (London, U. K.)*, 401(6755):775–778. doi:10.1038/44545
- Nuñez, F., and Norris, R.D., 2006. Abrupt reversal in ocean overturning during the Palaeocene/Eocene warm period. *Nature (London, U. K.)*, 439(7072):60–63. doi:10.1038/nature04386
- Pagani, M., Arthur, M.A., and Freeman, K.H., 1999. Miocene evolution of atmospheric carbon dioxide. *Paleoceanography*, 14(3):273–292. doi:10.1029/1999PA900006
- Pälike, H., Frazier, J., and Zachos, J.C., 2006a. Extended orbitally forced palaeoclimatic records from the equatorial Atlantic Ceara Rise. *Quat. Sci. Rev.*, 25(23–24):3138–3149. doi:10.1016/j.quascirev.2006.02.011
- Pälike, H., Moore, T., Backman, J., Raffi, I., Lanci, L., Parés, J.M., and Janecek, T., 2005. Integrated stratigraphic correlation and improved composite depth scales for ODP Sites 1218 and 1219. In Wilson, P.A., Lyle, M., and Firth, J.V. (Eds.), *Proc. ODP, Sci. Results*, 199: College Station, TX (Ocean Drilling Program), 1–41. doi:10.2973/odp.proc.sr.199.213.2005
- Pälike, H., Norris, R.D., Herrle, J.O., Wilson, P.A., Coxall, H.K., Lear, C.H., Shackleton, N.J., Tripathi, A.K., and Wade, B.S., 2006b. The heartbeat of the Oligocene climate system. *Science*, 314(5807):1894–1898. doi:10.1126/science.1133822
- Parés, J.M., and Moore, T.C., 2005. New evidence for the Hawaiian hotspot plume motion since the Eocene. *Earth Planet. Sci. Lett.*, 237(3–4):951–959. doi:10.1016/j.epsl.2005.06.012
- Paul, H.A., Zachos, J.C., Flower, B.P., and Tripathi, A., 2000. Orbitally induced climate and geochemical variability across the Oligocene/Miocene boundary. *Paleoceanography*, 15(5):471–485. doi:10.1029/1999PA000443

- Pearson, P.N., Ditchfield, P.W., Singano, J., Harcourt-Brown, K.G., Nicholas, C.J., Olsson, R.K., Shackleton, N.J., and Hall, M.A., 2001a. Warm tropical sea surface temperatures in the Late Cretaceous and Eocene epochs. *Nature (London, U. K.)*, 413(6855):481–487. [doi:10.1038/35097000](https://doi.org/10.1038/35097000)
- Pearson, P.N., McMillan, I.K., Wade, B.S., Dunkley Jones, T., Coxall, H.K., Bown, P.R., and Lear, C.H., 2008. Extinction and environmental change across the Eocene–Oligocene boundary in Tanzania. *Geology*, 36(2):179–182. [doi:10.1130/G24308A.1](https://doi.org/10.1130/G24308A.1)
- Pearson, P.N., Norris, R.D., and Empson, A.J., 2001b. *Mutabella mirabilis* gen. et sp. Nov., a Miocene microperforate planktonic foraminifer with an extreme level of intraspecific variability. *J. Foraminiferal Res.*, 31(2):120–132. [doi:10.2113/0310120](https://doi.org/10.2113/0310120)
- Peng, T.-H., Maier-Reimer, E., and Broecker, W.S. 1993. Distribution of  $^{32}\text{Si}$  in the world ocean: model compared to observation. *Global Biogeochem. Cycles*, 7(2):463–474. [doi:10.1029/93GB00686](https://doi.org/10.1029/93GB00686)
- Petronotis, K.E., 1991. Paleomagnetic studies of the skewness of Pacific plate marine magnetic anomalies 25–32R: implications for anomalous skewness and the motion of the Pacific plate and hotspots [Ph.D. thesis]. Northwestern Univ., Evanston, IL.
- Petronotis, K.E., Gordon, R.G., and Acton, G.D., 1994. A 57 Ma Pacific plate paleomagnetic pole determined from a skewness analysis of crossings of marine magnetic anomaly 25r. *Geophys. J. Int.*, 118(3):529–554. [doi:10.1111/j.1365-246X.1994.tb03983.x](https://doi.org/10.1111/j.1365-246X.1994.tb03983.x)
- Pisias, N.G., Mayer, L.A., Janecek, T.R., Palmer-Julson, A., and van Andel, T.H. (Eds.), 1995. *Proc. ODP, Sci Results*, 138: College Station, TX (Ocean Drilling Program). [doi:10.2973/odp.proc.sr.138.1995](https://doi.org/10.2973/odp.proc.sr.138.1995)
- Raffi, I., Backman, J., Fornaciari, E., Pälike, H., Rio, D., Lourens, L., and Hilgen, F., 2006. A review of calcareous nannofossil astrobiochronology encompassing the past 25 million years. *Quat. Sci. Rev.*, 25(23–24):3113–3137. [doi:10.1016/j.quascirev.2006.07.007](https://doi.org/10.1016/j.quascirev.2006.07.007)
- Raffi, I., Backman, J., and Pälike, H., 2005. Changes in calcareous nannofossil assemblages across the Paleocene/Eocene transition from the paleo-equatorial Pacific Ocean. *Palaeogeogr., Palaeoclimatol., Palaeoecol.*, 226(1–2):93–126. [doi:10.1016/j.palaeo.2005.05.006](https://doi.org/10.1016/j.palaeo.2005.05.006)
- Rea, D.K., and Lyle, M.W., 2005. Paleogene calcite compensation depth in the eastern subtropical Pacific: answers and questions. *Paleoceanography*, 20(1):PA1012. [doi:10.1029/2004PA001064](https://doi.org/10.1029/2004PA001064)
- Riedel, W.R., 1967. Radiolarian evidence consistent with spreading of the Pacific floor. *Science*, 157(3788):540–542. [doi:10.1126/science.157.3788.540](https://doi.org/10.1126/science.157.3788.540)
- Röhl, U., Ogg, J.G., Geib, T.L., and Wefer, G., 2001. Astronomical calibration of the Danian time scale. In Kroon, D., Norris, R.D., and Klaus, A. (Eds.), *Western North Atlantic Paleogene and Cretaceous Paleoceanography*. Geol. Soc. Spec. Publ., 183:163–184.
- Sager, W.W., and Pringle, M.S., 1988. Mid-Cretaceous to early Tertiary apparent polar wander path of the Pacific plate. *J. Geophys. Res., [Solid Earth]*, 93(B10):11753–11771. [doi:10.1029/JB093iB10p11753](https://doi.org/10.1029/JB093iB10p11753)
- Scher, H.D., and Martin, E.E., 2006. Timing and climatic consequences of the opening of Drake Passage. *Science*, 312(5772):428–430. [doi:10.1126/science.1120044](https://doi.org/10.1126/science.1120044)
- Shackleton, N.J., Hall, M.A., Raffi, I., Tauxe, L., and Zachos, J., 2000. Astronomical calibration age for the Oligocene–Miocene boundary. *Geology*, 28(5):447–450. [doi:10.1130/0091-7613\(2000\)28<447:ACAFTO>2.0.CO;2](https://doi.org/10.1130/0091-7613(2000)28<447:ACAFTO>2.0.CO;2)
- Shipboard Scientific Party, 1995. Leg 154 synthesis. In Curry, W.B., Shackleton, N.J., Richter, C., et al., *Proc. ODP, Init. Repts.*, 154: College Station, TX (Ocean Drilling Program), 421–442. [doi:10.2973/odp.proc.ir.154.109.1995](https://doi.org/10.2973/odp.proc.ir.154.109.1995)

- Shipboard Scientific Party, 2002. Leg 199 summary. In Lyle, M., Wilson, P.A., Janecek, T.R., et al., *Proc. ODP, Init. Repts.*, 199: College Station, TX (Ocean Drilling Program), 1–87. [doi:10.2973/odp.proc.ir.199.101.2002](https://doi.org/10.2973/odp.proc.ir.199.101.2002)
- Shipboard Scientific Party, 2004. Leg 208 summary. In Zachos, J.C., Kroon, D., Blum, P., et al., *Proc. ODP, Init. Repts.*, 208: College Station, TX (Ocean Drilling Program), 1–112. [doi:10.2973/odp.proc.ir.208.101.2004](https://doi.org/10.2973/odp.proc.ir.208.101.2004)
- Spero, H.J., Bijma, J., Lea, D.W., and Bemis, B.E., 1997. Effect of seawater carbonate concentration on foraminiferal carbon and oxygen isotopes. *Nature (London, U. K.)*, 390(6659):497–500. [doi:10.1038/37333](https://doi.org/10.1038/37333)
- Steiger, T.H., 2006. Biogenic sedimentology of radiolarian assemblages in a middle Eocene diatom-rich unit from the eastern equatorial Pacific: ODP Leg 199, Site 1219. In Wilson, P.A., Lyle, M., and Firth, J.V. (Eds.), *Proc. ODP, Sci. Results*, 199: College Station, TX (Ocean Drilling Program), 1–19. [doi:10.2973/odp.proc.sr.199.217.2006](https://doi.org/10.2973/odp.proc.sr.199.217.2006)
- Tarduno, J.A., Duncan, R.A., Scholl, D.W., Cottrell, R.D., Steinberger, B., Thordarson, T., Kerr, B.C., Neal, C.R., Frey, F.A., Torii, M., and Carvallo, C., 2003. The Emperor Seamounts: southward motion of the Hawaiian hotspot plume in Earth's mantle. *Science*, 301(5636):1064–1069. [doi:10.1126/science.1086442](https://doi.org/10.1126/science.1086442)
- van Andel, T.H., 1975. Mesozoic/Cenozoic calcite compensation depth and the global distribution of calcareous sediments. *Earth Planet. Sci. Lett.*, 26(2):187–194. [doi:10.1016/0012-821X\(75\)90086-2](https://doi.org/10.1016/0012-821X(75)90086-2)
- Wade, B.S., Berggren, W.A., and Olsson, R.K., 2007. The biostratigraphy and paleobiology of Oligocene planktonic foraminifera from the equatorial Pacific Ocean (ODP Site 1218). *Mar. Micropaleontol.*, 62(3):167–179. [doi:10.1016/j.marmicro.2006.08.005](https://doi.org/10.1016/j.marmicro.2006.08.005)
- Wade, B.S., and Pälike, H., 2004. Oligocene climate dynamics. *Paleoceanography*, 19(4)PA4019. [doi:10.1029/2004PA001042](https://doi.org/10.1029/2004PA001042)
- Zachos, J.C., Dickens, G.R., and Zeebe, R.E., 2008. An early Cenozoic perspective on greenhouse warming and carbon-cycle dynamics. *Nature (London, U. K.)*, 451(7176):279–283. [doi:10.1038/nature06588](https://doi.org/10.1038/nature06588)
- Zachos, J.C., Flower, B.P., and Paul, H., 1997. Orbitally paced climate oscillations across the Oligocene/Miocene boundary. *Nature (London, U. K.)*, 388(6642):567–570. [doi:10.1038/41528](https://doi.org/10.1038/41528)
- Zachos, J.C., Pagani, M., Sloan, L., Thomas, E., and Billups, K., 2001a. Trends, rhythms, and aberrations in global climate 65 Ma to present. *Science*, 292(5517):686–693. [doi:10.1126/science.1059412](https://doi.org/10.1126/science.1059412)
- Zachos, J.C., Quinn, T.M., and Salamy, K.A., 1996. High-resolution (10<sup>4</sup> years) deep-sea foraminiferal stable isotope records of the Eocene–Oligocene climate transition. *Paleoceanography*, 11(3):251–266. [doi:10.1029/96PA00571](https://doi.org/10.1029/96PA00571)
- Zachos, J.C., Shackleton, N.J., Revenaugh, J.S., Pälike, H., and Flower, B.P., 2001b. Climate response to orbital forcing across the Oligocene–Miocene boundary. *Science*, 292(5515):274–278. [doi:10.1126/science.1058288](https://doi.org/10.1126/science.1058288)
- Zeebe, R.E., and Wolf-Gladrow, D.A., 2001. *CO<sub>2</sub> in Seawater: Equilibrium, Kinetics, Isotopes*: Amsterdam (Elsevier).

Expedition 321 Preliminary Report

**Table T1.** Expedition 321 coring summary.

Hole	Latitude	Longitude	Seafloor depth DRF (m)	Cores (N)	Cored (m)	Recovered (m)	Recovered (%)	Drilled (m)	Total penetration (m)	Total depth DRF (m)	Time on hole (h)	Time on hole (days)
U1337A	3°50.0065'N	123°12.3558'W	4472.0	48	449.8	420.11	93.40	0.0	449.8	4921.8	141.75	5.9
U1337B	3°50.0067'N	123°12.3621'W	4472.0	28	250.9	242.65	96.71	1.0	251.9	4723.9	61.25	2.6
U1337C	3°50.0067'N	123°12.3755'W	4478.6	32	282.3	273.72	96.96	158.0	440.3	4918.9	63.25	2.6
U1337D	3°50.0067'N	123°12.3858'W	4476.5	49	442.9	431.97	97.53	0.0	442.9	4919.4	74.50	3.1
Site U1337 totals:				157	1425.9	1368.45	95.97	159.0	1584.9	NA	340.75	14.2
U1338A	2°30.4685'N	117°58.1623'W	4210.8	44	410.0	345.96	84.38	0.0	410.0	4620.8	67.75	2.8
U1338B	2°30.4692'N	117°58.1736'W	4209.9	45	413.6	417.18	100.87	2.5	416.1	4626.0	118.00	4.9
U1338C	2°30.4687'N	117°58.1842'W	4212.7	47	414.4	432.48	104.36	0.0	414.4	4627.1	75.25	3.1
U1338D	2°30.4689'N	117°58.1948'W	4212.6	3	23.9	24.79	103.72	0.0	23.9	4236.5	14.25	0.6
Site U1338 totals:				139	1261.9	1220.41	96.71	2.5	1264.4	NA	275.25	11.5
Expedition 321 totals:				296	2687.8	2588.86	96.32	161.5	2849.3	NA	616.00	25.7

Note: NA = not applicable.

**Figure F1.** Location map of sites drilled during Expeditions 320 and 321. Red stars = sites drilled during Expedition 320, red circles = sites drilled during Expedition 321, black circles = previous DSDP and ODP sites. F.Z. = fracture zone. The positions of Honolulu and Papeete are indicated for orientation.

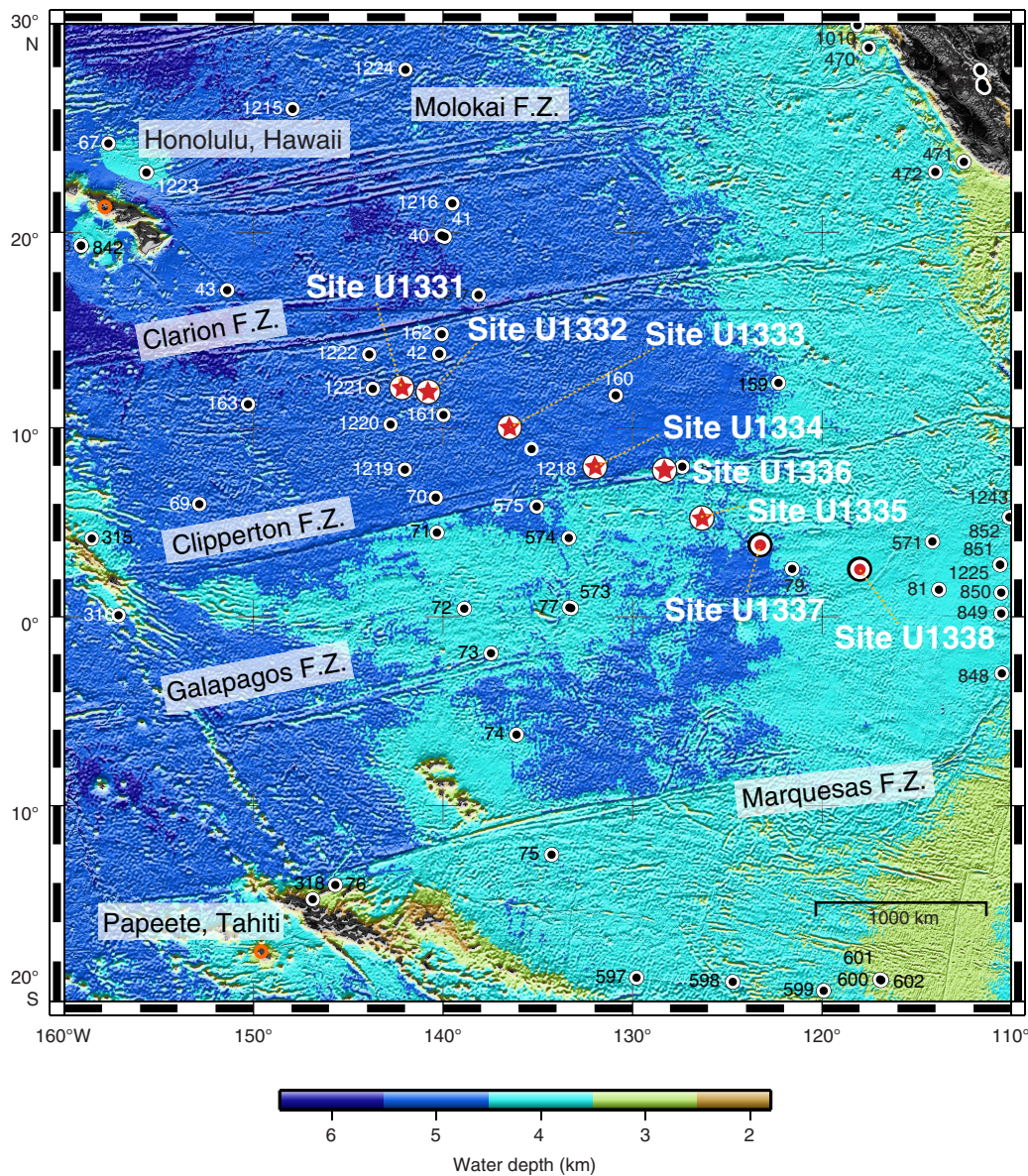


**Figure F2.** Evolution of oxygen stable isotopes ( $\delta^{18}\text{O}$ ) through the Cenozoic and related major phases of climate change (modified from Zachos et al., 2001b, 2008). Yellow boxes = time slices of interest for the PEAT program, green and blue boxes = ODP legs and sites previously drilled in the equatorial Pacific region; these additional sites will be used with the PEAT sites to obtain a nearly continuous Cenozoic record of the equatorial Pacific region. VPDB = Vienna Peedee belemnite. Oi-1 = Oligocene isotopic Event 1, Mi-1 = Miocene isotopic Event 1 (described in Miller et al., 1991). ETM2 = Eocene thermal maximum 2.

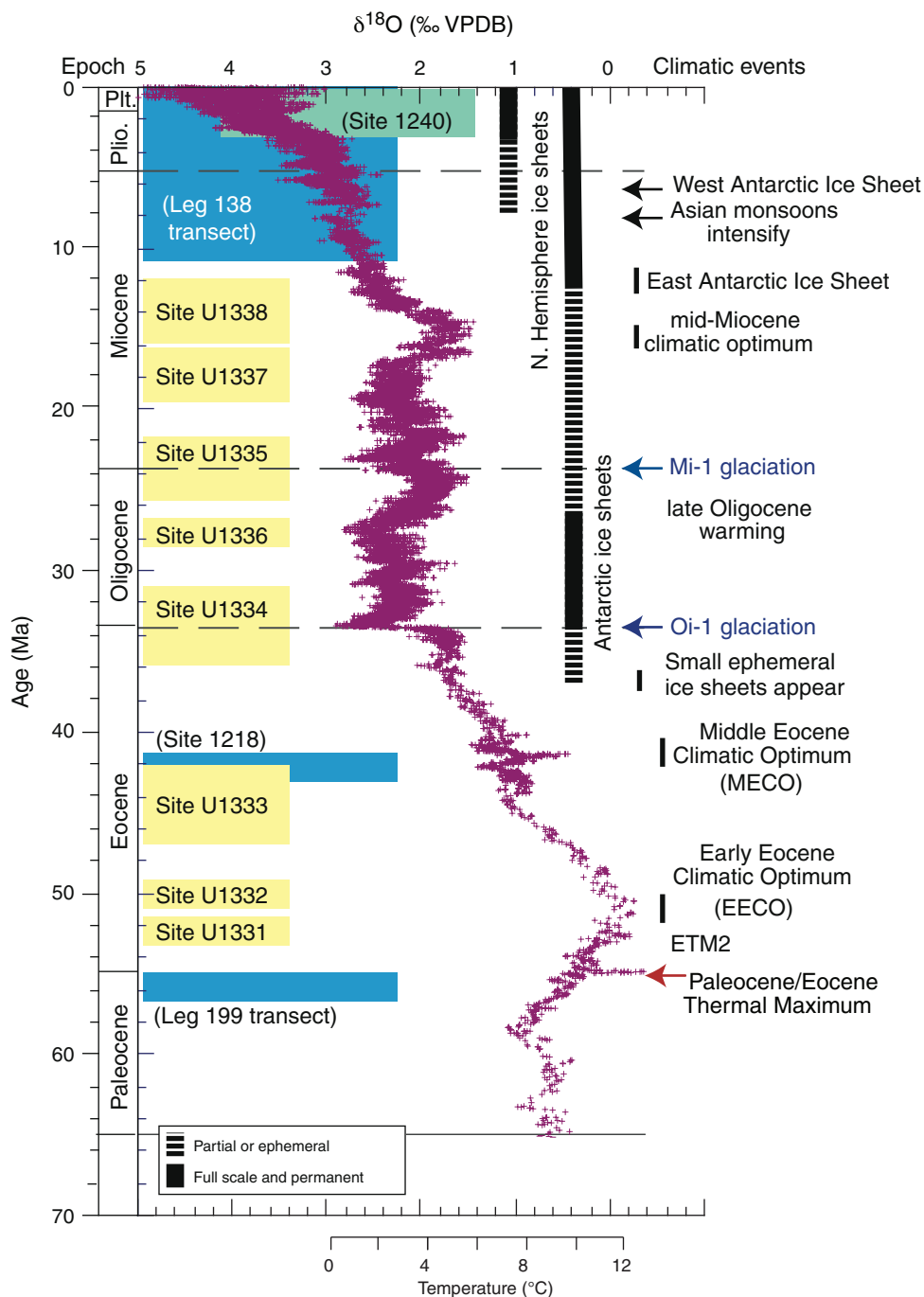


**Figure F3.** Targeting drill sites based on calcium carbonate compensation depth (CCD) history (van Andel, 1975), with new data from Leg 199 prior to coring. Colored boxes = critical time interval targeted for each site. Colored subsidence lines = time intervals when we expected carbonate to be deposited (i.e., when site is above CCD). Subsidence curves use a subsidence parameter calculated from estimated basement age of PEAT sites and their present-day depth ( $k = \sim 0.35$ ). Additional subsidence caused by sediment loading was not modeled.

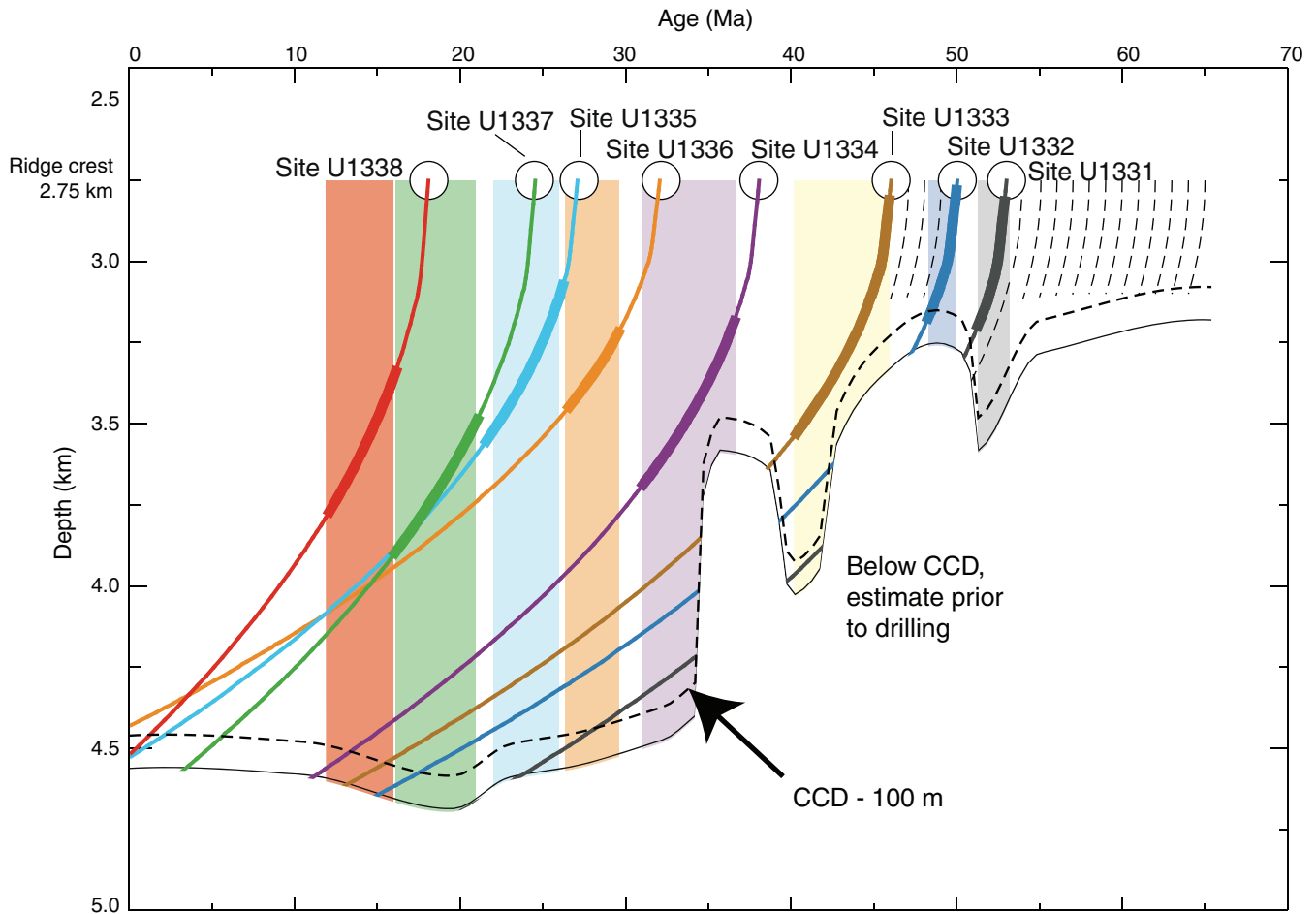




**Figure F5.** Backtracked latitudinal positions for PEAT sites and selected ODP sites (1218 and 1220) vs. geological age. Sites were backrotated along the flow line using stage poles from Koppers et al. (2001).

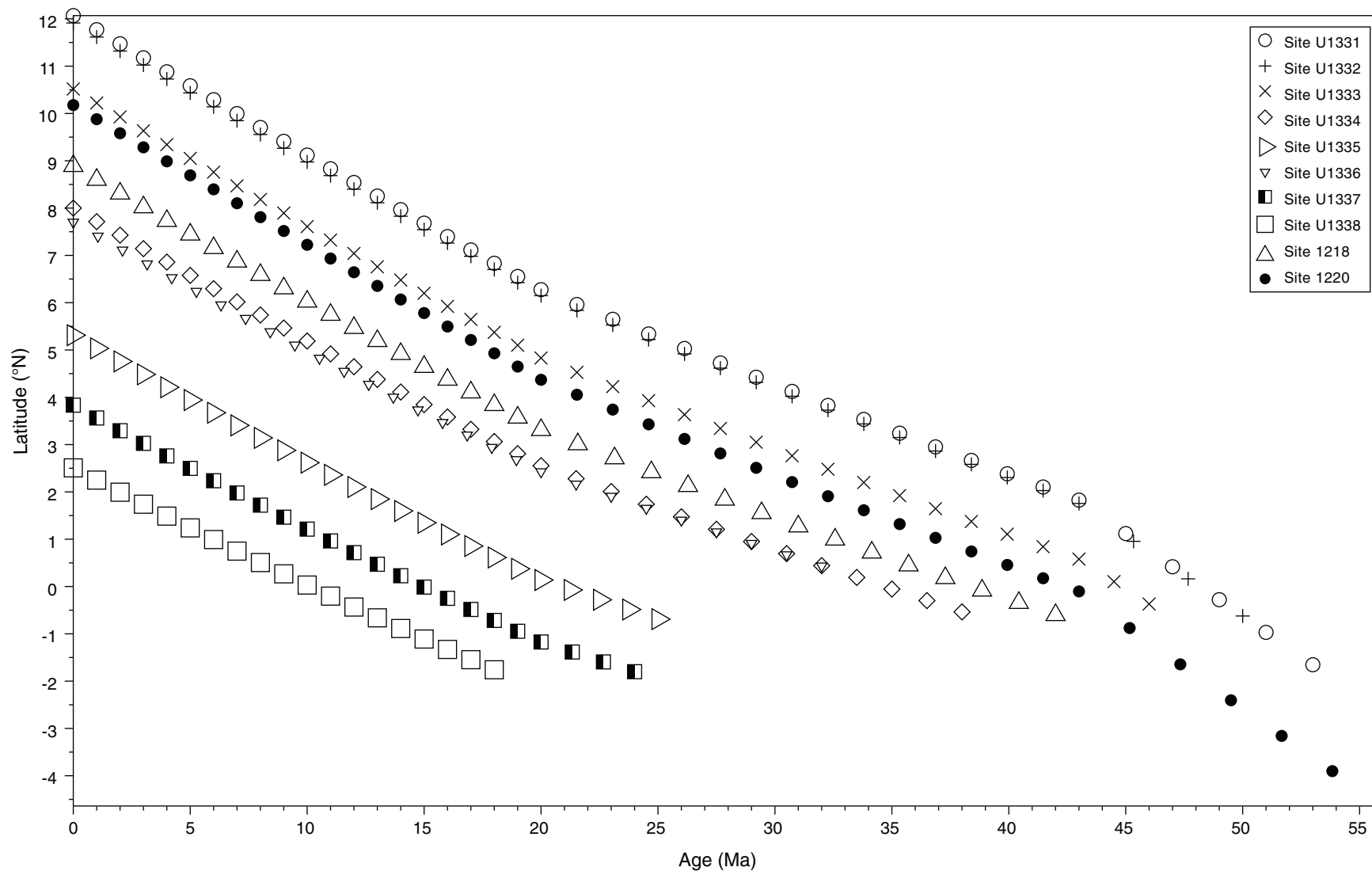


**Figure F6. A.** Backtracked positions for PEAT sites (red circles), using stage poles from Koppers et al. (2001) superimposed on a satellite-derived (GlobColour) map of present ocean chlorophyll-a concentrations (December 2005 mean monthly). Red = high productivity, blue = low productivity. Solid circles = previous DSDP and ODP sites. **B.** Backtracked positions for PEAT sites, with annotated positions every 10 m.y. back from present. Estimated basement ages for each site while situated at paleo-ridge crest are noted.

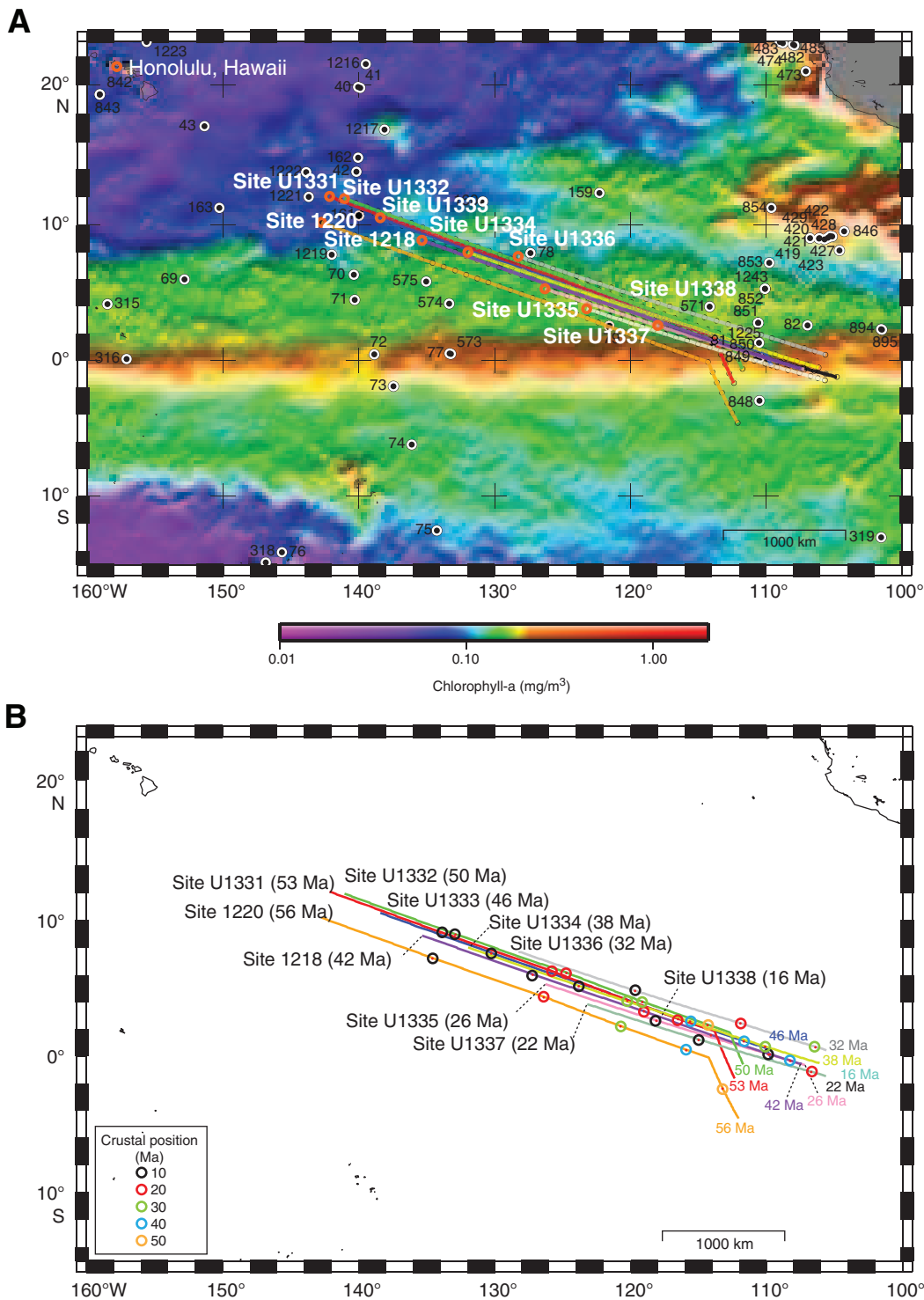


**Figure F7.** Times when PEAT sites (U1331–U1338) and selected DSDP and ODP sites (574, 572, 849, 851, and 1218) were positioned within paleoequatorial band. Equatorial band is defined as being within 2° latitude of Equator. Lighter shading = calcium compensation depth (CCD) (estimated prior to drilling for PEAT sites). Paleopositions were calculated with a fixed-hotspot model.

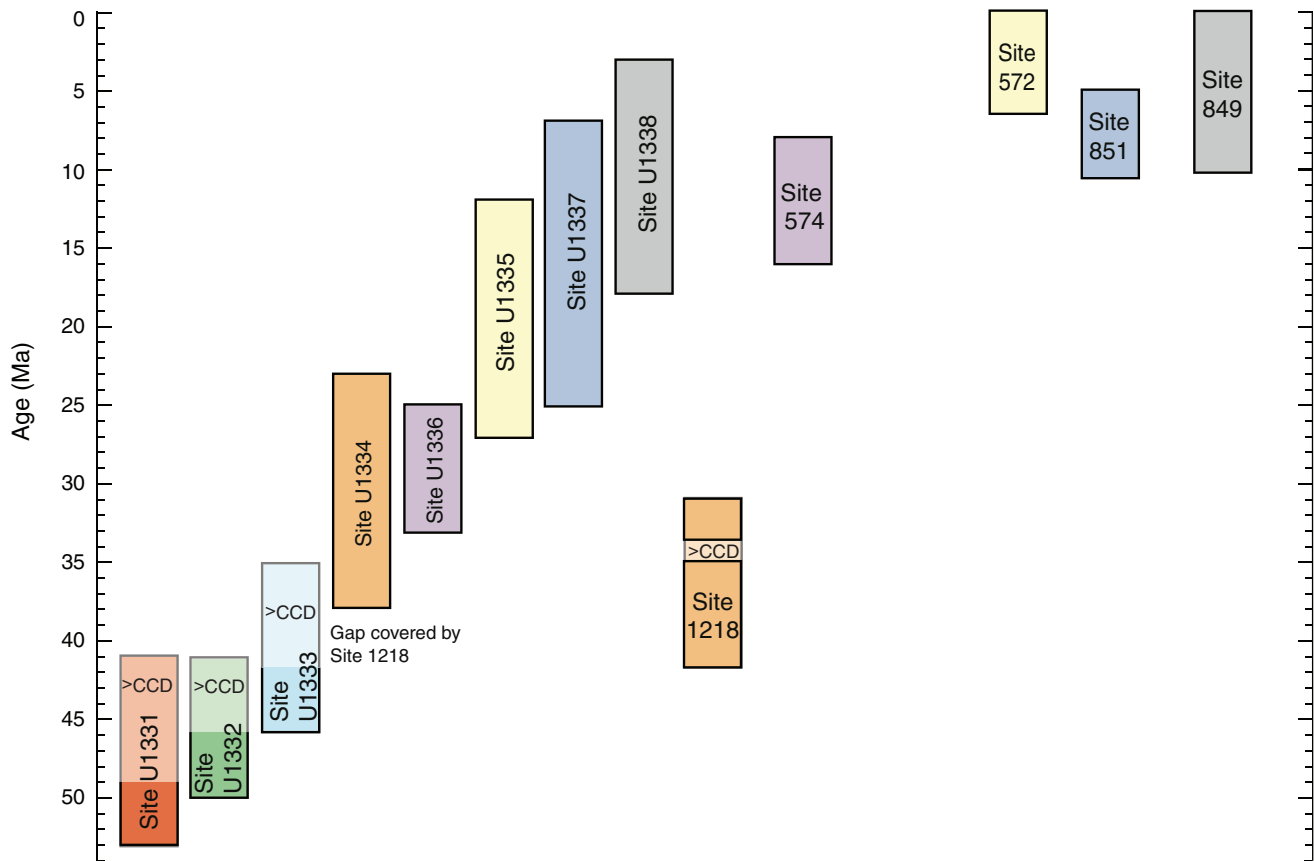


**Figure F8.** A. Model cross-section of equatorial sediment mound taking into account northward drift of Pacific plate. B. Mapped thickness of Pacific equatorial sediment mound. Color code = thickness of mound. (Both modified from Mitchell, 1998; Mitchell et al., 2003.)

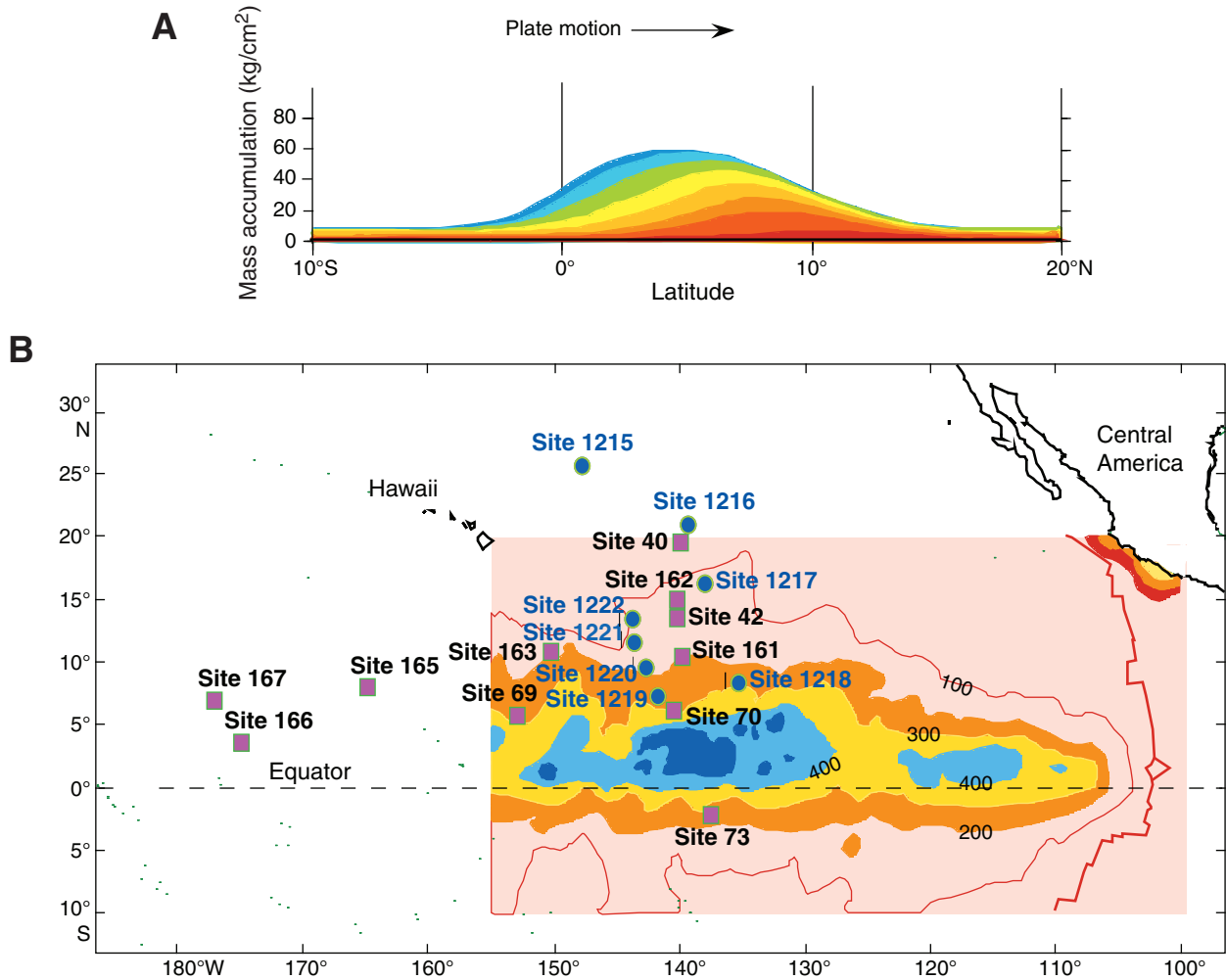


**Figure F9.** Coherence of sediment properties between widely separated drill sites in the equatorial Pacific is very high, allowing correlation of sediment properties over hundreds of kilometers. Figure shows Sites 1218 and 1219 (Shipboard Scientific Party, 2002), two sites >740 km apart. VGP = virtual geomagnetic pole, GRA = gamma ray attenuation,  $L^*$  = lightness reflectance value of sediment as defined in the LAB color model. GRA and magnetic susceptibility were completed on board. (**Figure shown on next page.**)

Figure F9 (continued). (Caption shown on previous page.)

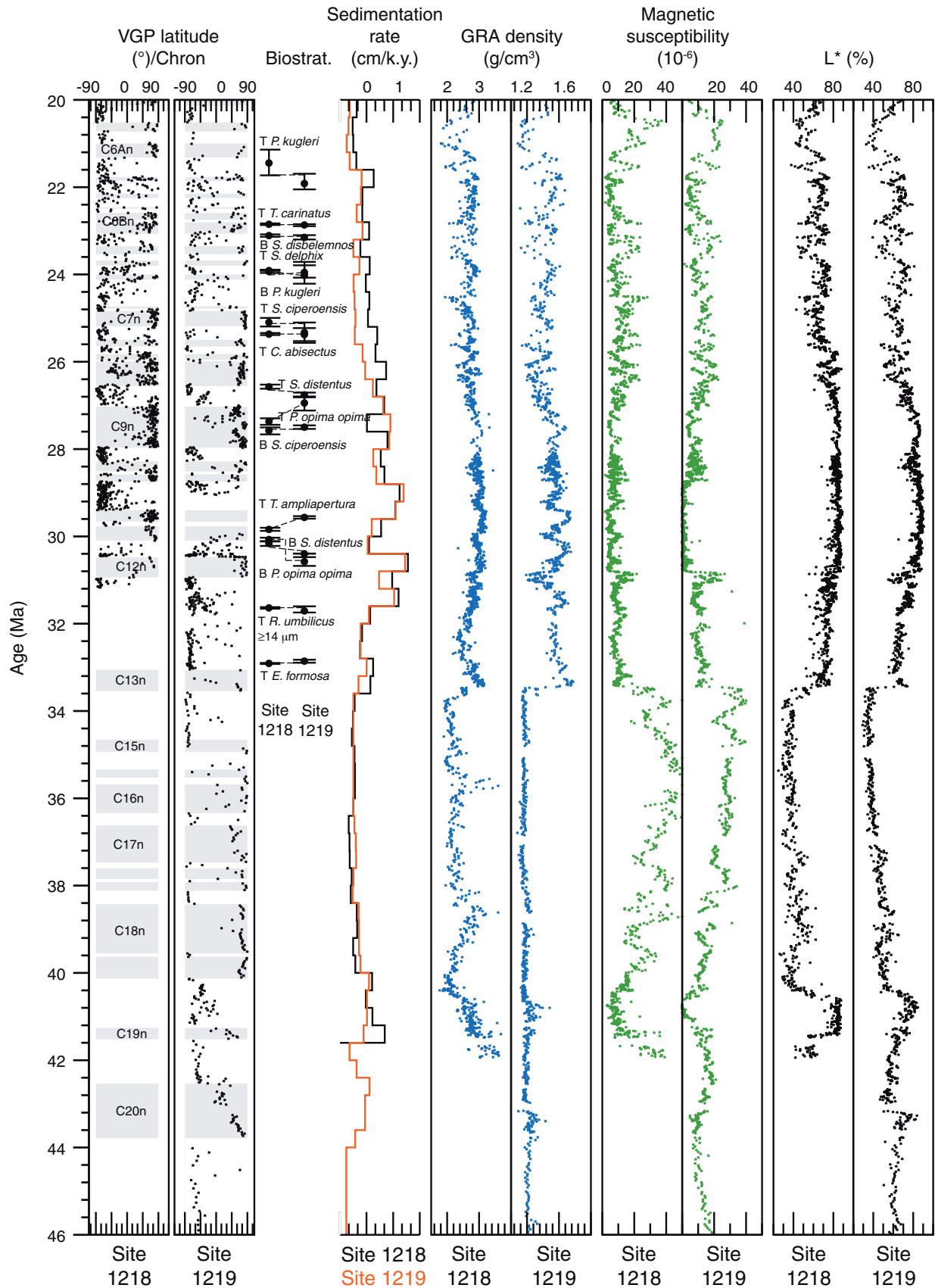


**Figure F10.** Model of early Eocene equatorial upwelling from Huber (2002), showing global land-sea distribution and annual average upwelling into thermocline (56 Ma sites, fixed-hotspot paleopositions). Red = regions of vigorous upwelling, green to blue = regions of weak upwelling, white = areas of average downwelling. Current streamlines at ~100 m ocean depth are shown for the Pacific Ocean. All map views are projected on a Mollweide projection. Upwelling region in eastern Pacific was broader than that of the modern region, primarily because of secondary upwelling centers on edges of region.

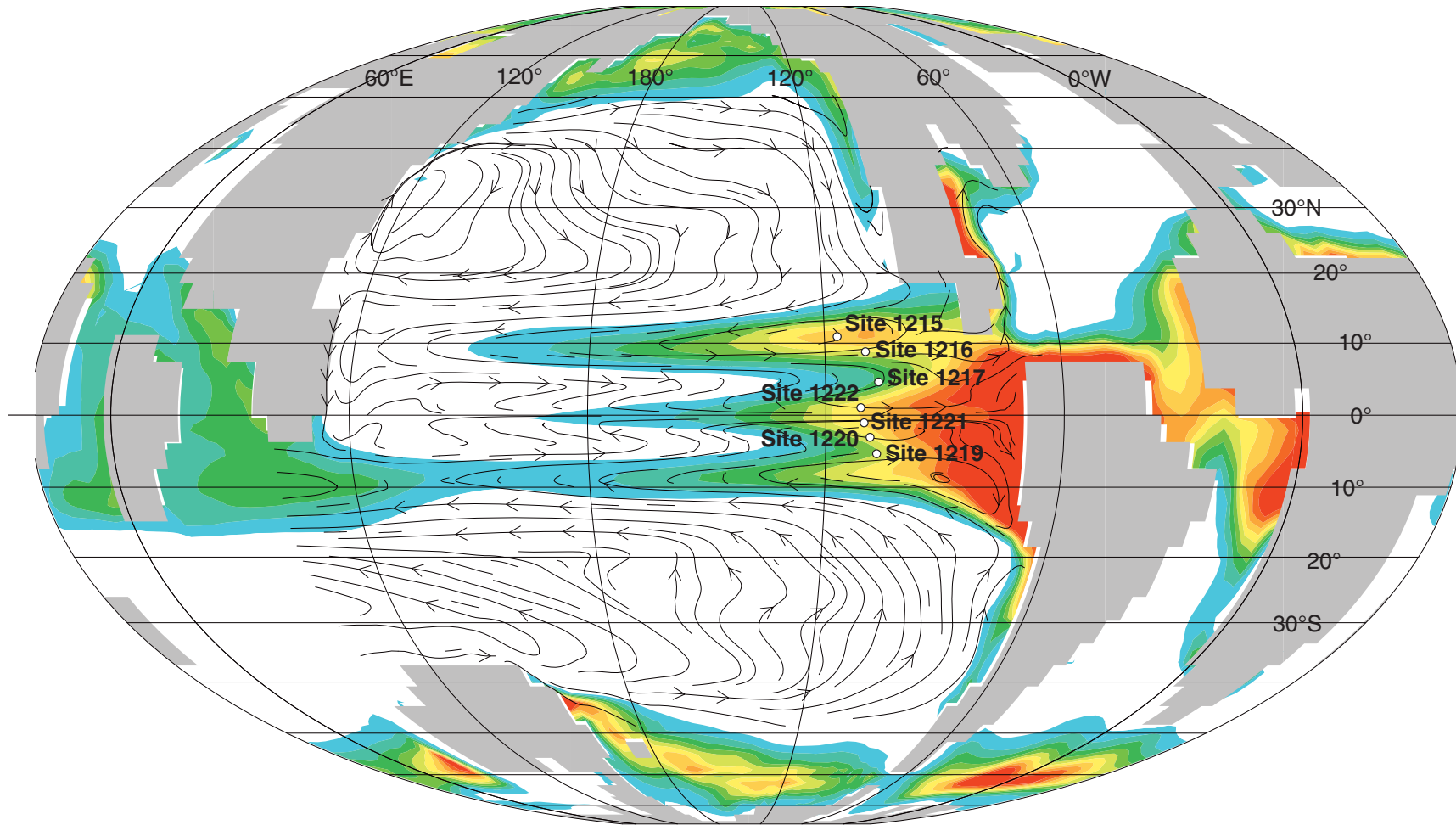


**Figure F11.** Average sedimentation rate for the interval 40–46 Ma, given in m/m.y. (after Moore et al., 2004). DSDP and ODP site positions are backtracked to their estimated position at 43 Ma. Site locations are colored according to sediment type for the time interval: blue = carbonate, green = siliceous-carbonate, red = siliceous, brown = clay. Contours are at 1, 5, and 10 m/m.y. Red dashed line = approximate geographic paleoequator based on the sediment archive, with a notable difference compared to the fixed-hotspot based rotation. Two regions of relatively high accumulation occur on both sides of the paleoequator in addition to the primary upwelling center.

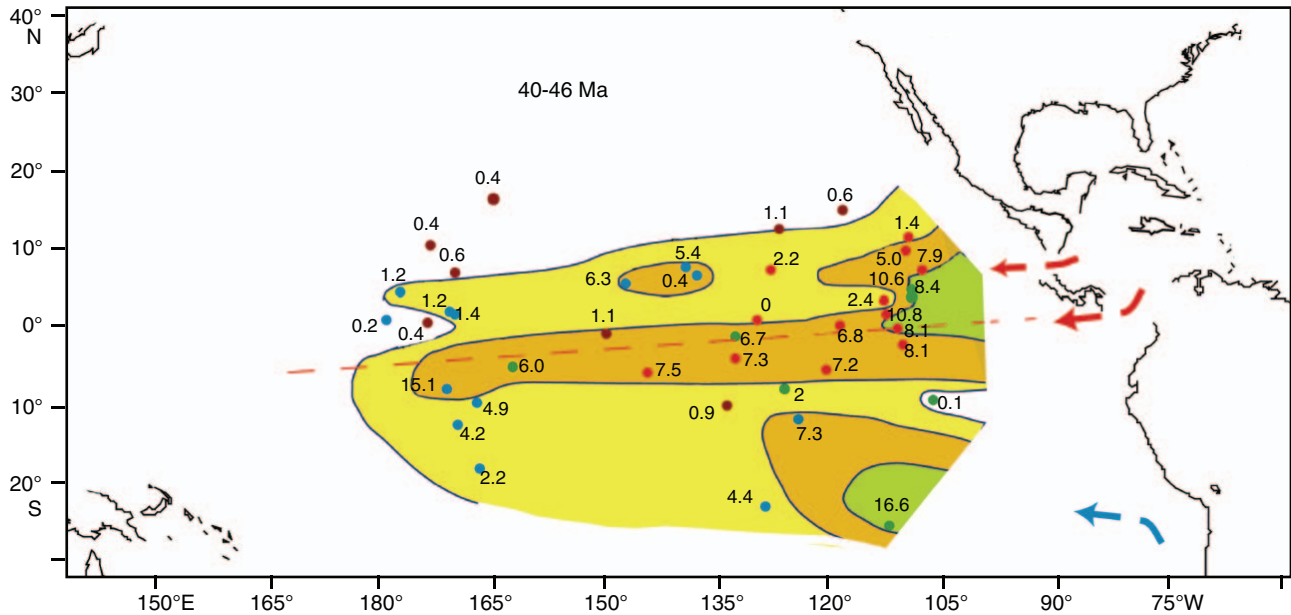


**Figure F12.** Summary of sedimentation rates derived from age-depth models at each PEAT (Expedition 320/321) site plotted vs. corrected core composite depth, method A (CCSF-A).

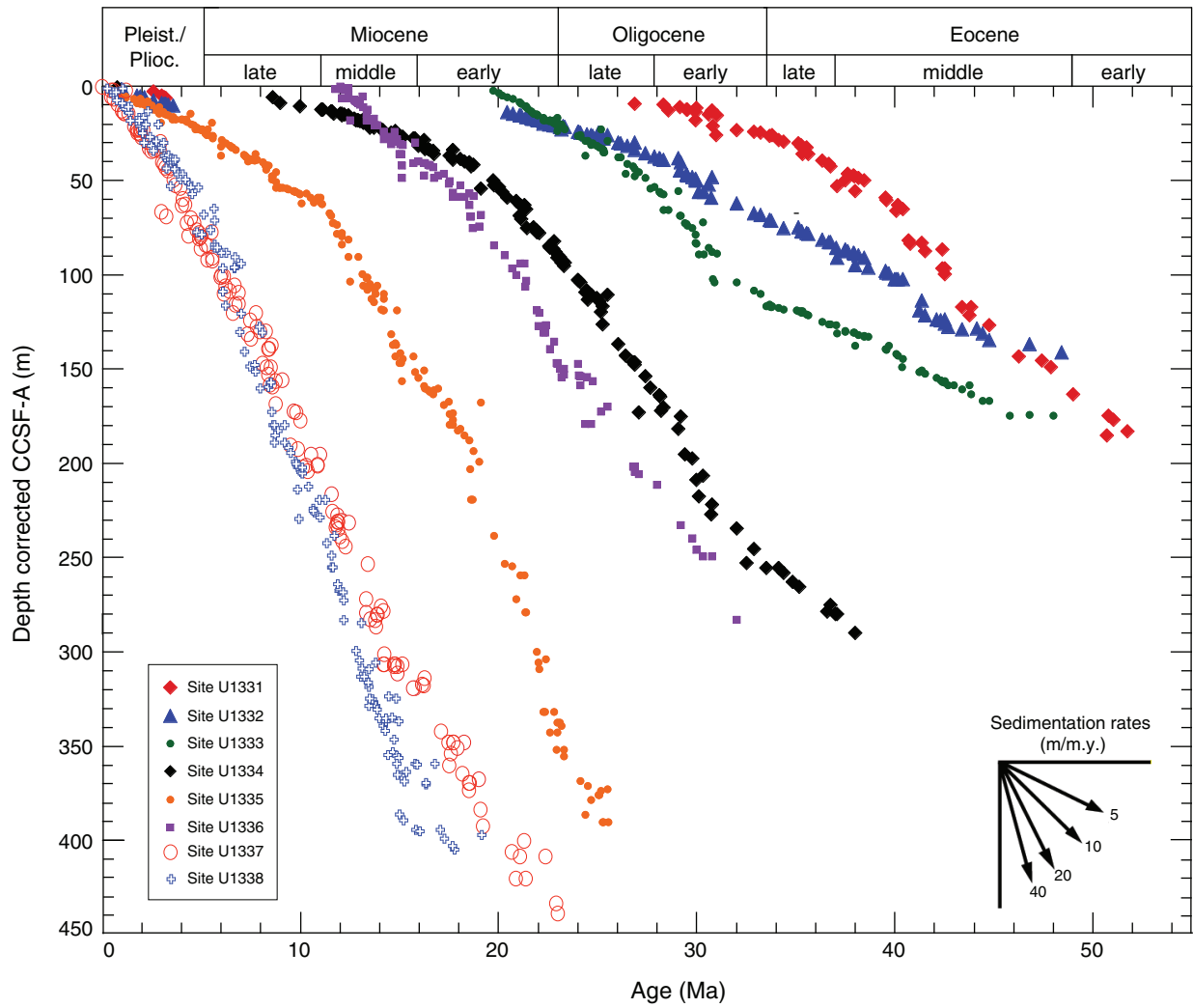


**Figure F13.** Stratigraphic summary plots, PEAT Sites U1334–U1338 and ODP Site 1218. Green = Eocene, blue = Oligocene, yellow = Miocene, pink = Pliocene–Pleistocene. CSF-A = core depth below seafloor, method A; DSF = drilling depth below seafloor.

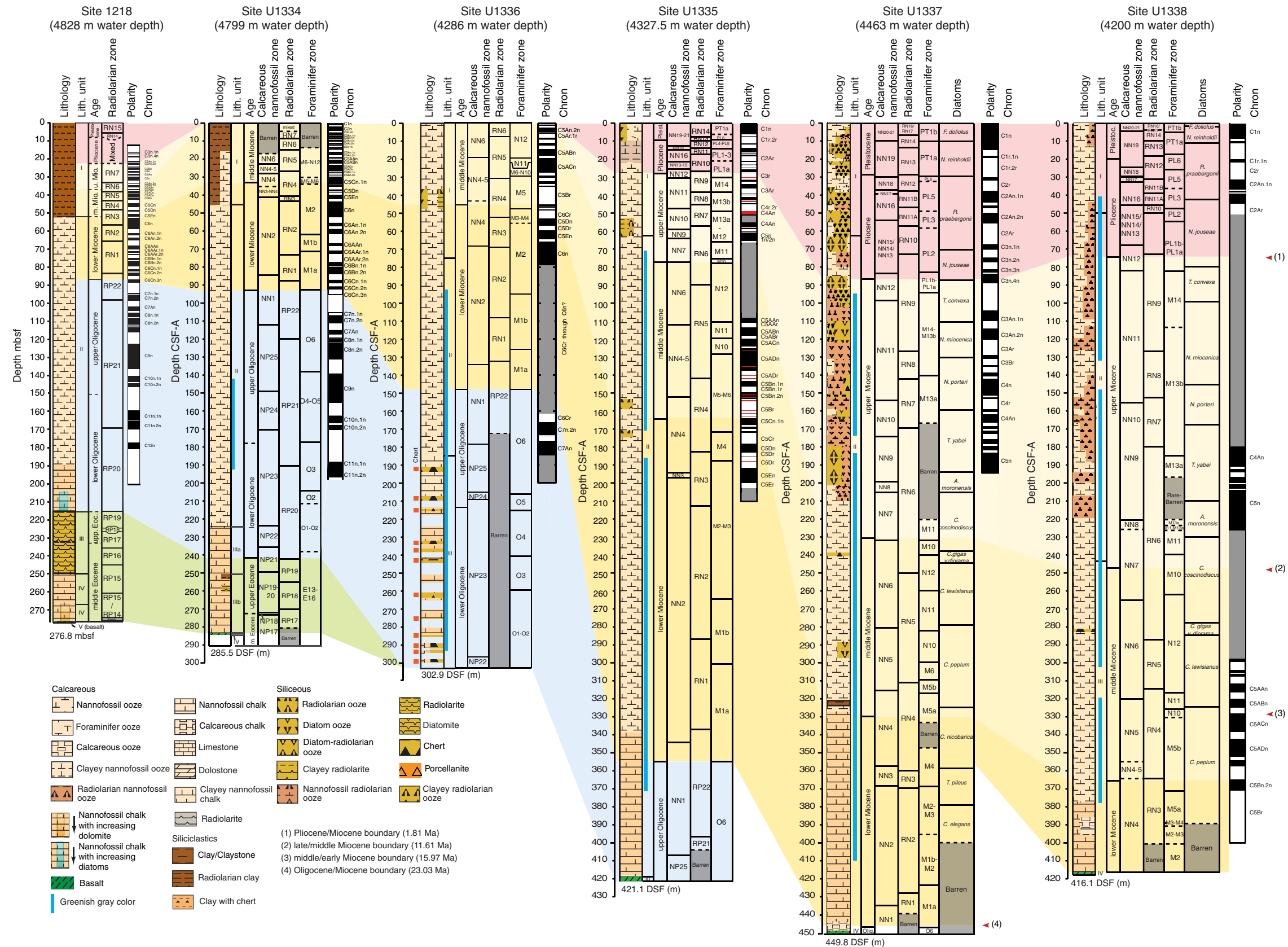


**Figure F14.** Expedition 320/321 Sites U1334–U1338 and ODP Site 1218 plotted against the PEAT timescale. Sites are plotted approximately ordered by site longitude and basement age. Estimated crustal ages are shown underneath each stratigraphic column. Carbonate accumulation events (CAE) appear as defined by Lyle et al. (2005). MECO = Middle Eocene Climatic Optimum.

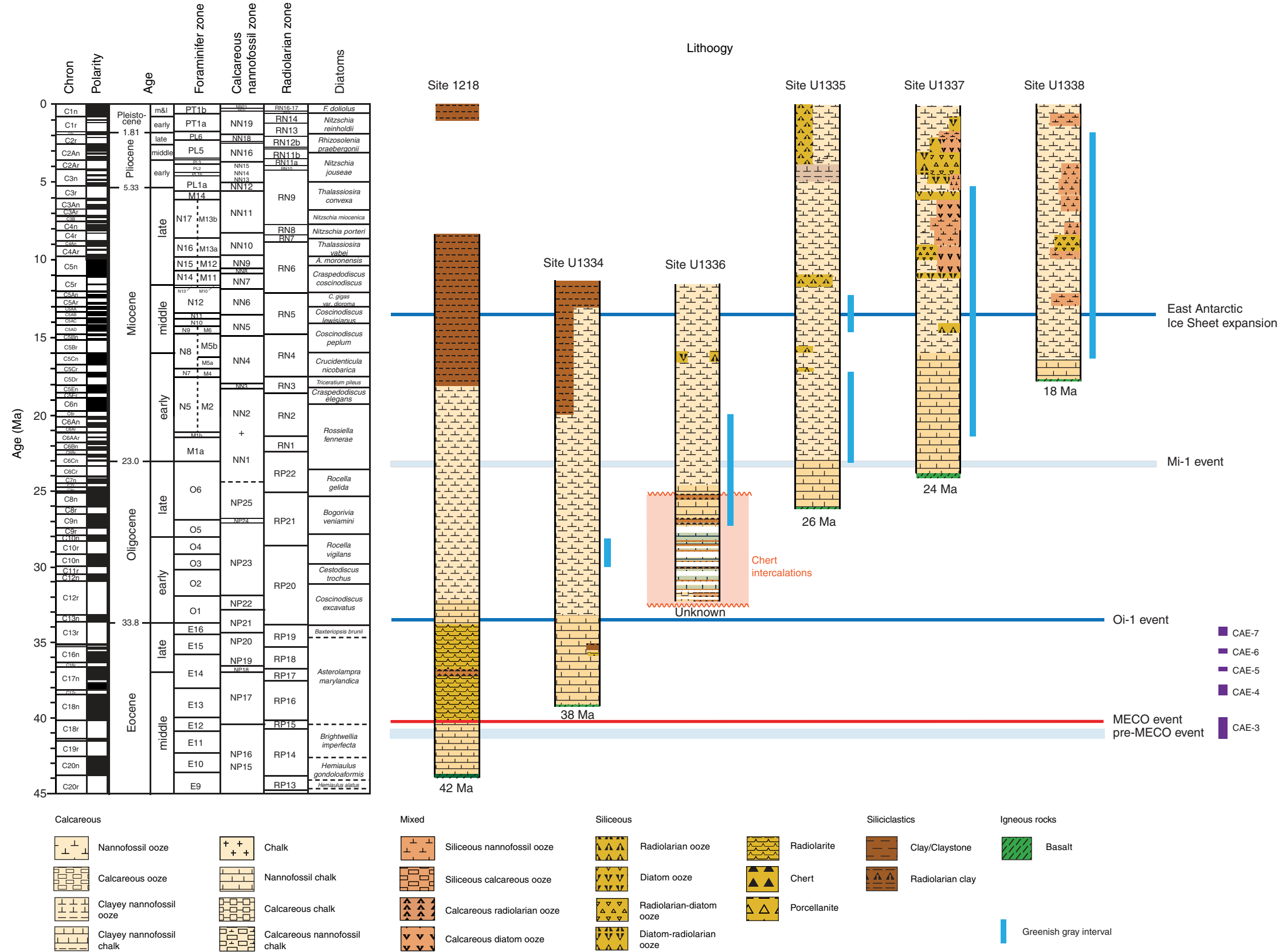
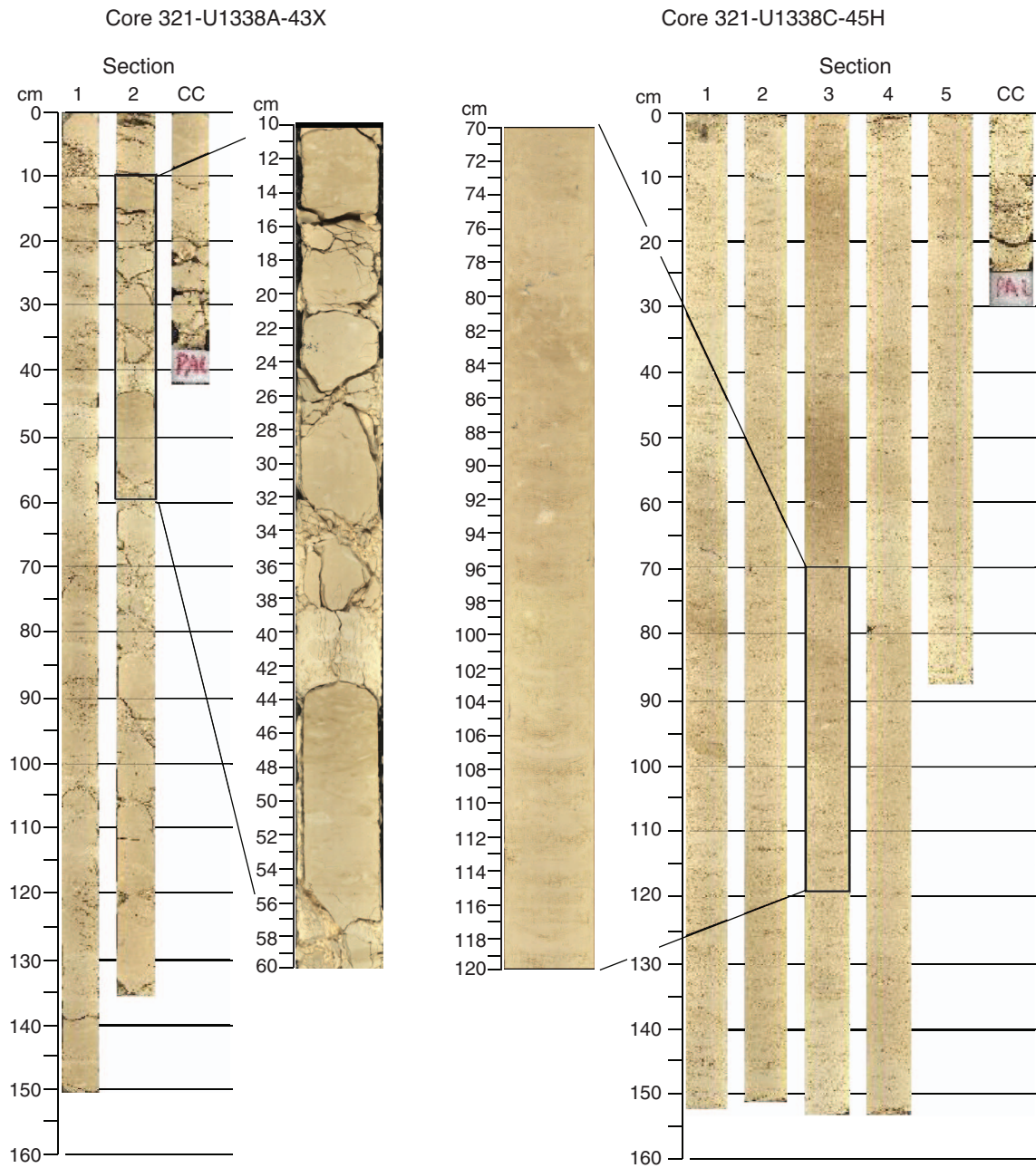
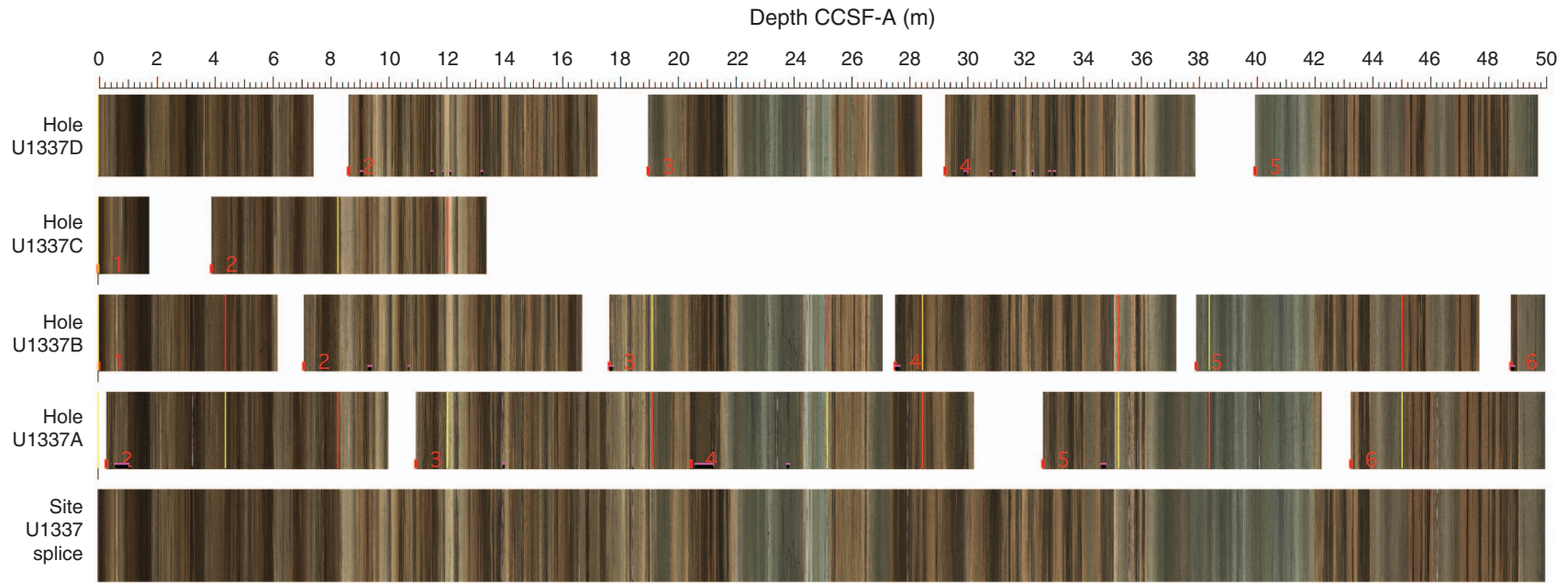


Figure F15. Comparison of XCB vs. APC drilling recovery in roughly equivalent intervals, Site U1338.



**Figure F16.** Digital line scan images, Site U1337. Red lines = base of a splice interval (tie point), yellow lines = top of the next splice interval (tie point). Images were depth registered by Roy Wilkens using IGOR-Pro software.



**Figure F17.** Depth vs. natural gamma radiation (NGR), Sites U1331–U1338. CSF-A = core depth below seafloor, method A.

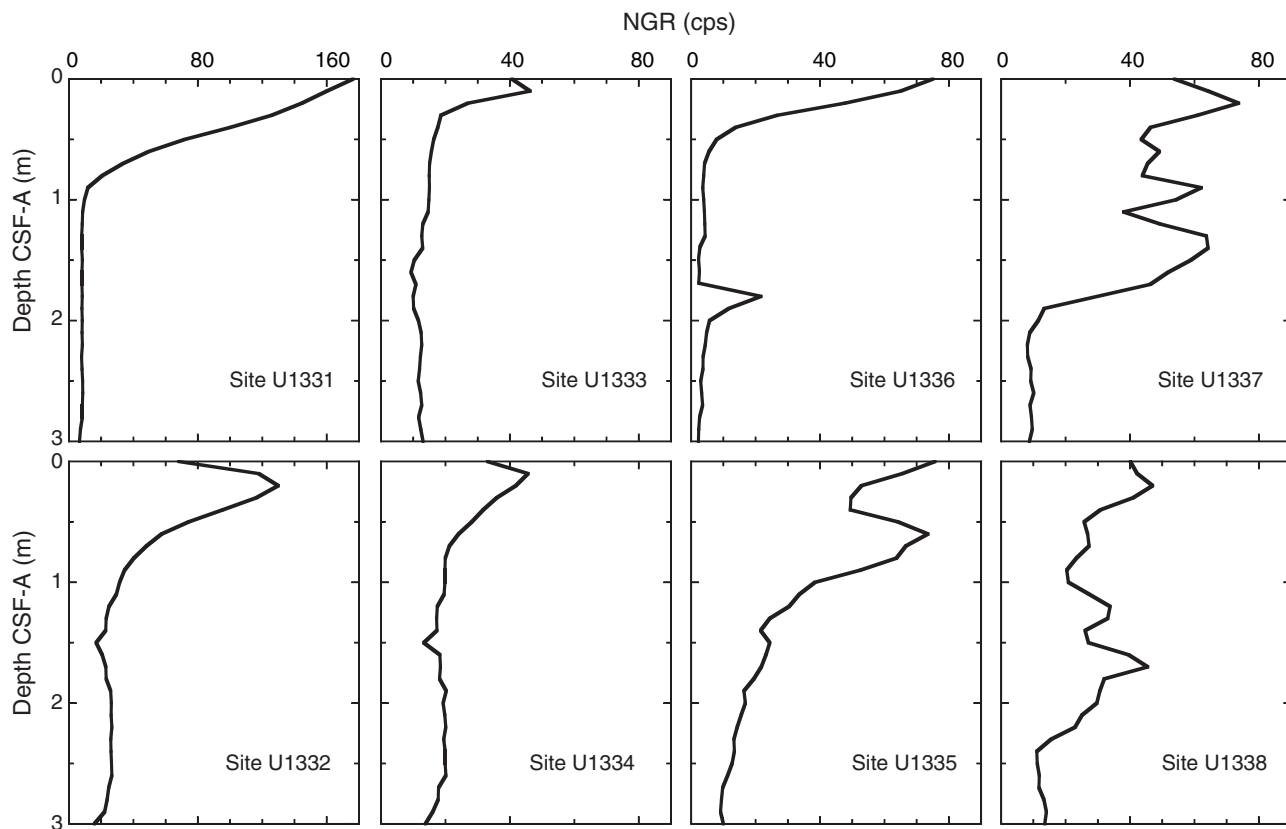


**Figure F18.** Downhole variation of paleomagnetic declination (green) and magnetostratigraphic interpretations, Sites U1334–U1338. Red lines = possible geomagnetic excursions. CSF-A = core depth below seafloor, method A.

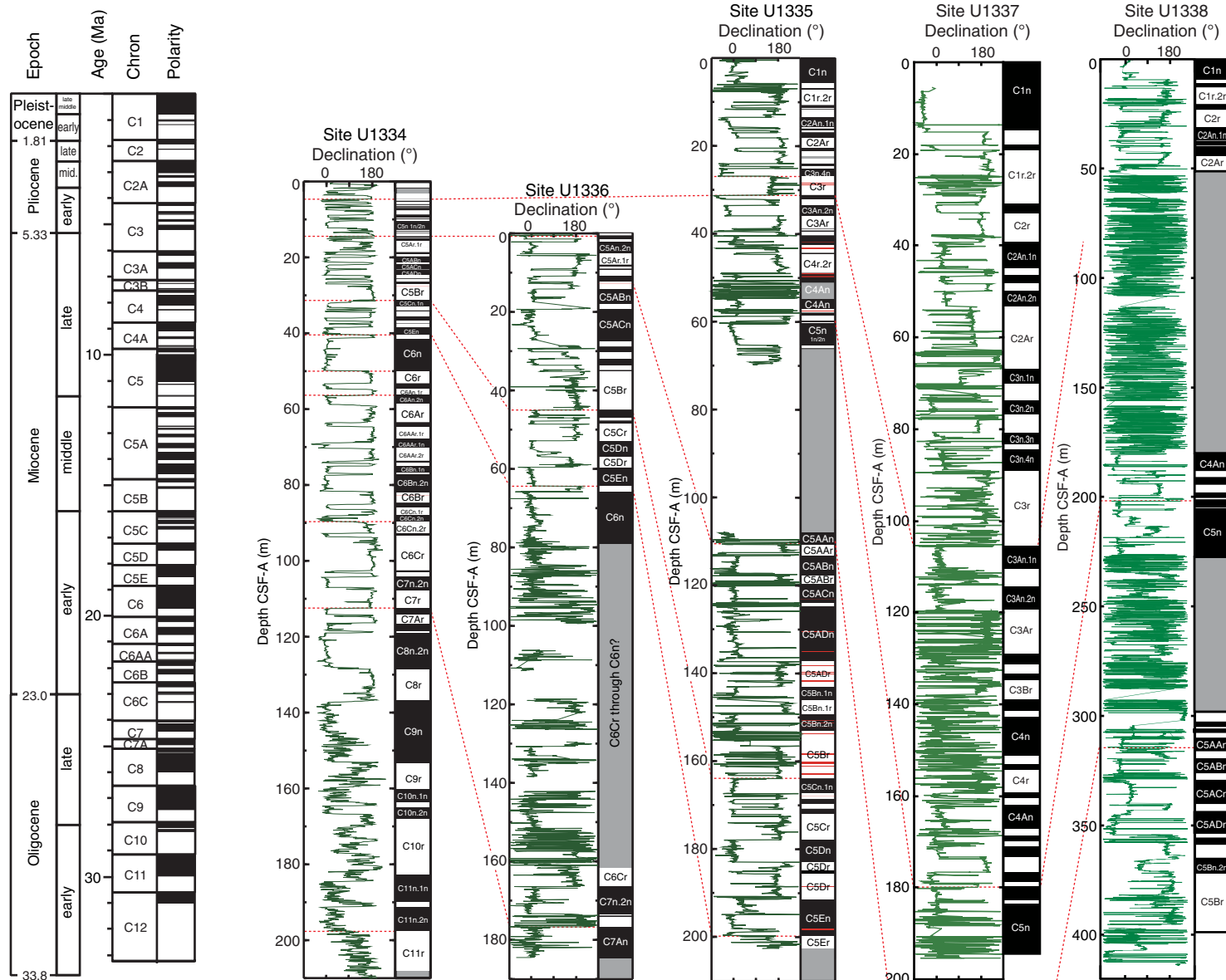


**Figure F19.** Planktonic foraminifer assemblage variations, Holes U1337A and U1338A. Correlation lines based on biochronologic data. CSF-A = core depth below seafloor, method A.

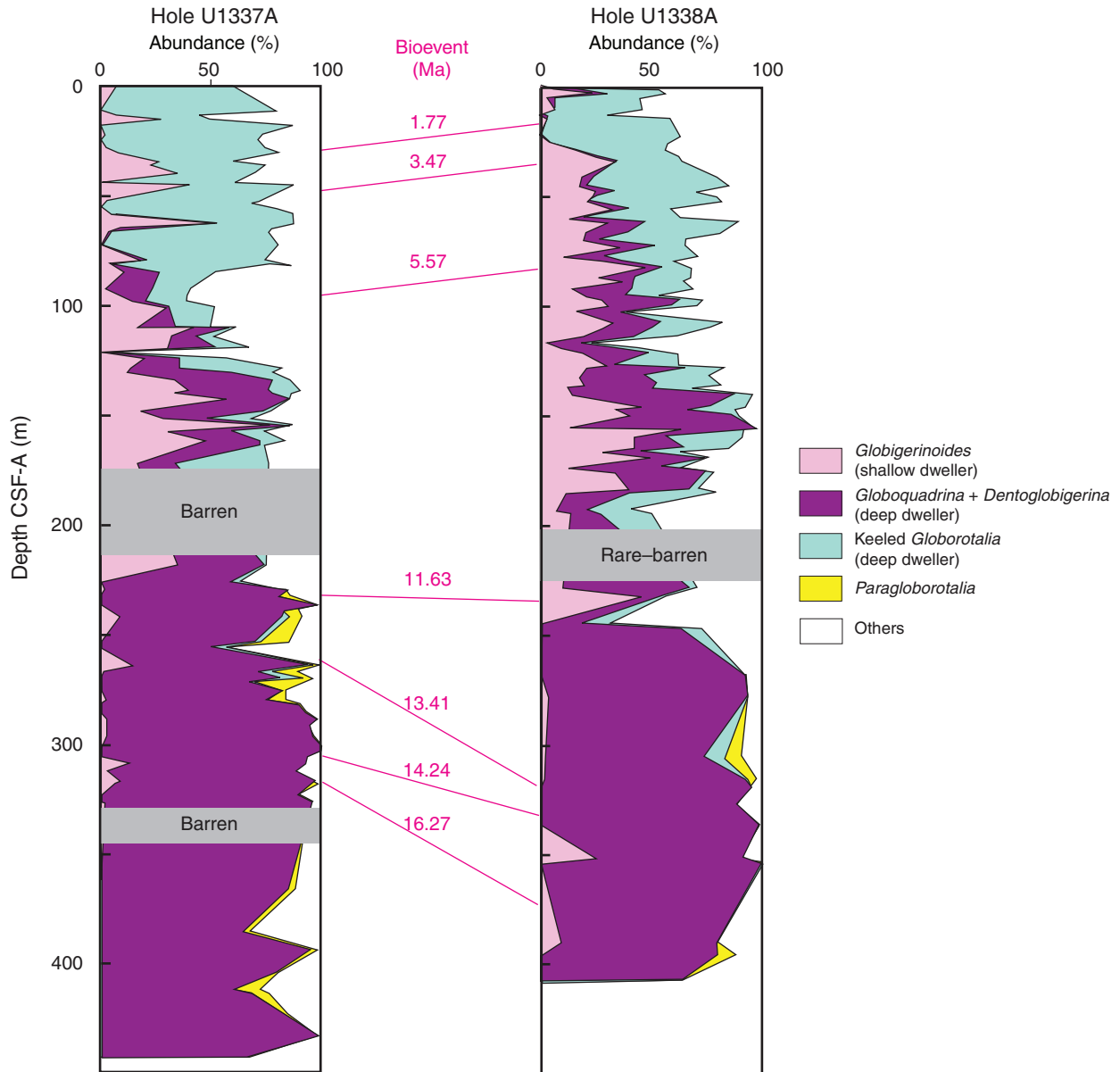


**Figure F20.** Planktonic foraminifer abundance and benthic/planktonic foraminifer ratios, Sites U1337 and U1338. Red line = average values. Light blue shading = low-carbonate (dissolution) interval (“carbonate crash”) (Lyle et al., 1995). Downcore variations in planktonic vs. benthic foraminifers reflect intervals of dissolution during the Pleistocene to early Miocene. Benthic foraminifers are more resistant to dissolution than most planktonic forms. PF = planktonic foraminifer.

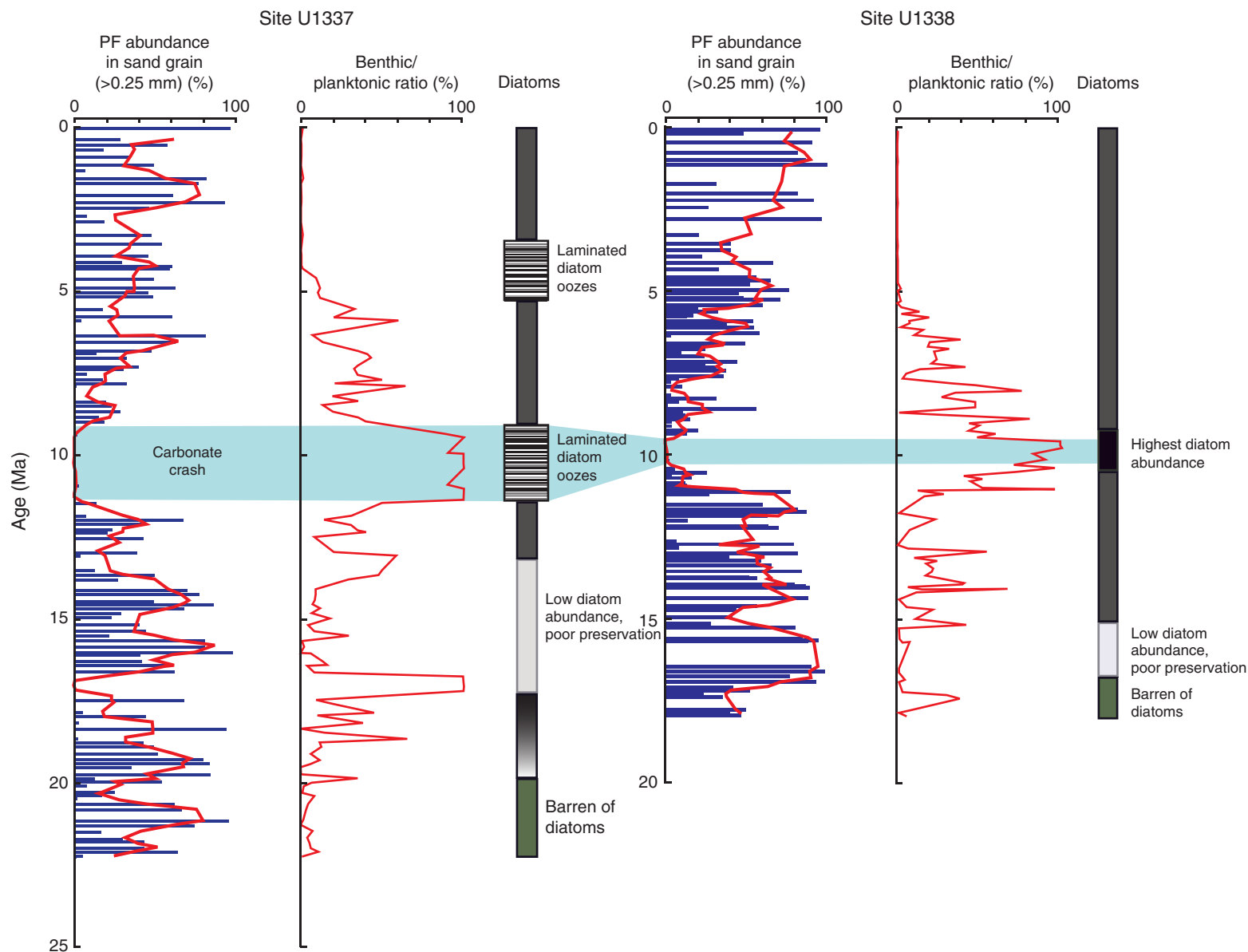


**Figure F21.** Stratigraphic compilation of diatom abundance in sediments from Expedition 320/321 and ODP Site 1218. Data for the Expedition 320/321 sites are from shipboard analysis. Data from Site 1218 are from Steiger (2006).

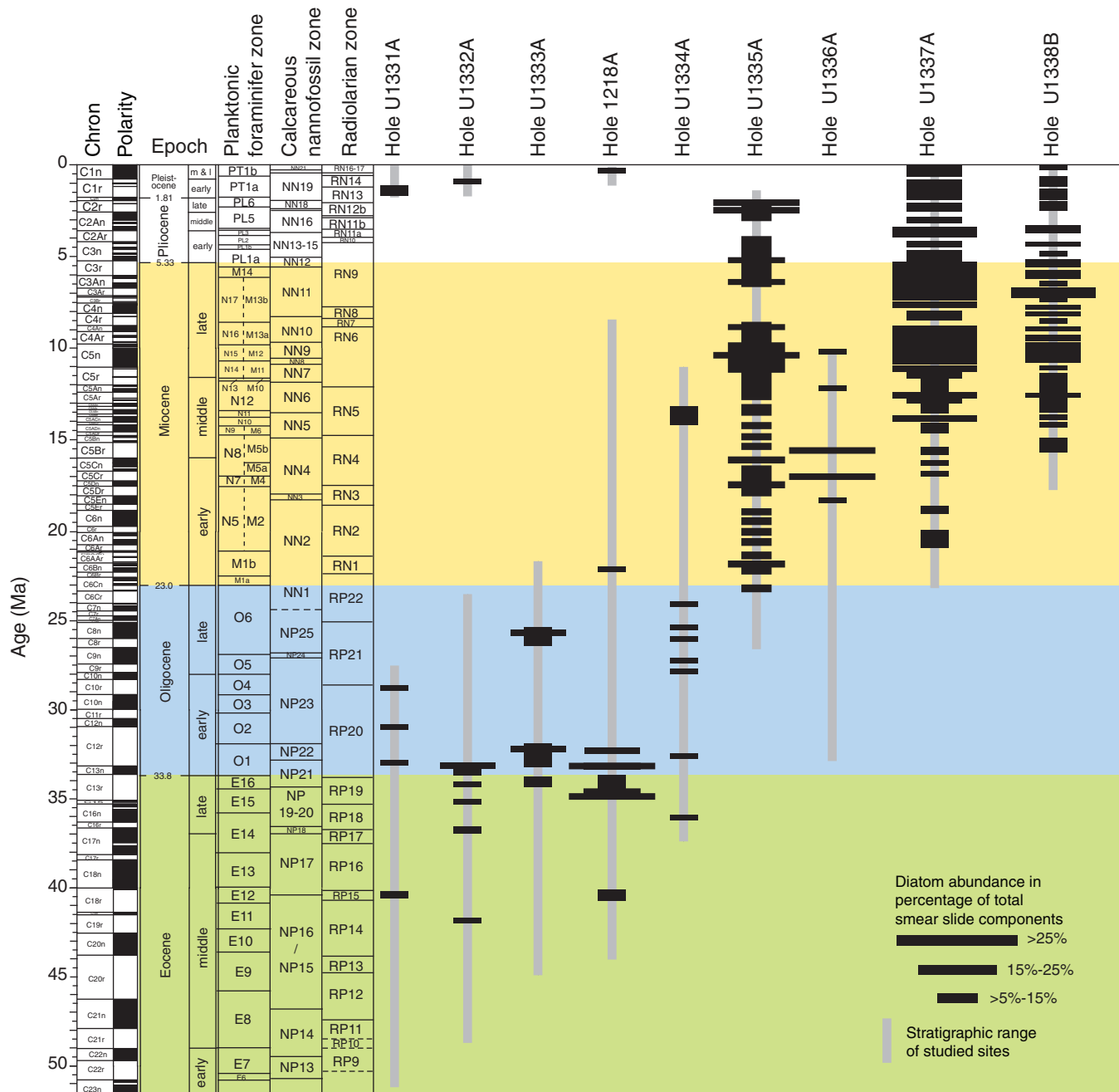


**Figure F22.** A. Digital line scan image of diatom mat from Section 321-U1337C-6H-2. B. Light microscope photograph (plane-polarized light, 400×) of *Thalassiothrix* diatom mat.

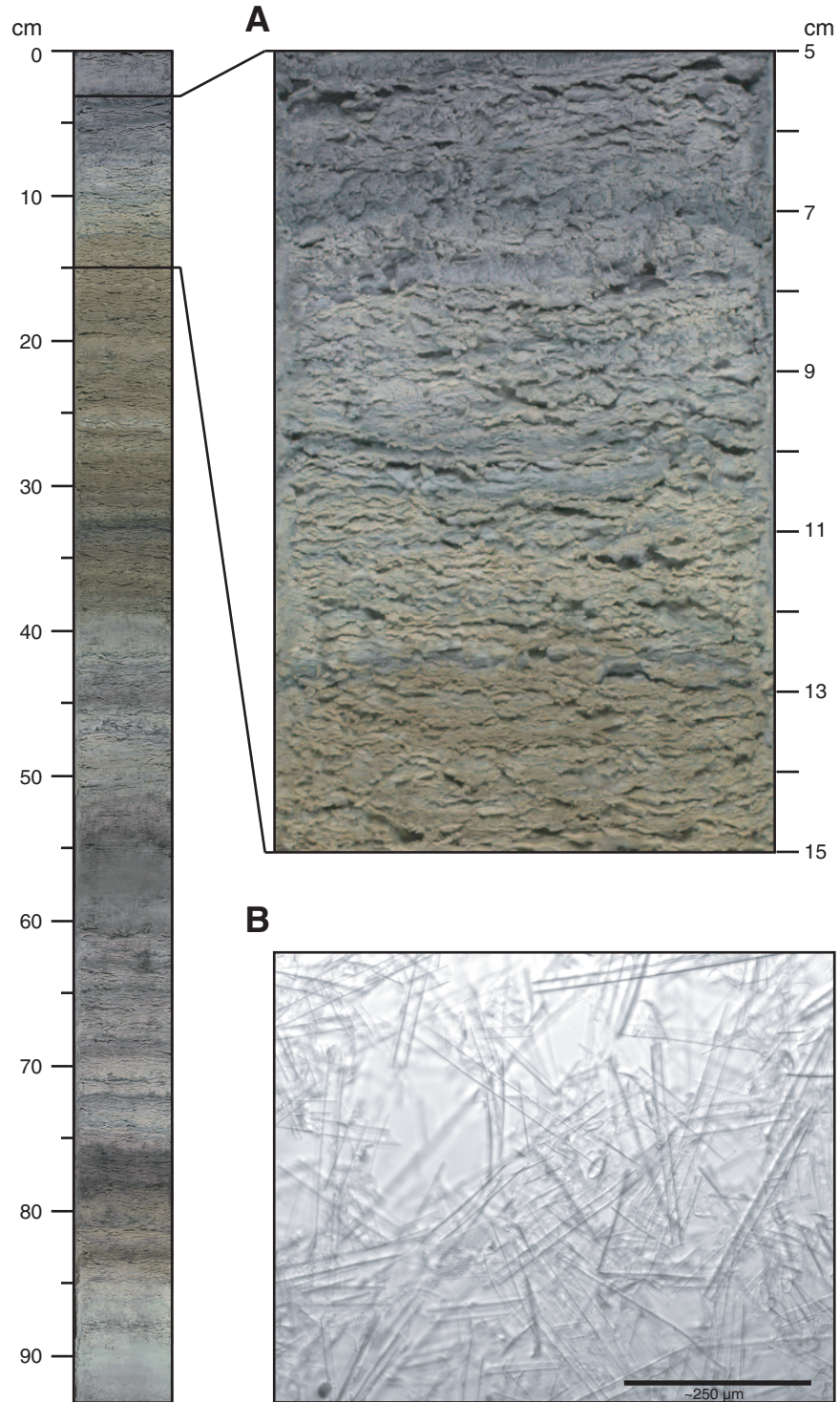


**Figure F23.** Summary of occurrence vs. age of recovered intervals of diatom mats and diatom-rich sediments, Expedition 321 Sites U1337 and U1338; ODP Sites 844, 847, and 849–851; and DSDP Site 572.

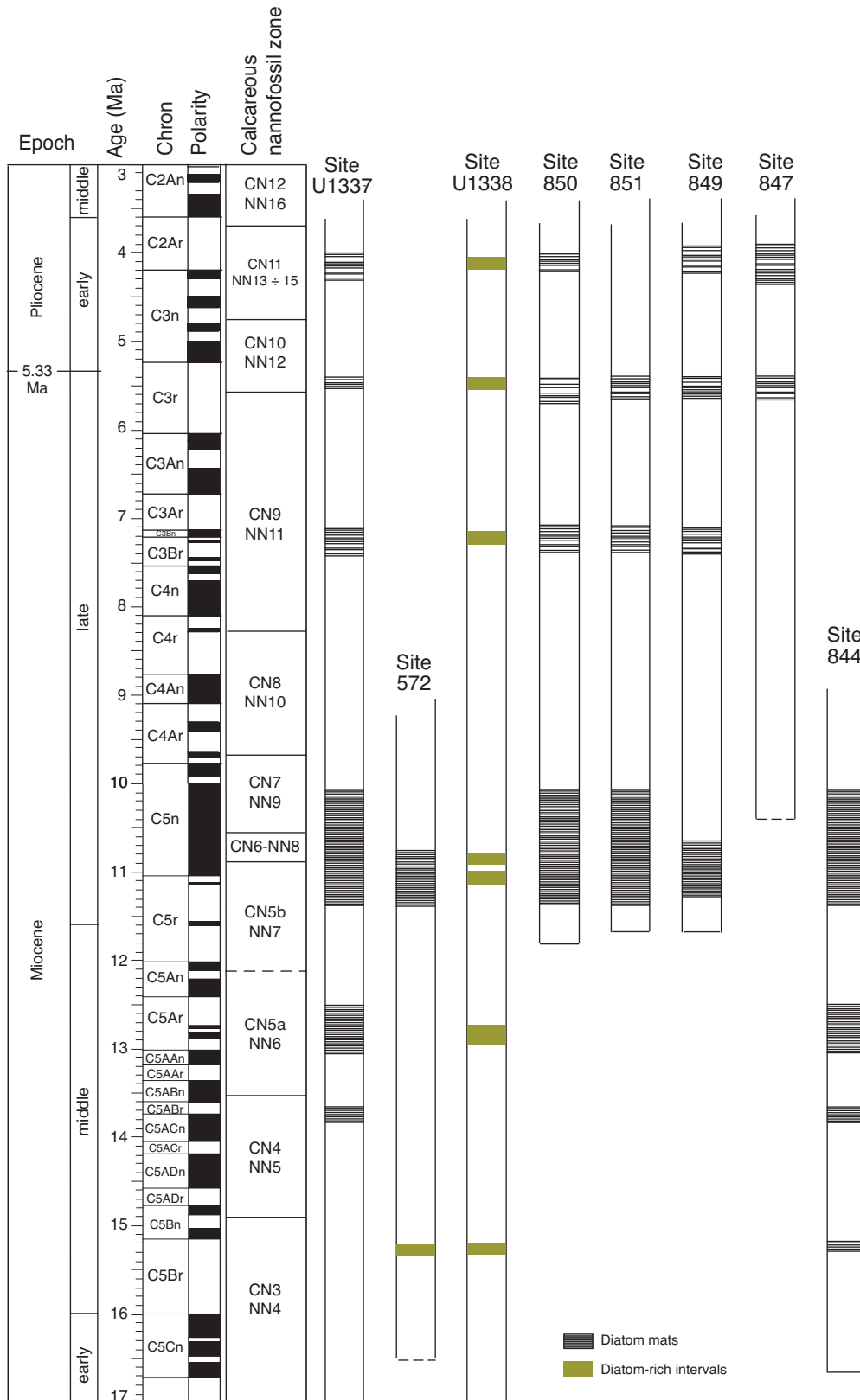


**Figure F24.** High-resolution bulk density downhole logs from Holes U1337A (black) and U1338B (red) with depth scales shifted and stretched to match the different sedimentation rates at the two sites. Blue = nannofossil events and respective ages. Pa, Rp, Dh, Cm, Dk, Sh, Dc = calcareous nannofossil biostratigraphic datum levels. Depths of nannofossil events are core depths below seafloor and may differ from wireline log matched depth below seafloor (WMSF) by several meters.

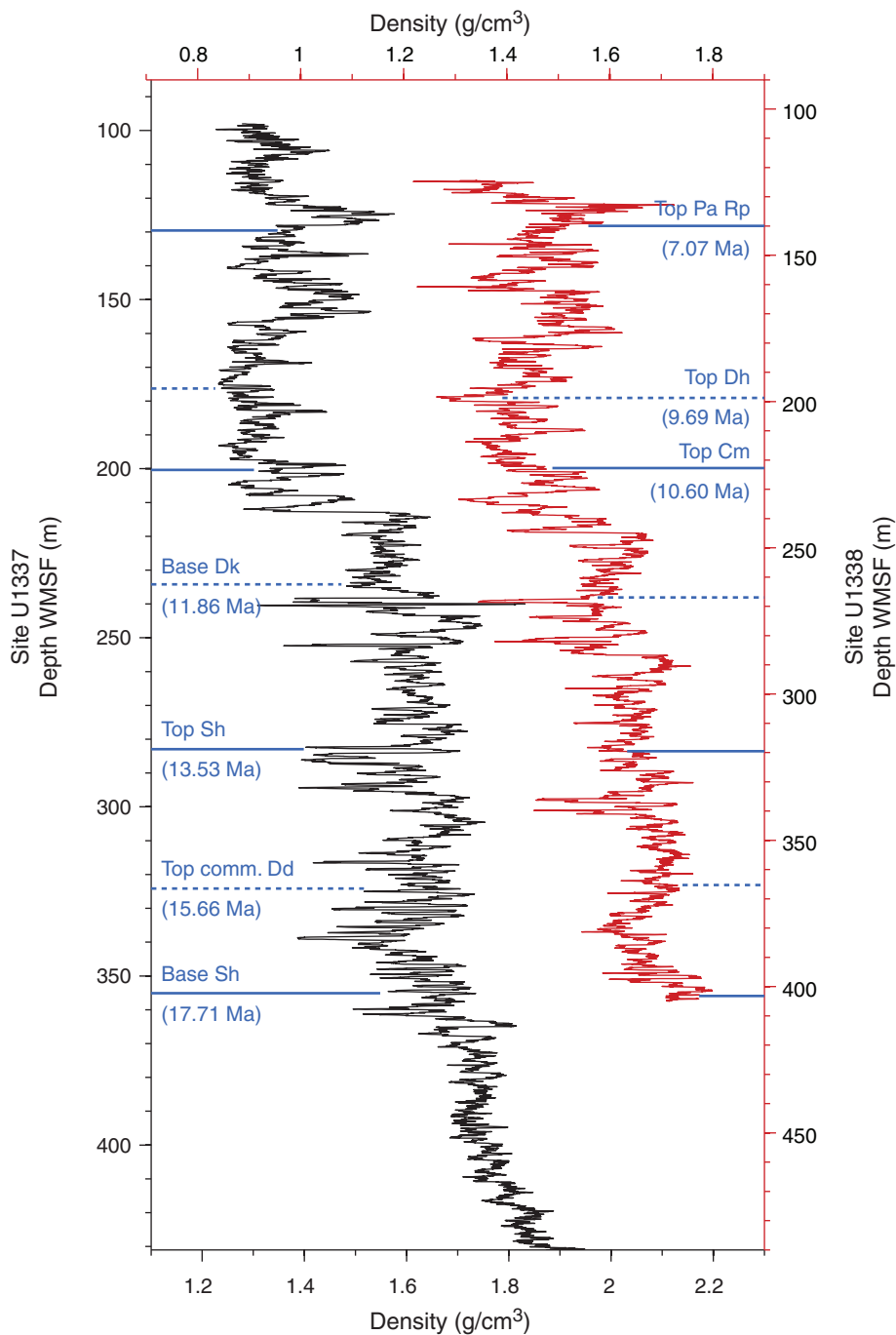


**Figure F25.** Correlation between seismic reflection records from DSDP Site 574, Site U1337 seismic imaging, and logging data from Hole U1337A. MAD = moisture and density, p1 = uplog pass 1, p2 = uplog pass 2, IMPH = medium induction phasor-processed resistivity, SFLU = spherically focused resistivity, VSP = vertical seismic profile, WMSF = wireline log matched depth below seafloor.

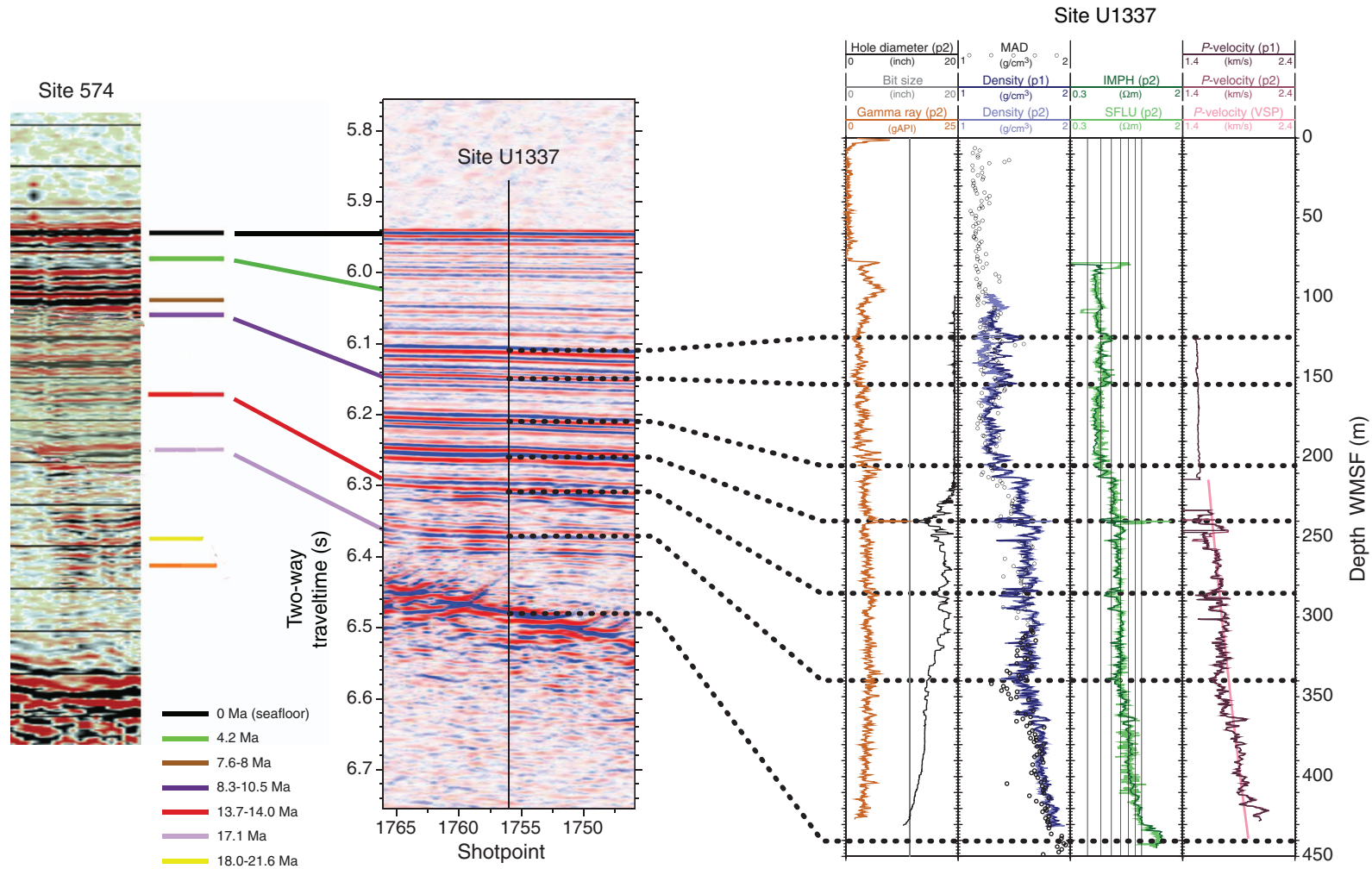


**Figure F26.** Formation MicroScanner (FMS) and downhole log curves highlighting the location of a thin “baby chert” layer at Sites U1337 (A, B, and C) and U1338 (D). **A.** Total gamma ray measured by Hostile Environment Gamma Ray Sonde (triple combination tool string). **B.** Bulk density measured by Hostile Environment Litho-Density Sonde. **C, D.** FMS four-pad downhole resistivity images. Depth interval of baby chert layer in A and B is slightly offset ( $\sim 0.4$  m) from the FMS image (C). WMSF = wireline log matched depth below seafloor.

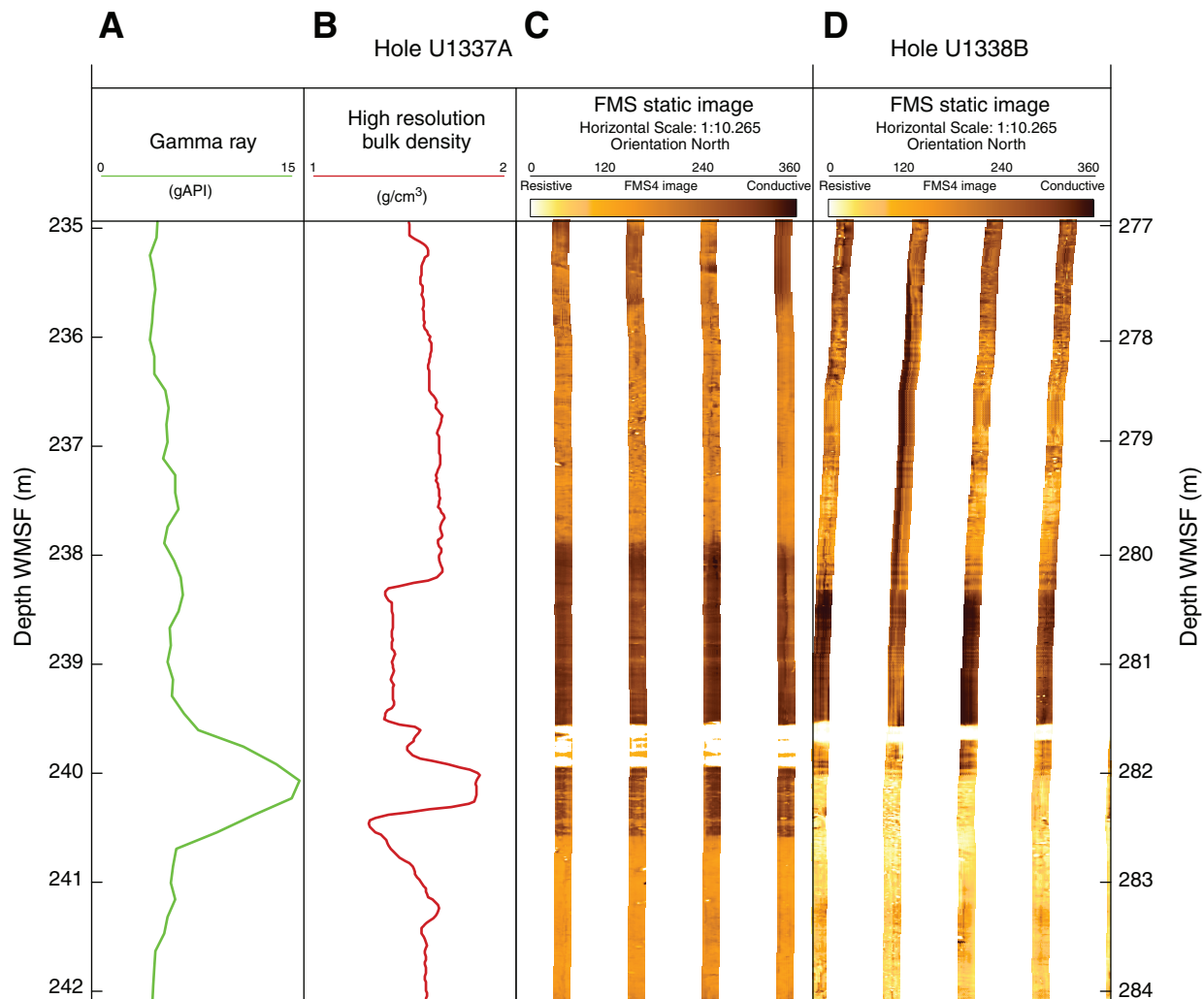
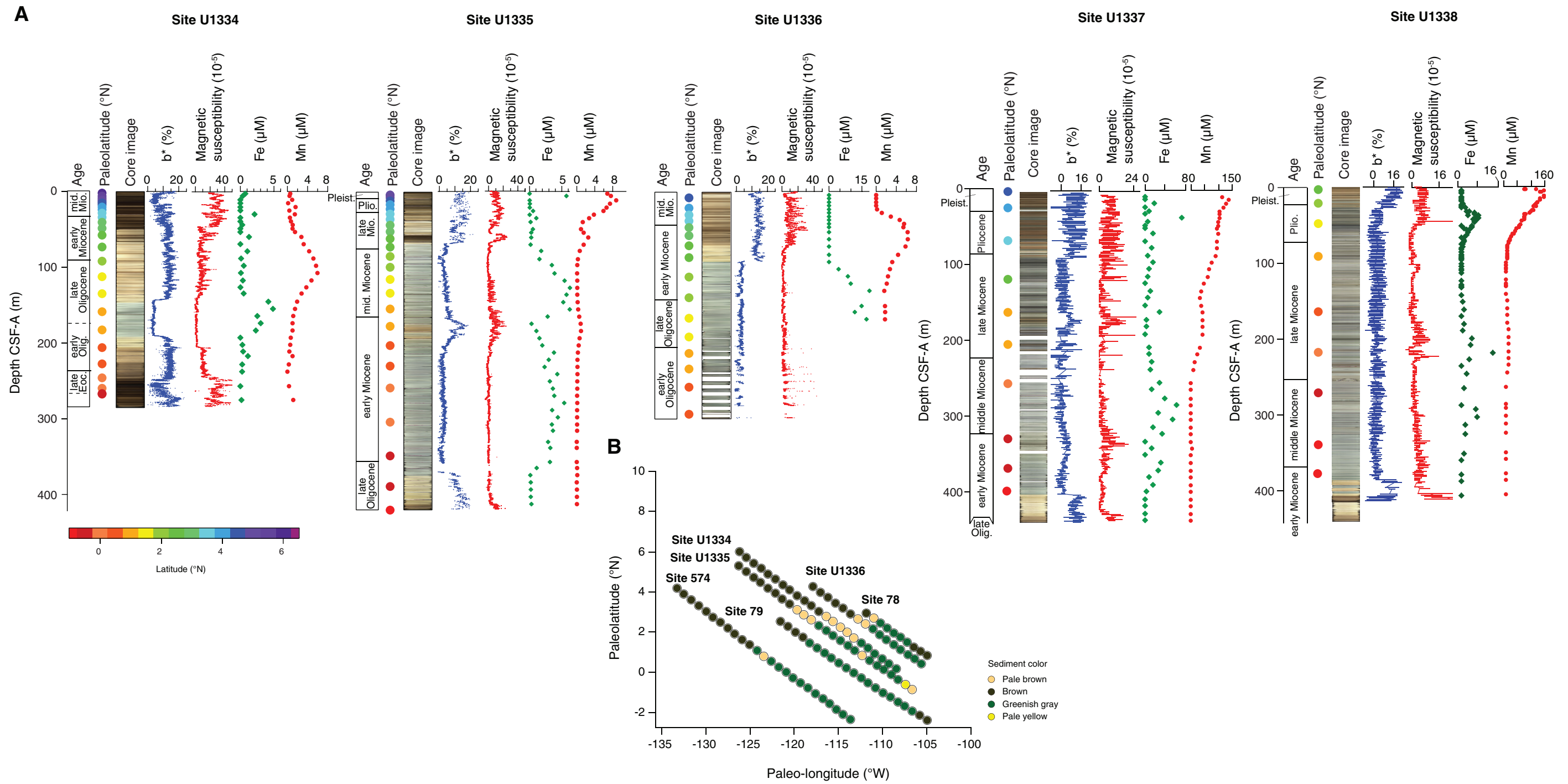


Figure F27. Sediment color and interstitial water chemistry change summaries. A. Site summaries. B. Sediment color changes superimposed on site backtrack curves as interpreted from visual core descriptions.



**Figure F28.** Calcium carbonate concentrations and total organic carbon (TOC) contents, Sites U1336–1338. TOC contents determined by acidification method.

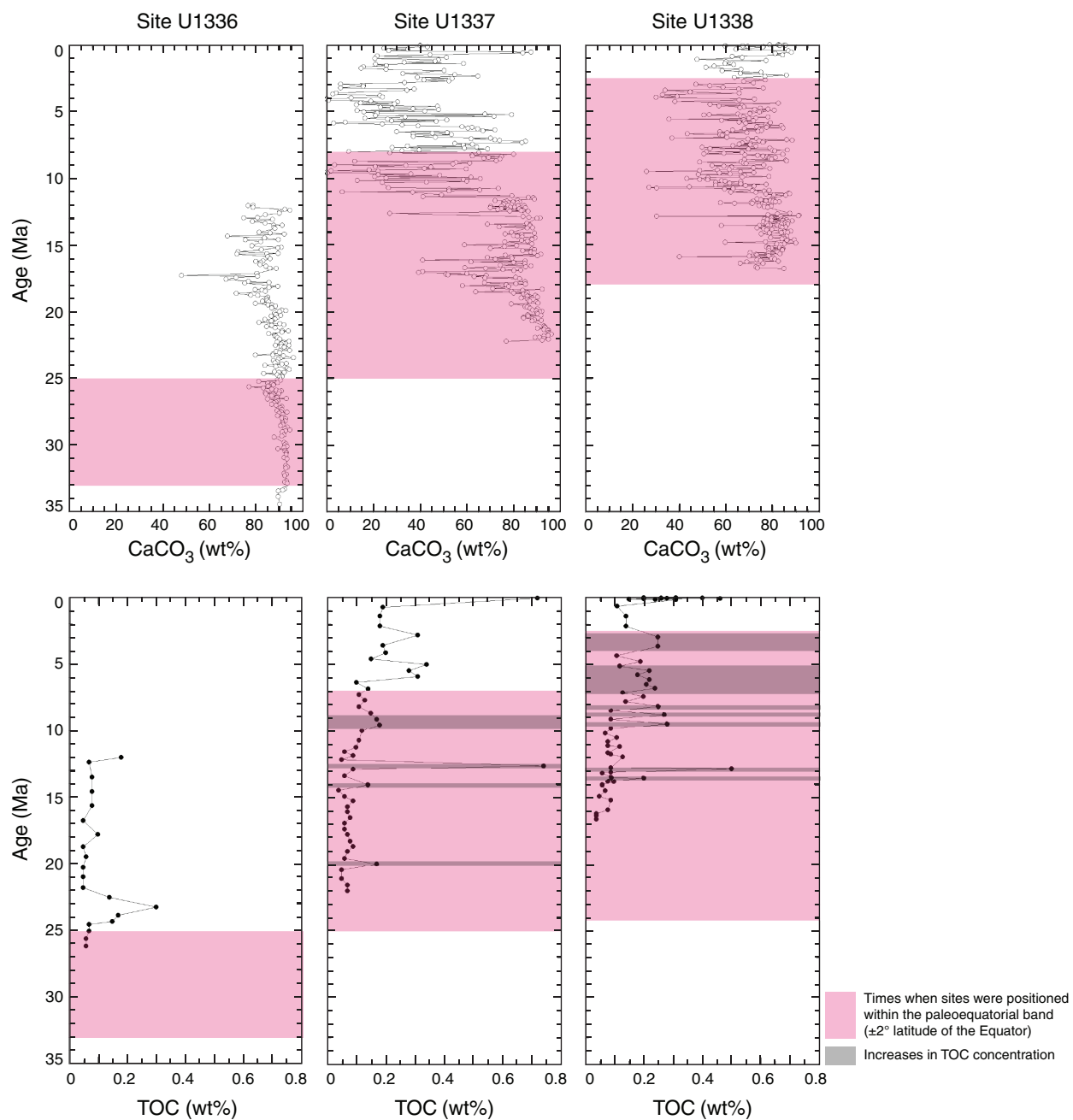
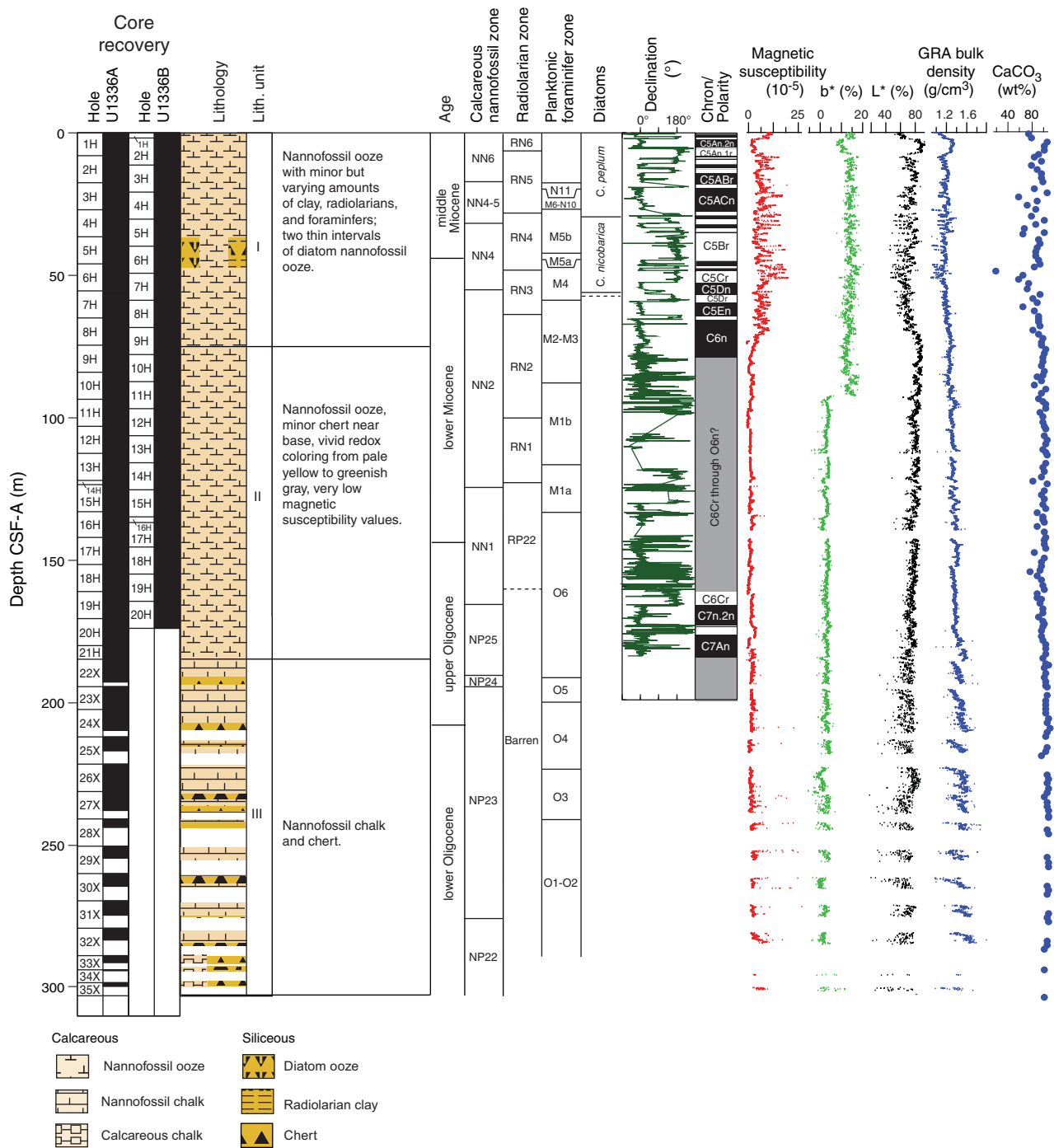
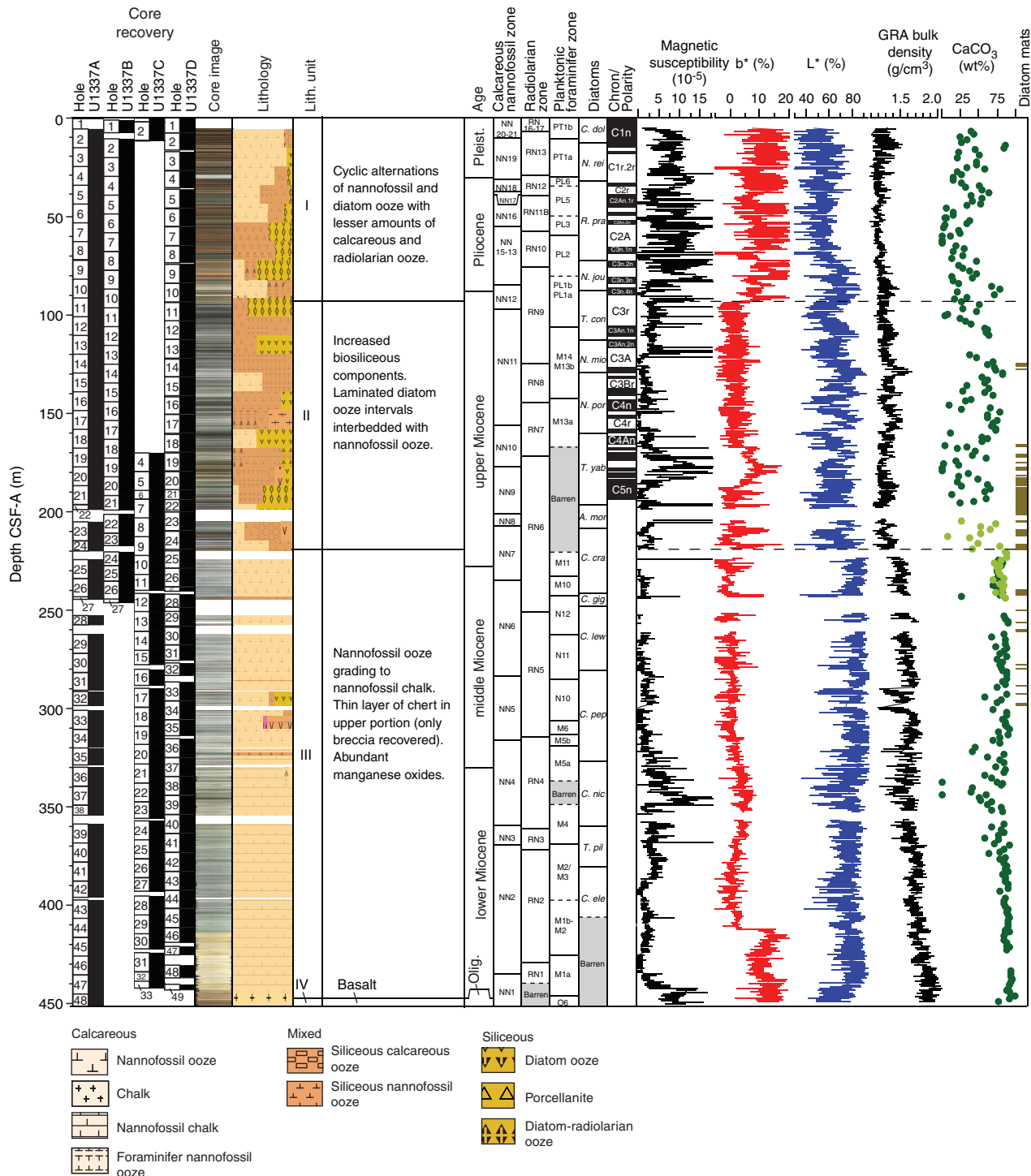


Figure F29. Site U1336 summary. CSF-A = core depth below seafloor, method A.



**Figure F30.** Site U1337 summary. Light green circles = CaCO<sub>3</sub> contents from Hole U1337B. Diatom mat intervals are from Hole U1337D. Core depth below seafloor, method A (CSF-A) depths for Holes U1337D and U1337B were converted to CSF-A depths for Hole U1337A. Magnetic stratigraphy represents a spliced record from all holes and is plotted relative to corrected core composite depth below seafloor, method A.



**Figure F31.** Downhole log measurement summary, Hole U1337A. MAD = moisture and density, p1 = uplog pass 1, p2 = uplog pass 2, IMPH = medium induction phasor-processed resistivity, SFLU = spherically focused resistivity, VSP = vertical seismic profile, WMSF = wireline log matched depth below seafloor.

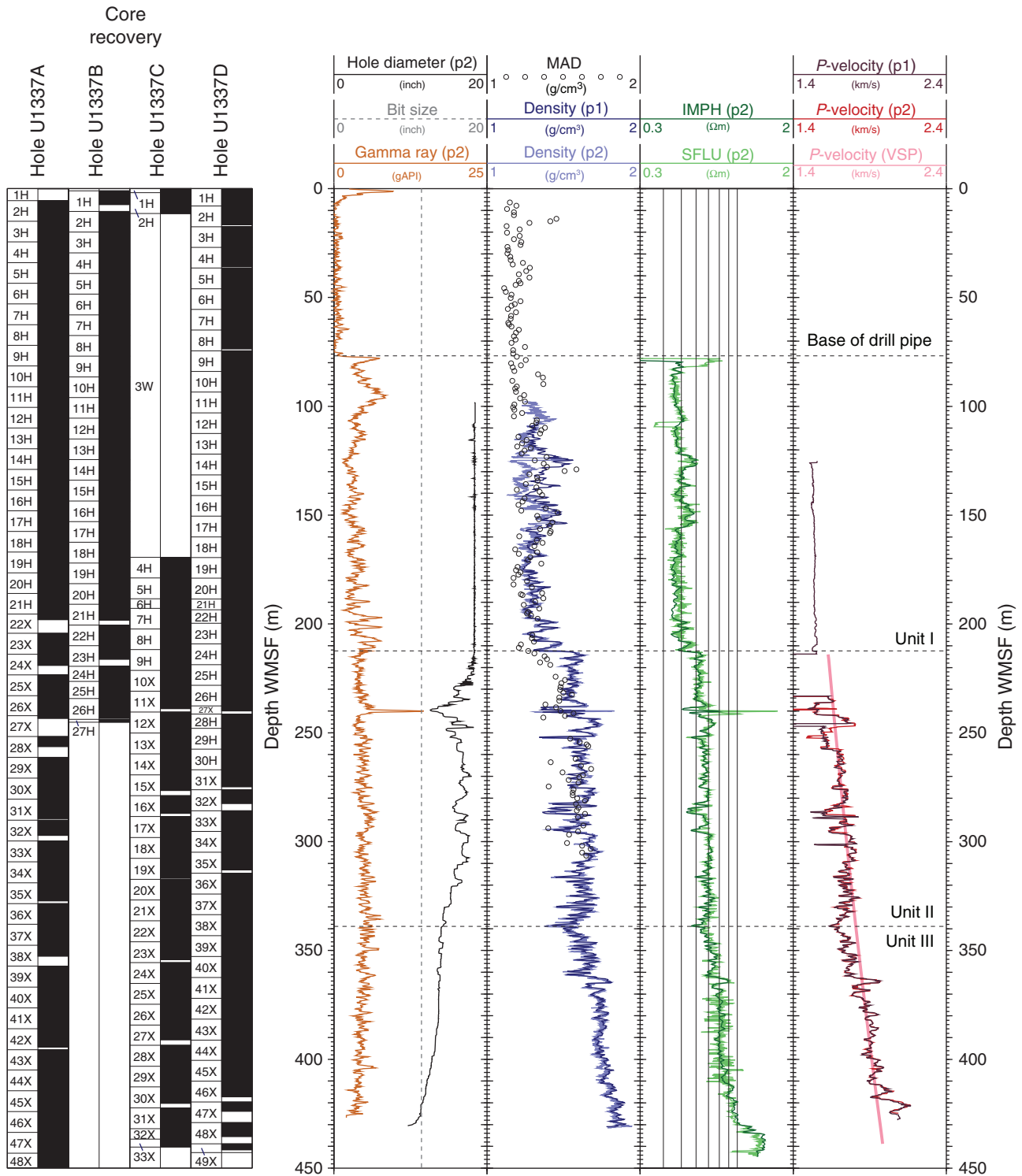


**Figure F32.** Site U1338 summary. Biostratigraphic zones and CaCO<sub>3</sub> contents mainly based on Hole U1338A. Light green circles = CaCO<sub>3</sub> contents from Hole U1338B. Core depth below seafloor, method A (CSF-A), depths for CaCO<sub>3</sub> samples from Hole U1338A were converted to CSF-A depths from Hole U1338B. Magnetostratigraphy represents a spliced record from all holes and is plotted relative to corrected core composite depth below seafloor, method A.

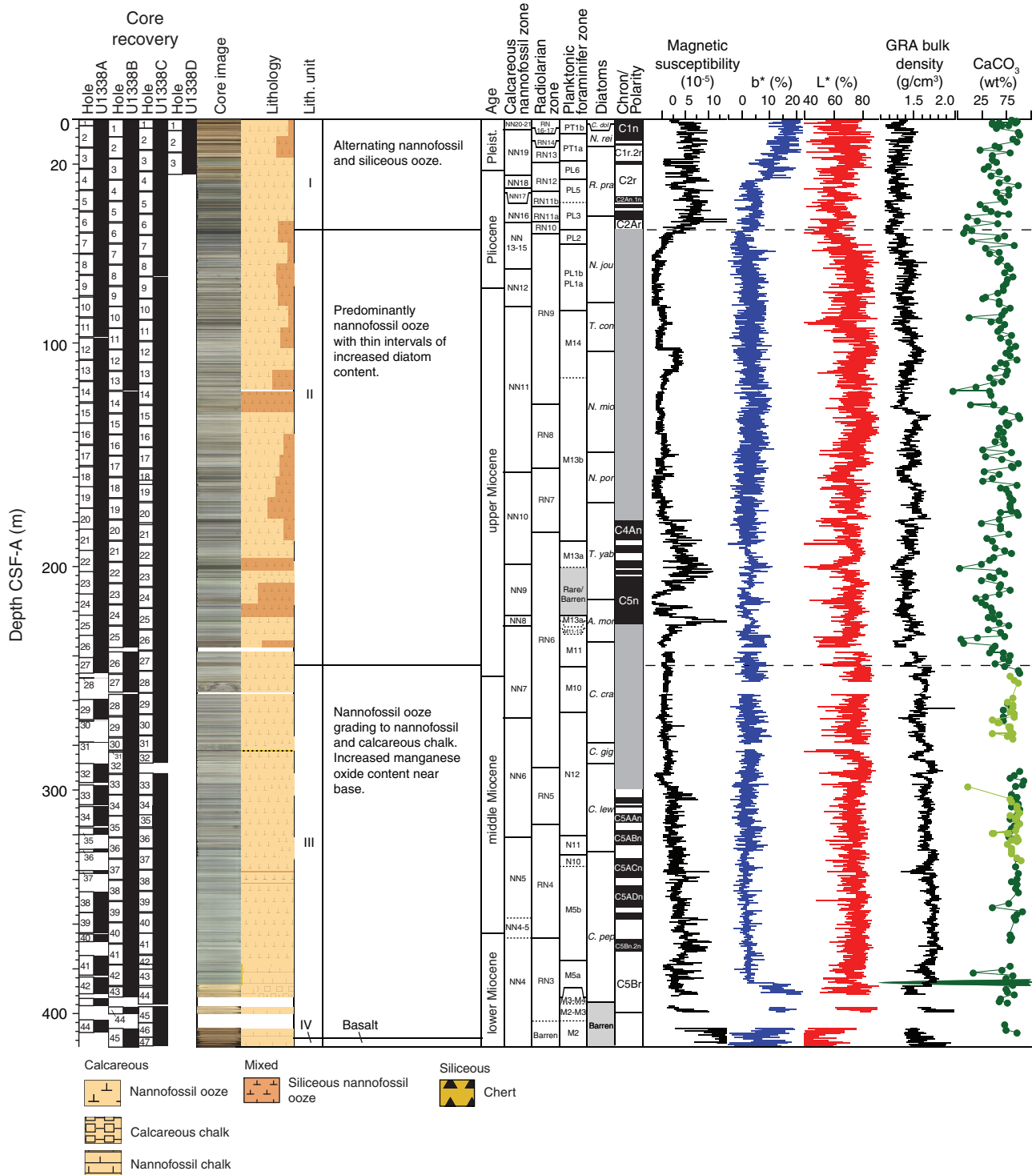


**Figure F33.** Downhole log measurement summary, Hole U1338B. TC = triple combo, IMPH = medium induction phasor-processed resistivity, SFLU = spherically focused resistivity, VSP = vertical seismic profile, WMSF = wireline log matched depth below seafloor.

